

Diss. ETH No. 18744

Optimisation of Fixation Techniques for Proximal Humeral Fractures

A dissertation submitted to the
ETH Zurich

for the degree of
Doctor of Sciences

presented by

DANIEL BAUMGARTNER
Dipl. Masch.-Ing. ETH

born October 26th 1976
Citizen of Oensingen, SO

Accepted on the recommendation of

Prof. Dr. Edgar Stüssi, examiner
Robert Mathys, co-examiner
Prof. Dr. Christian Gerber, co-examiner
Prof. Dr. Jess Snedeker, co-examiner

2009

Gewidmet Alex Stacoff und Markus Kissling.

Sie haben mir die Faszination der Technik aufgezeigt und mich in meinem beruflichen Weg inspiriert.

Summary

Introduction: Humeral fractures represent one of the most common fracture types of the skeletal system. One in four fractures of the upper extremities affects the proximal humerus. Hemiarthroplasty represents one type of surgical intervention to replace the detached head of the humerus by shoulder prosthesis. Additional fragments like the greater and lesser tuberosity are attached to the prosthesis stem and to the proximal part of the humerus by wires and sutures. However, fragment displacement is present in about 25-30 % of all cases by clinical follow-up studies. Muscular force transmission to the tendon insertions on the fragments is assumed to be the reason for such displacements. The chance of a proper bone healing due to an increased interfragmentary distance and compromised nutritional supply is decreased. Thus, resulting fragment non-unions correlate with poor clinical outcome. As a consequence, fragment fixation is important to guarantee primary stability of the prosthesis and to prevent secondary fragment dislocation. Optimisation of the stability of such reconstructions is therefore highly relevant to improve clinical outcome and thus patient satisfaction.

In existing biomechanical testing of fixation techniques, static unidirectional loading without simulating cyclic loads is applied. Requirements for an optimised fixation technique are derived by analysing failure mechanisms of existing techniques during physiological loading.

The aim of this work is the optimisation of the primary stability of fixation techniques for a reconstructed humerus. The following steps are included:

- Analysis and comparison of existing fixation techniques for proximal humeral fracture reconstruction in hemiarthroplasty.
- Realisation of a fracture model and a corresponding biomechanical testing device to apply a physiological, cyclic loading to a reconstructed humerus.
- Development and testing of an optimised fixation technique based on the biomechanical analysis of existing fixation techniques.
- Finite Element Analysis (FEA) of a reconstructed humerus to investigate bone-to-implant interactions, in particular maximum stresses in the bone and fragment displacements.

Experimental method: A four-part fracture was simulated according to a standardised fracture classification. Idealised, straight line fractures were cut with a saw in artificial bone samples (Last-a-Foam, ASTM-F 1836). Muscular loads were applied by artificial tendons (polyester webbing) to the corresponding anatomical insertion sites. In total 6 human humeri were included in the study and fractured similarly to the artificial model. The fractures were reconstructed with two clinically established fixation techniques. Type A fixation comprised two vertical suture loops (connecting the tuberosities to the shaft) and a horizontal loop (connecting both tuberosities together). Type B was additionally stabilised by a horizontal cable cerclage. For each type, n=6 tests were performed with the artificial model, and n=3 tests for type A using human samples. Fragment kinematics (distance and angulation relative to the humerus shaft) during loading was determined by images on axes perpendicular to the scapular plane. The number of cycles-to-failure was determined as the “migration rate”, a number to quantify the progress of dislocation per loading cycle (increment). Based on the performance of the existing techniques, requirements for an optimised fixation technique were defined and a novel design concept was derived.

The experimental testing device represents a free hanging arm model, which is mobilised by muscular activation of the rotator cuff muscles. The subscapularis, teres minor and superior/inferior infraspinatus muscles actively stabilise the joint in the scapular plane, whereas supraspinatus and deltoideus apply an increasing load to the humerus until a maximum glenohumeral (GH) abduction angle of 70°. The testing device records the glenohumeral joint force and the muscular forces of the supraspinatus and deltoideus using a load cell. By applying the tendon travel method, the muscular moment arms are determined.

FE-Analysis: The Finite Element Analysis (FEA) is based on a mathematical algorithm which calculates resulting stresses and displacements for a given geometry, predetermined material properties and the applied boundary conditions. FEA was used to determine the direct interaction of the fixation technique with the bone; with the goal of reducing the risk of migration into the bone by optimising pressure distribution. Additionally, resulting fragment displacements were analysed and compared with the results from the experiment. The geometry of the fractured humerus was chosen according to the experimental tests, while material properties of the bone were defined based on the literature. Loading of the rotator cuff muscles was simulated by a total tensional load of 40 N. Cable placement of type B' and the novel design (type C') were simulated. Implant-to-bone friction was set equal to zero to simulate a worst case scenario. The healed and consolidated fracture represented a control.

Experimental validation was done using speckle interferometry to compare the resulting strain distribution on the bone surface with FEA results.

Experimental Results: Applied muscle forces, moment arms and joint forces were within the range reported in literature. Deltoideus and supraspinatus applied 150 N each, additional muscles of infraspinatus/teres minor and subscapularis applied approx. 100 N each, which resulted in a glenohumeral contact force of 500 N at maximum abduction angle of 70°. Muscle and joint forces were reproducible for all samples with the variation of less than 10 % with respect to the mean forces.

Superior fragment dislocation was detected during cyclic loading for clinically established fixation techniques, which is in agreement with documented literature in clinics. Cutting-through effects of the sutures in the greater and lesser tuberosity fragments occurred with subsequent tilt-out of the humerus in the scapular plane, as a result of an asymmetric loading. Type A fixation withstood 2.5 cycles (human 2.4 cycles), type B 5.5 loading cycles on average, which shows significant higher durability ($p = 0.04$).

Requirements for an improved technique were derived based on failure mechanisms of existing designs: the placement of a rigid shaft-to-tuberosity connection counteracting the muscular force vectors to prevent superior displacement. Second, cutting-effects in the bone due to peak-stresses applied by sutures can be prevented by better and more evenly distributed load transmission. As a result, the novel design (type C) uses a cable construction which is guided and supported by the anchor points. The anchor points enable crossing and perpendicular placement of the cables. The described type C fixation failed after 8 loading cycles (human samples 7.5 cycles), therefore demonstrating a significantly higher survival rate than type A ($p = 0.02$). Migration rate of type C was about three times less for the greater tuberosity (A: 0.5mm/cycle, B: 0.2 mm/cycle, C: 0.1 mm/cycle) . Failure occurred due to sliding effects of the anchor points on the bone surface. The artificial bone model showed similar failure mechanisms when comparing the fixations A and C. Fragment kinematics and sustained loading cycles were comparable to the human samples what proves the reliability of the artificial bone model. Furthermore, detected fragment kinematics in the experiments (superior migration combined with rotational tilting) is in agreement with clinical observations based on x-ray.

FE-Results: Stress concentrations were shown at two specific regions at the bone-to-implant interface such as the insertion holes of the cables into the bone and on the lateral surface of the proximal humerus. Type B' applied contact stresses on the bone surface similar to the

bone anchors of type C'. Risk of bone anchor subsidence by using type C' was therefore not increased in comparison to clinically established technique of type B'. The interfragmentary distance between the humeral shaft and the lesser tuberosity varied between 40 μm (type C') and 80 μm . (type B'). Tuberosity fixation by guiding the cable through the prosthesis (type B) revealed reduced fragment dislocations of around 50 % in comparison to type A'. Experimental speckle interferometry revealed similar strains in the healed bone and in the fragmented bone which confirms the results of FEA.

Summary: Two different methods are elaborated in this work, aiming to test the stability of fixation techniques for the fractured humerus. The experiment allows a biomechanical analysis of a cyclically loaded, fractured and reconstructed humerus. The FE Analysis is used to provide detailed analysis of the implant-to-bone interaction, such as the resulting stresses during loading. A novel fixation technique was developed and optimised by means of these methods. The novel technique showed an increased survival rate during cyclic loading while potentially reducing the risk of subsidence and damage of the underlying tissue. In the future work, in vivo tests have to be performed to investigate the biological behaviour after implantation.

Zusammenfassung

Einleitung: Rund 20 % aller auftretenden Frakturen am skeletalen System betreffen die oberen Extremitäten, wovon jede vierte Fraktur eine proximale Humerusfraktur ist. Als mögliche Behandlung bietet sich eine Schultergelenksprothese an, die den gebrochenen Humeruskopf, insbesondere dessen Gleitfläche ersetzt. Zusätzliche Fragmente des proximalen Humerus wie die grosse und kleine Tuberkula (GT und LT) werden an die Prothese und an den Humerusschaft fixiert. In rund 30 % aller klinisch nachuntersuchten Fälle tritt eine Verschiebung der Fragmente auf, wobei die muskuläre Lastübertragung auf die Fragmente ein Grund für die Dislokation zu sein scheint. Eine solche Dislokation kann einer Einheilung der Fragmente infolge eines erhöhten Frakturspaltes entgegenwirken. Ein Nicht-einheilen der Fragmente hat ein nicht befriedigendes klinisches Ergebnis zur Folge. Eine Fixation der Fragmente mittels Drähten und Fäden soll deshalb eine Primärstabilität gewährleisten und sekundäre Dislokationen verhindern. Der Verbesserung der Primärstabilität der Rekonstruktion kommt demzufolge eine hohe Bedeutung zu. Bestehende in-vitro Testverfahren zur Analyse der Stabilität von Fixationstechniken beinhalten nur statische Armpositionen mit Lasteinleitung bis zum Versagen und simulieren keine dynamischen zyklischen Belastungen, wie sie im Patientenalltag auftreten. Anforderungen an ein neues Design können aus den Versagensmechanismen bestehender Fixationstechniken definiert werden, um eine Stabilitätsverbesserung zu erreichen.

Das Ziel dieser Arbeit ist eine Optimierung der Primärstabilität durch verbesserte Fixationstechniken, die im Rahmen einer Hemiarthroplastik bei Schulterfrakturen angewandt werden. Um dieses Ziel zu erreichen, werden folgende Schritte durchlaufen:

- Analyse bestehender Fixationstechniken für Humerusfrakturen, die im Rahmen eines Schultergelenksersatzes (insbes. bei Hemiarthroplastiken) angewandt werden.
- Entwicklung eines Frakturmodells und einer Testapparatur mit physiologischen Lastszenarien, um die Stabilität bestehender Fixationstechniken zu analysieren.
- Optimiertes Design einer neuen Fixationstechnik basierend auf den Anforderungen, die aus Erkenntnissen der Testung bestehender Techniken hervorgeht.
- Finite Elemente Analyse (FEA) einer fixierten Fraktur, um den Effekt der Fixationstechnik auf den Knochen (Spannungen und Verschiebungen) bei Belastung zu bestimmen.

Experimentelle Methode: Als Grundlage für alle Testungen diente eine Vier-Fragment-Fraktur analog zur offiziellen Frakturklassifikation. Die Frakturlinien wurden kontrolliert mit Hilfe einer Säge gesetzt. Als Kunstknochen-Material wurde ein Polyurethanschaum verwendet (Last-a-Foam, Tacoma US, ASTM-F 1836). Die Muskelkräfte wurden mittels künstlicher Sehnen aus Polyester auf die anatomischen Insertionsstellen eingeleitet. Als Vergleich zum Kunstknochenmodell wurden sechs Humanpräparate mit analoger Fraktur-Geometrie verwendet.

Die Fraktur wurde mit zwei klinisch etablierten Fixationstechniken stabilisiert. Typ A bestand aus zwei vertikalen und einer horizontalen Schlaufe aus Nahtfäden (Variante Balgrist Universitätsklinik, Dr. Betsy McAllister). Bei Typ B wurde zusätzlich mit einem zirkulären Kabel stabilisiert. Es wurden von jedem Typ n=6 Testungen für das Kunstmodell und n=3 Testungen für die Humanpräparate für Typ A durchgeführt. Die Kinematik der Fragmente relativ zum Humerusschaft (Distanz und Winkel der Fragmente) wurde mittels planarer Projektion in jeweils statische Abduktions-Positionen von 15°, 30°, 45°, 60° und 70° photometrisch evaluiert. Die Ergebnisse dieser Projektion wurden mit manuellen Messungen des Frakturspaltes mit Hilfe der Schiebelehre verglichen. Es wurde die Lebensdauer, d.h. die Anzahl Zyklen bis Erreichen des Abbruchkriteriums/Instabilität gezählt. Zudem wurde eine kinematische Kennzahl zur Quantifizierung der Dislokation pro Lastzyklus definiert, die so genannte „Migrationsrate“. Die Erkenntnisse aus den Versagensmechanismen der bestehenden Techniken dienen als Grundlage für die Entwicklung eines optimierten Designs.

Die experimentelle Testapparatur basiert auf dem Konzept eines frei hängenden Arm-Modells, der durch die muskulären Zugkräfte der Rotatorenmanschetten-Muskeln im konkaven Glenoid stabilisiert wird. Supraspinatus und mittlerer Deltoid abduzieren den Humerus mit Hilfe einer aktiv ansteigenden Kraft. Subscapularis, teres minor, infraspinatus superior und inferior stabilisieren mit vier unabhängigen kontraktile pneumatischen Aktuatoren den Humerus in der Scapula-Ebene. Als physiologisches Lastszenario für die experimentelle Testapparatur wurden relevante Bewegungsmuster im Rahmen der Rehabilitation gewählt. Das Lastszenario bestand aus einer zyklischen Abduktionsbewegung bis 70°. Die Testapparatur misst die glenohumerale Gelenkskraft mit einer Kraftmessdose und die einzelnen Muskelkräfte mit Hilfe der Druckwerte und der Kontraktionslänge der pneumatischen Aktuatoren. Der Verlauf der muskulären Hebelarme wird mittels der Sehnen-Exkursionsmethode gemessen.

Methode der Finiten Elemente Analyse: Die Methode der Finiten Elemente Analyse wurde verwendet, um den Effekt der Fixationstechnik auf den Knochen evaluieren zu können. Die FE-Analyse basiert auf numerischer Simulation, welche mit Hilfe der bekannten Geometrie, den Materialeigenschaften und Kräften die resultierenden Dehnungen und Fragmentdislokationen berechnet. Entstehende maximale Dehnungen und Verschiebungen am Knochen wurden für verschiedene Punkte auf der Knochenoberfläche analysiert. Die Geometrie der Fraktur wurde analog zum experimentellen Setup gewählt, Materialeigenschaften anhand bekannter Werte für spongiösen Knochen definiert. Die Fraktur wurde mit drei unterschiedlichen Fixationstechniken A', B', C' fixiert, wobei B' und C' ähnlich zu Typ B und Typ C aus dem Experiment sind. Als Kontrolle zur Fraktur diente der eingehelte Knochen mit Prothese. Die Fraktur wurde einer Zugkraft von 40 N ausgesetzt, die proportional zu den Querschnitten der Rotatorenmanschetten-Muskeln verteilt war. Die Reibung zwischen Knochen und Prothese wurde dabei gleich Null gesetzt, um eine maximal mögliche Verschiebung zu simulieren. Es erfolgte eine experimentelle Validierung mittels der Speckle-Interferometrie.

Experimentelle Resultate: Die mit der Testapparatur ermittelten Hebelarme, Muskelkräfte und Gelenkskräfte liegen im Bereich der Literaturdaten. Deltoideus und supraspinatus erzeugen nach linearem Anstieg je 150 N bei maximalem Abduktionswinkel von 70°, subscapularis und infraspinatus/teres minor je 100 N, was in einer glenohumeralen Gelenkskraft von maximal 500 N resultierte. Die Muskel- und Gelenkskräfte konnten für alle durchgeführten Tests reproduziert werden und variierten im Verlauf der Testung um weniger als 10 %. Die beiden klinisch etablierten Techniken zeigen eine Fragmentdislokation des GT nach proximal mit gleichzeitiger Rotation um die antero-posteriore Achse. Hauptgrund für das Versagen war das Einschneiden des Fadens in die Fragmente mit anschließender Instabilität des Humerus (Abkippen aus der Frontalebene) aufgrund asymmetrischer Lasteinleitung. Typ A überdauerte 2.5 Zyklen bis zur Instabilität (human 2.4 Zyklen), wogegen Typ B mit 5.5 Zyklen eine signifikant längere Überlebensrate aufweist ($p=0.04$). Die charakteristische Kennzahl zur Beschreibung der Kinematik, die Migrationsrate, zeigt eine grössere Zunahme des Fragmentspalts in der Scapula-Ebene bei Typ A im Vergleich zu B (A: 0.5 mm/Lastzyklus, B: 0.2 mm/Lastzyklus für das Tuberculum majus).

Die Anforderungen an ein optimiertes Design der Fixationstechnik beinhaltet deshalb eine rigide Verbindung in Richtung der muskulären Kraftwirkungslinien, wobei die Fragment-Migration nach proximal verhindert werden soll. Hierfür sind sogenannte Ankerplatte auf den

Fragmenten und auf dem Humerusschaft vorgesehen, die das Kreuzen und Fixieren zweier Drahtkabel zueinander ermöglicht. Zudem ist das Kabel auf den Ankerplatten abgestützt, um eine Schädigung des Periosts und dessen Durchblutung zu reduzieren.

Die neue Fixationstechnik weist eine mittlere Lebensdauer von 8 Zyklen (human 7.5 Zyklen) und ist im Vergleich zu Typ A signifikant ($p=0.02$), und gegenüber Typ B tendenziell höher. Zudem wurden für Typ A reduzierte Fragment-Migrationsraten festgestellt (0.1 mm/Abduktionszyklus). Versagen trat infolge Abgleiten der Ankerplatten auf der Knochenoberfläche auf. Das Kunstknochenmodell hat sich aufgrund des ähnlichen biomechanischen Verhaltens (vergleichbare Migrationsraten, Versagensmechanismen und Zyklenzahl bis Bruch) im Vergleich zu den Humanpräparaten als geeignet erwiesen. Zudem sind proximale Verschiebungen der Fragmente auch klinisch beobachtet worden.

FE-Analyse: Orte maximaler Spannungen wurden im Interface zwischen der Fixation und Knochenoberfläche aufgezeigt, einerseits bei der Kabel-Insertionsstelle in den Knochen, andererseits bei der lateralen Linienauflage (Typ B') und Auflage der Ankerplatten (Typ C'). Die Ankerplatten zur Kabelführung übertragen ähnlich hohe Spannungen am Knochen wie die direkte Linienauflage der Kabel. Folglich ist das Risiko eines Einsinkens der Ankerplatte in den Knochen nicht erhöht. Die Fragmentverschiebung rechtwinklig zur Frakturlinie im Halsbereich betrug je nach Fixationstechnik zwischen 40 μm (Typ C') und 80 μm (Typ B'). Die Kabel-Schleife durch die Prothese und die Fragmente hindurch erwies sich dabei als vorteilhaft und zeigte um 50 % reduzierte Verschiebungen. Die FE-Analyse eignet sich als Berechnungsmethode, um die Interaktion diverser Fixationstechniken mit dem Knochen unter einheitlichen Bedingungen zu evaluieren. Die experimentelle Speckle-Interferometrie wies vergleichbare Oberflächen-Dehnungen wie die FE-Analyse auf.

Zusammenfassung: In der vorliegenden Arbeit wurden zwei Testmethoden zur Evaluation der Primärstabilität als Folge verschiedener Fixationstechniken für den frakturierten proximalen Humerus erarbeitet. Das Experiment erlaubte eine Analyse des biomechanischen Verhaltens der Rekonstruktion bei zyklischer Belastung. Die FE-Analyse lieferte eine detaillierte Betrachtung der Interaktion zwischen Knochen und Fixation. Die optimierte Fixationstechnik hat eine Festigkeitserhöhung im Vergleich zu den etablierten klinischen Methoden ergeben, was das Verbesserungspotential für die Primärstabilität der bestehenden Techniken aufzeigt. Zudem ist, wie die FE-Analyse zeigt, das Risiko einer Migration in den Knochen nicht gegeben. Die klinische Umsetzung wird aufzeigen, ob aufgrund erhöhter in-vitro Primärstabilität auch verbesserte Patientenergebnisse resultieren.

Acknowledgement / Danksagung

Die vorliegende Arbeit beinhaltet vielschichtige Themengebiete und beanspruchte deshalb den wissenschaftlichen Input aus verschiedensten Bereichen. Angefangen bei der Formulierung der klinischen Problemstellung über die technische Realisierung von Testaufbauten und Prototypen bis zur Interpretation der Resultate war die Arbeit bereichsübergreifend.

Meinem Doktorvater Prof. Edgar Stüssi danke ich für seinen grossen Input sowie seine strategischen Entscheide, die zum Erfolg des Projekts geführt haben. Ich hab die fachlichen Diskussionen nicht zuletzt dank seiner umgänglichen Art als sehr angenehm empfunden. Er hat mir ermöglicht, meine wissenschaftlichen Ziele zu erreichen. Auch danke ich seinem Nachfolger Prof. Ralph Müller für die Unterstützung und wünsche Ihm und dem gesamten IFB alles Gute.

Einen herzlichen Dank gebührt Dr. Hans Gerber, der als Leiter Technik einen wichtigen Beitrag ins Projekt mit einbrachte. Die Unterstützung durch seine Crew mit Peter Schwilch, Marco Hitz sowie den Lehrlingen war für die Arbeit Gold wert. Dr. Jachen Denoth und Dr. Alex Stacoff danke ich für ihren Beitrag und auch Sofia Delamanis hat in organisatorischer Hinsicht wesentlich zur Arbeit beigetragen.

Die Zeit mit meinen Kollegen während der Doktorarbeit möchte ich nicht missen. Mit Dr. Renate List hab ich mich durch Vorlesungen im wahrsten Sinne des Wortes „durchgeboxt“, Dr. Silvio Lorenzetti hat mich in inhaltlicher Hinsicht und bei meiner Vorgehensweise sehr unterstützt und auch Urs Stöcker und Mauro Foresti haben mich während meiner Zeit am Institut begleitet. Dr. Heidi Ruckstuhl-Knüsel hatte eine Vorreiterrolle inne, denn sie bearbeitete als erste Doktorandin am IFB die Biomechanik der Schulter. Thomas Ukelo danke ich unter anderem für unsere Trainings-Partnerschaft über die Mittagspausen.

Die RMS Foundation hat mein Projekt nicht nur finanziell getragen – sondern auch einen wichtigen Beitrag an die Umsetzung geliefert. Robert Mathys als Initiant des Projekts stellte sein fachliches Wissen vollumfänglich zur Verfügung. Ich danke Ihm, dass er die Aufgabe des Co-Referenten übernommen hat. Dr. Beat Gasser danke ich für die Manuskript-Korrekturen und die saubere Zusammenarbeit bei der Patentierung. Paul Brotschi als Leiter der Versuchsmechanik in der RMS gebührt ein grosser Dank für die Prototypenfabrikation.

Ein grosser Dank gebührt dem Universitäts-Spital Balgrist, wo ich trotz hektischem Klinik-Alltag das benötigte Wissen abrufen konnte. Insbesondere Dr. Betsy McAllister danke ich für ihre Hilfe bei den experimentellen Tests. Prof. Jess Snedeker hat hinsichtlich biomechanischer Fragestellungen meinen Horizont erweitert. Es ist nicht selbstverständlich, dass ich mit dem Klinikdirektor in Form von Herrn Prof. Christian Gerber im Rahmen von spontanen Meetings zusammensitzen durfte. Philippe Favre danke ich für die fachlichen Diskussionen rund um die Schulter-Biomechanik.

Mathys AG Bettlach, insbesondere Roger Baumgartner und Frank Dallmann danke ich für die Bereitstellung der Implantate und OP-Sets. Der Festo AG danke ich für die grosszügige Unterstützung mit Pneumatik-Elementen für den experimentellen Schulter-Tester. Der Repla AG in Solothurn und insbesondere meinem Vater danke ich für die Fertigung der Oberarm-Kunstmodelle.

Einen grossen Beitrag für die Durchführung des „Strain Mapping“ am proximalen Humerusmodell hat das Institut für Baumaterialien IFB geliefert. Prof. Van Mier erlaubte die Benutzung der Geräte; Daniel Caduff hat mich in die Verwendung der Ausrüstung eingeführt.

Dr. Sven Knecht, Dr. Aldemar Hegewald, Robert Spörri sowie möchte ich für die abwechslungsreiche Zeit danken, in der für einmal die Wirbelsäule als Auflockerung zur Schulter diente.

Eine Reihe von Praktikantinnen und Praktikanten haben mich während der Arbeit unterstützt. Erich Roffler, Tamara Horn, Dave Burkhardt, Matthias Schlüssel. Stefan Schmid, Stefan Schori, Martin Walti danke ich für die sauber abgefassten Literaturarbeiten. Nicht zuletzt gebührt der Dank den zahlreichen Englisch-Korrigierenden Alina Levchuck, André Butscher, Duncan Webster, Carmen Hauser, Renate List, Hedy Dobler und Christoph Wille.

Meinen Eltern, den beiden Schwestern sowie natürlich meiner Freundin danke ich für ihre Rücksichtnahme, als ich gegen Ende der Arbeit meine Zeit eher der Arbeit widmete als familiären Angelegenheiten.

Table of Contents

SUMMARY.....	IV
ZUSAMMENFASSUNG.....	VIII
ACKNOWLEDGEMENT / DANKSAGUNG	XII
TABLE OF CONTENTS.....	XIV
TERMINOLOGY.....	XVII
ABBREVIATIONS	XVIII
1 INTRODUCTION.....	1
1.1 ANATOMICAL BACKGROUND.....	1
1.1.1 OVERVIEW OF THE SHOULDER JOINT.....	1
1.1.2 THE PROXIMAL HUMERUS	1
1.2 CLINICAL BACKGROUND	6
1.2.1 INCIDENCE OF FRACTURES AT THE PROXIMAL HUMERUS	6
1.2.2 FRACTURE CLASSIFICATIONS	7
1.2.3 GENERAL STRATEGIES IN FRACTURE TREATMENT	8
1.2.4 POSTOPERATIVE REHABILITATION	11
1.3 AIM OF THE PROJECT	13
2 LITERATURE ANALYSIS	14
2.1 DETAILED ANALYSIS OF EXISTING FIXATION TECHNIQUES	14
2.1.1 INTRODUCTION.....	14
2.1.2 RESULTS OF THE LITERATURE REVIEW.....	17
2.1.3 DISCUSSION AND CONCLUSIONS	23
2.2 EXISTING EXPERIMENTAL SHOULDER TESTING DEVICES	26
2.2.1 INTRODUCTION.....	26
2.2.2 MATERIAL & METHODS	28
2.2.3 RESULTS OF THE LITERATURE REVIEW.....	29
2.2.4 DISCUSSION AND CONCLUSIONS	39

2.3	CONCLUSION BASED ON THE LITERATURE REVIEW	41
<u>3</u>	<u>MATERIAL & METHODS</u>	<u>42</u>
3.1	EXPERIMENTAL TESTING OF FIXATION TECHNIQUES	42
3.1.1	EXISTING TESTING STRATEGIES FOR FRACTURE RECONSTRUCTIONS.....	42
3.1.2	FOUR-PART FRACTURE MODEL.....	45
3.1.3	EXPERIMENTAL TESTING DEVICE	53
3.1.4	DATA ACQUISITION DURING TESTING	58
3.1.5	REPRODUCIBILITY OF THE APPLIED JOINT AND MUSCLE FORCES.....	60
3.1.6	ANALYSIS OF THE FRAGMENT KINEMATICS	66
3.1.7	ERROR ESTIMATION AND REPRODUCIBILITY OF FRAGMENT DISPLACEMENT MEASUREMENTS	71
3.2	FINITE ELEMENT ANALYSIS OF PROXIMAL HUMERAL FIXATION	76
3.2.1	INTRODUCTION.....	76
3.2.2	MATERIAL & METHODS	76
3.2.3	FE VALIDATION STUDY USING SPECKLE INTERFEROMETRY	81
<u>4</u>	<u>RESULTS.....</u>	<u>82</u>
4.1	RESULTS OF THE EXPERIMENTAL TESTING.....	82
4.1.1	APPLIED MUSCLE AND CONTACT FORCES.....	82
4.1.2	MOMENT ARMS AND TRANSLATION OF THE ROTATION CENTRE.....	86
4.1.3	BIOMECHANICAL FAILURE ASSESSMENT OF EXISTING FIXATION TECHNIQUES	88
4.1.4	THE NOVEL FIXATION TECHNIQUE (TYPE C).....	91
4.1.5	BIOMECHANICAL PERFORMANCE OF FIXATION TECHNIQUES.....	93
4.2	RESULTS OF THE FINITE ELEMENT ANALYSIS	105
4.2.1	REGIONS OF HIGH VON MISES STRESSES	105
<u>5</u>	<u>DISCUSSION</u>	<u>110</u>
5.1	EXPERIMENTAL TESTING	110
5.2	FINITE ELEMENT ANALYSIS FEA.....	112
<u>6</u>	<u>CONCLUSIONS AND OUTLOOK</u>	<u>115</u>

<u>7</u>	<u>APPENDIX A: SUTURE MATERIAL PROPERTIES</u>	<u>119</u>
7.1	BIOMECHANICAL BEHAVIOUR OF SUTURES UNDER DYNAMIC LOADING	119
7.1.1	INTRODUCTION.....	119
7.1.2	MATERIAL & METHODS	120
7.1.3	RESULTS	122
7.1.4	DISCUSSION AND CONCLUSIONS.....	123
<u>8</u>	<u>APPENDIX B: ARTIFICIAL BONE MODEL AND PROSTHESIS DESIGN</u>	<u>124</u>
8.1	ARTIFICIAL BONE MODEL.....	124
8.2	PROSTHESIS DESIGN.....	124
<u>9</u>	<u>APPENDIX C: CURRICULUM VITAE</u>	<u>125</u>
<u>10</u>	<u>BIBLIOGRAPHY</u>	<u>127</u>

Terminology

Arthroplasty.....	Joint replacement by using prosthetic devices
Cancellous bone	Trabecular bone
Compacta.....	Cortical bone
Constant Score.....	Clinical outcome score for the shoulder function
Diaphysis.....	Main or mid section of a long bone
Footprint	Tendon insertion
Four-part fracture	Humeral fracture with four fragments (head segment, LT, GT, shaft)
Greater Tuberosity.....	lat.: tuberculum majus
Hemiarthroplasty.....	Replacement of the humeral head by prosthesis
Lesser Tuberosity	lat.: tuberculum minus
Osteoporotic	Condition of bone with reduced mineral density
Osteotomy	Surgical cutting of bone
Reduction	Anatomical reposition of the fragments
Scaption.....	Abduction in the scapular plane
Tension band technique.	Suture or cable construction to compress fragments together
Testing device	Experimental shoulder testing machine used in this report

Abbreviations

AC	Acromioclavicular
a. / m. / p. DELT.....	Anterior, middle, posterior Deltoideus muscle
CAD	Computer Aided Design
CS	Constant Score
COR.....	Centre of Rotation
DOF.....	Degree of Freedom
EMG	Electromyogram
FE(M)	Finite Element (Modelling)
GH	Glenohumeral
GT.....	Greater Tuberosity
IAR.....	Instantaneous Axis of Rotation
ISP.....	Infraspinatus
LD.....	Latissimus Dorsi
LT	Lesser Tuberosity
ORIF.....	Open Reduction and Internal Fixation
PCSA.....	Physiological Cross Sectional Area
PM.....	Pectoralis Major
ROM.....	Range of Motion
SC	Sternoclavicular
SSC.....	Subscapularis
SSP	Supraspinatus
TM.....	Teres Minor
TMAJ	Teres Major
TH.....	Thoracohumeral
3D	Three Dimensional

1 Introduction

1.1 Anatomical background

Preamble: The analysis of the shoulder joint anatomy represents important background information for the understanding of the shoulder function. The bone morphometry and the geometric placement of the muscles have direct influence on the shoulder biomechanics. It is therefore evident to provide a basic description of the human shoulder complex.

1.1.1 Overview of the shoulder joint

The complex musculoskeletal system of the shoulder joint enables a three-dimensional placement of the arm in the working space. The huge range of motion of the shoulder exceeds the range of motion of any other joint by a simultaneous, coordinated movement of different articulations. The shoulder complex is built by four bones, comprising the sternum, the clavicle, the scapula and the humerus. The humerus and the articulating surface in the scapula, the glenoid, form the glenohumeral joint. Both joint surfaces are covered by cartilage layers enabling a low-friction cartilage-to-cartilage articulation. The coracoid process, which is part of the scapula, and the acromion process of the clavicular part form the coracoacromial arch, which is located above the glenohumeral joint. This description is based on the anatomy of Gray et al. [1]. The glenohumeral joint is a ball-and-socket joint which provides considerable range of motion and is stabilised by surrounding tendons, ligaments and muscles. The tendons mainly restrict glenohumeral translation, whereas the glenohumeral ligaments limit the rotational movement capacity of the joint. Further passive stabilisers of the glenohumeral joint are the glenohumeral joint capsule with its negative, intraarticular pressure, the glenoid fossa and the labrum glenoidale.

1.1.2 The proximal humerus

1.1.2.1 The proximal humeral bone shape

The proximal humeral bone consists of a large hemispherical head, which articulates in the glenoid cavity of the scapula (Figure 1). Distally from the head, the circumference of the articular surface is slightly constricted and termed the anatomical neck. The surgical neck joins the anatomical neck more distally. In between the head and the lateral side of the humeral shaft, the greater and lesser tuberosities are located. The outer surface of the greater tuberosity is convex and continuous with the outer side of the shaft. The lesser tuberosity is

smaller than the greater but more prominent. Both tuberosities are separated by the bicipital groove, in which the biceps tendon is guided from proximal to distal and which comprises as well a branch of the anterior circumflex artery.

Generally, the proximal humerus is often described two-dimensionally. Only few investigations deal with the analysis of the three-dimensional shape. An anthropometric study of the proximal humerus revealed a variation on a wide scale, that makes adaptable implant sizes necessary [2]. The proximal shaft of the humerus is almost cylindrically shaped and becomes prismatic in its cross section in distal direction.



Figure 1: Anterior (left) and posterior view (right) of a left proximal humerus.

1.1.2.2 Acting muscles at the proximal humerus

In total four muscles are inserted to the proximal humerus, namely the supraspinatus (SSP), subscapularis (SSC), infraspinatus (ISP) and teres minor (TM). They form a functional unit called the rotator cuff. The rotator cuff stabilises and guides the glenohumeral joint by individual activation of the single muscles. The origin of the supraspinatus is located superior to the spina scapulae and inserts in the proximal facet of the greater tuberosity. The large origin site of the infraspinatus is found below the spina scapulae and inserts on the middle facet of the greater tuberosity. The origin of the teres minor is found along the middle third of the margo lateralis, whereas its insertion is located on the distal part of the greater tuberosity. The large origin of the subscapularis is found on the anterior side of the scapula and leads to the lesser tuberosity [3]. Generally, muscles with large insertions are divided up into multiple functional segments such as superior, middle or inferior subscapularis/infraspinatus. In particular, the deltoideus is divided into anterior, middle and posterior segment. The segments

of the deltoideus cover the rotator cuff in the proximal part and wrap around the bony structures. The deltoideus muscle is therefore not characterised by a straight line of action.

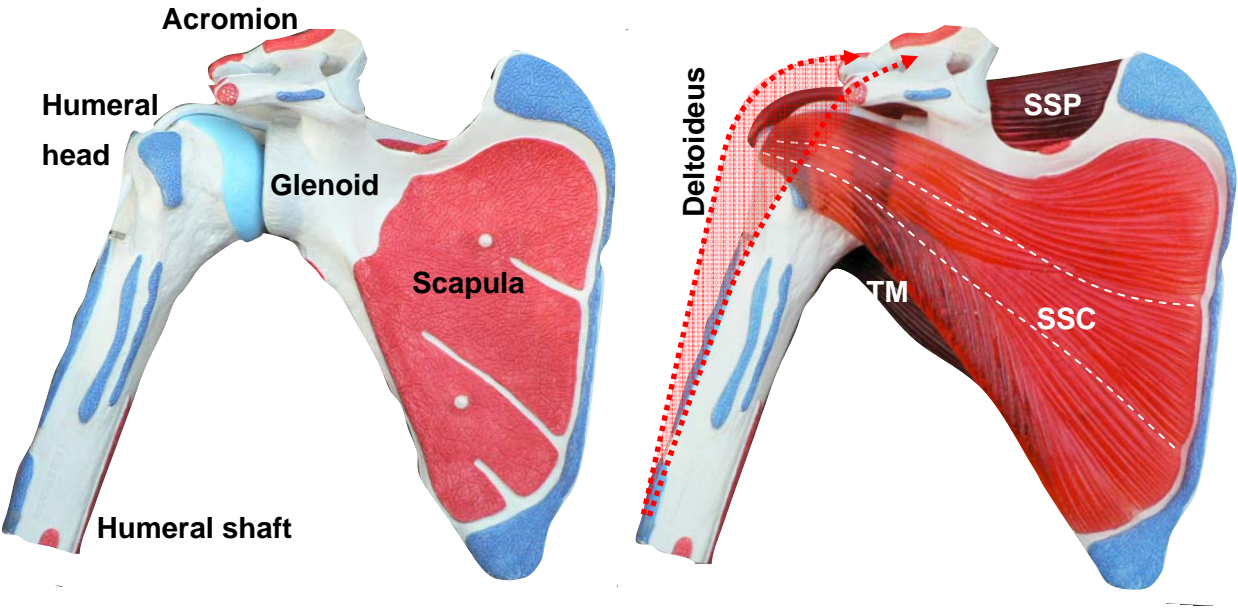


Figure 2: Anterior view on the shoulder complex with the involved bone morphometry (left) and corresponding placement of the muscles (right).

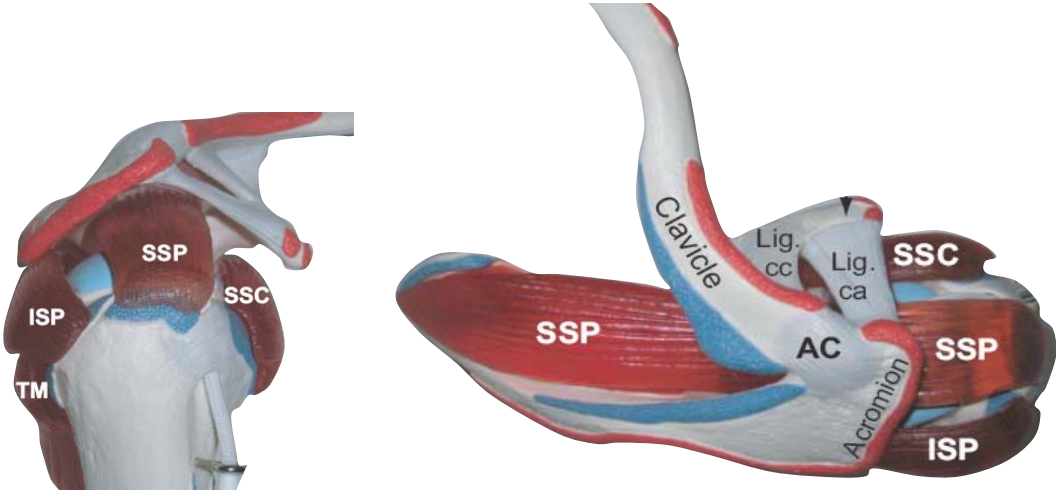


Figure 3: Rotator cuff from the medial view (left) and top view (right).

1.1.2.3 The vascular system at the proximal humerus

Nutritional supply of the proximal humeral bone is provided by an dense arterial distribution [4, 5] (Figure 4). The vascular system is well documented by Laing et al., the directions of the vessel branches were evaluated based on perfusion techniques by using contrast agents [6]. Although Seggl et al. detected a slight anatomic variation of the vascular system comparing different samples, an identical overall orientation of the arteries at the endosteum of the proximal humerus is assumed [7]. The arteries are located on the bone surface of the proximal humerus, originating from the arteria axillaris.

The anterior humeral circumflex and posterior humeral circumflex arteries are leading to the anterior and posterior proximal humeral surface: The posterior humeral circumflex artery originates from the arteria axillaris at the same level of the lower border of the subscapularis. The vessel proceeds parallel to the axillary nerve, between the subscapularis and teres major, before it turns around the neck of the humerus and is connected to the anterior humeral circumflex artery. The anterior humeral circumflex artery opposes opposite the posterior humeral circumflex artery and has a slightly smaller vessel diameter. It is oriented horizontally in front of the humerus at the same height as the surgical neck. At the bicipital groove, one branch originates proximally (ramus ascendens) and enters in the sulcus to supply the head of the humerus.

A rich extraosseous anastomosis is seen between the anterior humeral circumflexa and the posterior humeral circumflex artery. Gerber et al. concluded that the anterior circumflex artery was the final pathway to the humeral head and that the articular surface was exclusively supplied by an intraosseous branch called the arcuate artery [8]. The posteromedial vessels originating from the posterior humeral circumflexa supply only a small inferior articular area. In contrast to the general assumption that long bones with open growth plate show independent epiphyseal and metaphyseal circulations, Brooks et al. revealed an arterial communication between the epiphyseal and metaphyseal system in some of the investigated samples, where the metaphyseal artery was connected to the arcuate artery [9].

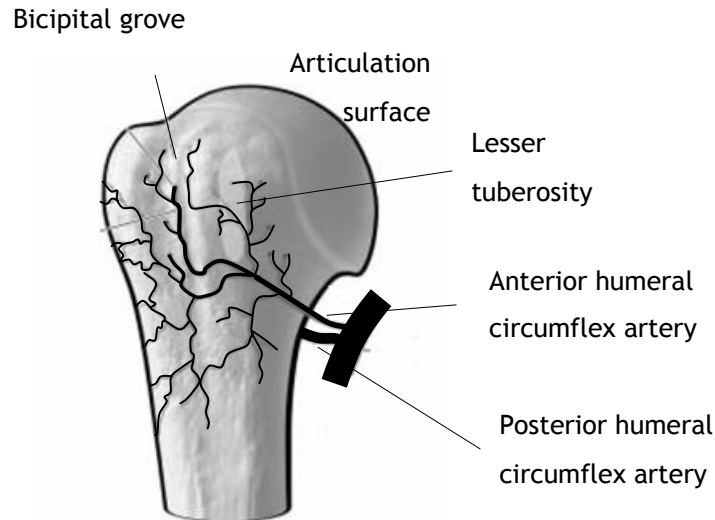


Figure 4: Vascular system at the proximal humerus [10].

1.1.2.4 The fractured proximal humerus

Fractures may negatively compromise the function of the vascularisation system. The severity of an injured humerus with a displaced four-part fracture is related to the vascular compromise of the bone tissue. The importance of vascular supply of the fragments after fracture was documented by Meyer et al. [11]. A fracture in the surgical neck region tends to interrupt the ascending branch of the anterior humeral circumflex artery as it is wrapped around the proximal humerus and enters at the tuberosities around the bicipital groove [12]. It is assumed that revascularisation of a severely displaced humeral head fragment does not occur in case of a four-part fracture. The complete interruption of the vascular system leads to avascular necrosis in the majority of the cases, thus surgical intervention is required [13, 14]. Beside the replacement of the articulating part of the proximal humerus, the preserved tuberosities still have to be provided by nutritional supply. The endosteal vessels are at risk in fractures which involve one or both tuberosities. Four-part fractures are particularly susceptible since they include disruption of both tuberosities and are associated with a high incidence of avascular necrosis, ranging from 34 % to 85 % [15-17].

A fracture is often stabilised by surgical interventions such as osteosynthesis techniques. Bone plates or cables fix the fragments to prevent interfragmentary motion and subsequent secondary dislocation. Therefore, a stable reconstruction of the fracture supports a potential revascularisation of the bone tissue. Nevertheless, the fixation of such rigid metallic devices

may apply also high pressure on the periosteum and on the underlying bone structures. This effect may disturb the microvascular endosteal supply [18] leading to accelerated degeneration of the bone. Additionally, tendon ageing is a further negative effect on the biological structures [19].

1.2 Clinical background

1.2.1 Incidence of fractures at the proximal humerus

Five percent of all fractures affecting human skeleton are related to the proximal humerus. This type of fracture represents the third most frequent fracture in elderly people after hip and distal forearm fractures [20], (Figure 5). Recent studies show an increase of proximal humerus fractures normalised to the growth of the population [21]. Considering the clinical interventions in joint arthroplasty in Switzerland, an increase of approximately 45 % of shoulder prosthesis operations were performed from 2002 to 2005 [22]. Fractures of the humerus are technically demanding and need intensive rehabilitation. An appropriate choice of treatment method based on the clinical diagnosis is therefore of high importance.

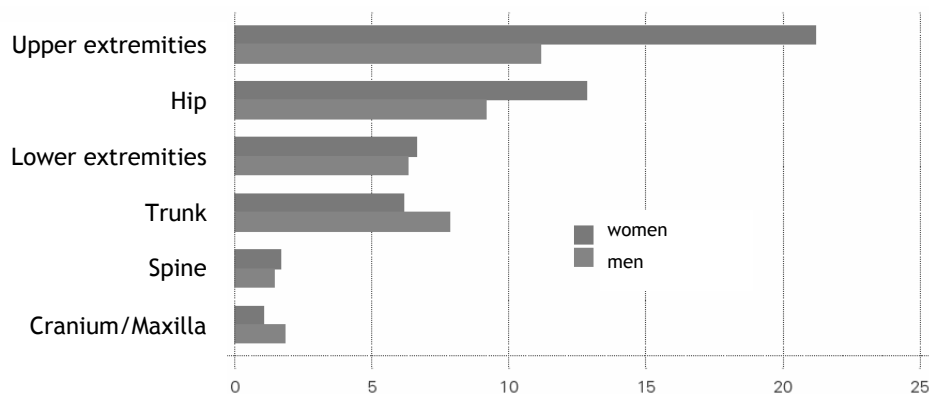


Figure 5: Upper extremity fractures represent the most frequent fracture type. (Bundesamt für Gesundheit BAG 2007).

1.2.2 Fracture classifications

Three different classifications exist for the proximal humerus to determine the fracture type. Codman's definition is based on the fact that the fracture lines follow the epiphyseal plate. The AO-classification is divided into three subsequent categories based on the severity of injury and the presence of avascular necrosis of the humeral head [23]. If no vascular isolation of the articular segment is detected, the fracture is defined as type A. Type B fractures describe a partial vascular isolation of the articular segment and in type C fractures, a total isolation of the articular segment is seen. The Neer classification system includes 4 segments (Figure 6). Displacement and vascular isolation are also considered. A fracture is considered to be displaced if more than 1 cm of interfragmentary distance and/or 45° of angulation of any one fragment with respect to the others is observed [24, 25].

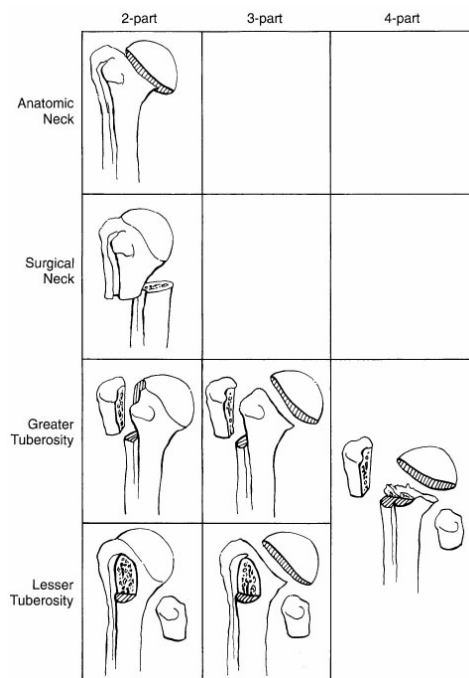


Figure 6: Fracture classification according to Neer [25].

Four-part fractures show the highest incidence of all proximal humerus fractures (Figure 7) and often appear in a standardised pattern [26]. The predetermined fracture lines are consistent with regard to the morphology and weakest points in the bone: the longitudinal fracture line parallel to the shaft axis follows the bicipital groove, the fracture perpendicular to the long bone axis is observed in the surgical neck in the epiphysis, resulting in four fragments of shaft, GT, LT and humeral head fragment. This type of trauma represents a

typical indication to perform a hemiarthroplasty. As a consequence, it was focused on that specific type of fractures in this thesis.

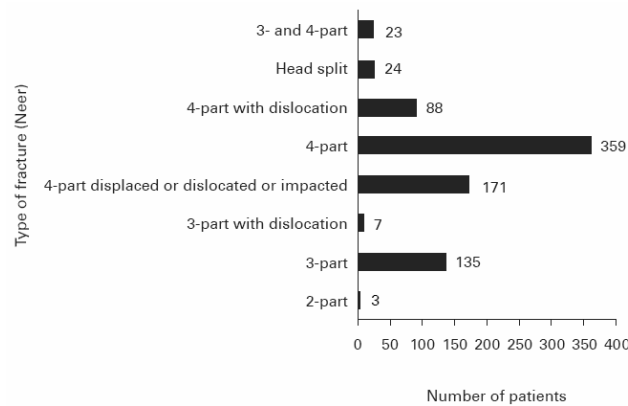


Figure 7: Four-part fractures represent the highest incidence of proximal humeral fractures according to the Neer fracture classification [26].

1.2.3 General strategies in fracture treatment

Up to now, no generally accepted strategy exists for the treatment of unstable and displaced fractures. Although intensive clinical documentation and fracture classification is defined, the indications using osteosynthesis plates with screws, intramedullary nailing or hemiarthroplasty are overlapping and similar for many cases, particularly in the osteoporotic bone, as shown by Szyszkowitz et al. [27]. Therefore, direct comparisons of the outcome of plating and hemiarthroplasty were performed in clinical studies by Dietrich et al. [28]. It was shown that using an angle stable locking plate, better results in comparison to the arthroplasty are achieved. In contradiction to that study, Bastian et al. performed a prospective comparison of osteosynthesis and hemiarthroplasty and discovered similar functional results and comparable patient satisfaction [29]. In that case, osteosynthesis has been chosen when adequate reduction and stable conditions for revascularisation were obtainable. Reuther et al. postulated that hemiarthroplasty represents a good alternative treatment for comminuted and severely displaced fractures with osteoporotic bone [30].

1.2.3.1 Postoperative outcome of fractures treated with hemiarthroplasty

The clinical outcome of proximal humeral fractures treated with joint arthroplasty often show unsatisfactory results [31, 32]. In Table 1, a summary presents resulting clinical results for dislocated four-part fractures by hemiarthroplasty. Clinical scores such as the Constant Score

assess the functional outcome after shoulder surgery. Maximum Constant Score results around 60 points out of 100 which refers to a satisfactory classification. Resorption of the fixed tuberosities is shown in 30-70 % of all cases after a shoulder arthroplasty, shown by Kralinger et al. [33]. Hasan et al. detected a significant correlation between resorbed tuberosities and low constant score [34]. Displaced and healed tuberosities in non-anatomical position showed worse clinical results than anatomically healed fragments [35]. Thus, a stable reconstruction of the fragments is of high importance in order to avoid instability and secondary dislocation. Dislocation of the fragments results in a modified position of the muscular insertion points and subsequent dysfunction. In addition, articular surface incongruency may be followed by consecutive osteoarthritis, shown by Ruckstuhl-Knuesel et al. [36].

<i>Reference</i>	<i># Cases</i>	<i>Follow-up [Mts]</i>	<i>Ø-Age [Years]</i>	<i>Constant Score</i>	<i>Prosthesis Type</i>
<i>Ambacher [37]</i>	27	42	69	65	<i>Neer II, Aequalis</i>
<i>Becker [38]</i>	27	45	67	45	<i>Global</i>
<i>Boileau [31]</i>	66	27	66	56	<i>Aequalis</i>
<i>Boileau [39]</i>	43	29	68	60	<i>Aequalis</i>
<i>Bosch [32]</i>	40	43	68	54.2	<i>Neer II</i>
<i>Boss [40]</i>	20	32	77	52	<i>Neer II</i>
<i>Christoforakis [41]</i>	26	50	65	70.4	<i>Cofield, Global, Aequalis</i>
<i>Demirhan [42]</i>	32	35	58	68	<i>Fenlin, Bio-Modular, Neer II</i>
<i>Kollig [43]</i>	46	62	60	66	<i>Neer II</i>
<i>Kralinger [33]</i>	167	29	70	55.4	<i>Global, Neer II, Aequalis</i>
<i>Reuther [30]</i>	37	39	71	46	<i>Articula</i>
<i>Zyto [44]</i>	36	12.4	72	57.5	<i>Neer II, Biomodular</i>
<i>Loew [45]</i>	21	29.3	74.1	51.5	<i>Aequalis anat. / Aequalis fract.</i>
<i>Mehlhorn [46]</i>	26	17	70.3	52	<i>Epoca</i>
<i>Fialka [47]¹</i>	35	12	74	70.4 / 46.2*	<i>Epoca / HAS</i>
<i>Grönhagen [48]</i>	46	53	72	42	<i>Bigliani-Flatow</i>
<i>Wiedemann [49]²</i>	13 / 34	40 / 44	72.9/61.6	45 / 50	<i>Aequalis</i>
<i>Besch [50]²</i>	18 / 16	60	-	54.9 / 48.5	-

Table 1: Clinical outcome of treated four-part fractures by hemiarthroplasty.

¹ Fialka et al. demonstrated a significant difference of two fixation techniques with respect to the clinical outcome.

² Primary arthroplasty shows better outcome than secondary arthroplasty.

1.2.3.2 Factors influencing the postoperative outcome

Many parameters influence the clinical outcome after fracture treatment on the proximal humerus [35]. Patient specific parameters which influence the clinical outcome are age, gender, level of ambulation, mental status, rehabilitation, tobacco & alcohol consumption and bone quality. Injury related parameters like the time to surgery after injury, presence of fragment dislocation, neurological deficit and type and grade of the fracture have a direct impact on the clinical result. Intraoperative parameters are considered to be important like the prosthesis type or the fixation technique as previously mentioned. A recent study has shown significant difference between two different types of fixation techniques with respect to the clinical outcome [47]. Although the detailed decisive factors are not clear, it is assumed that the clinical result can be directly influenced by the selection of the technique.

To preserve the tendon insertions of the rotator cuff muscles, biologically integrated tuberosities are highly required for satisfactory clinical outcome [31]. To support the biological healing process (Figure 8), stable fixed tuberosities are a prerequisite for bone consolidation. Due to the fact that an osteotomy of the greater tuberosity does lead to unsatisfactory results [51], the preservation of the proximal bone by surgical fixation represents a reliable alternative.

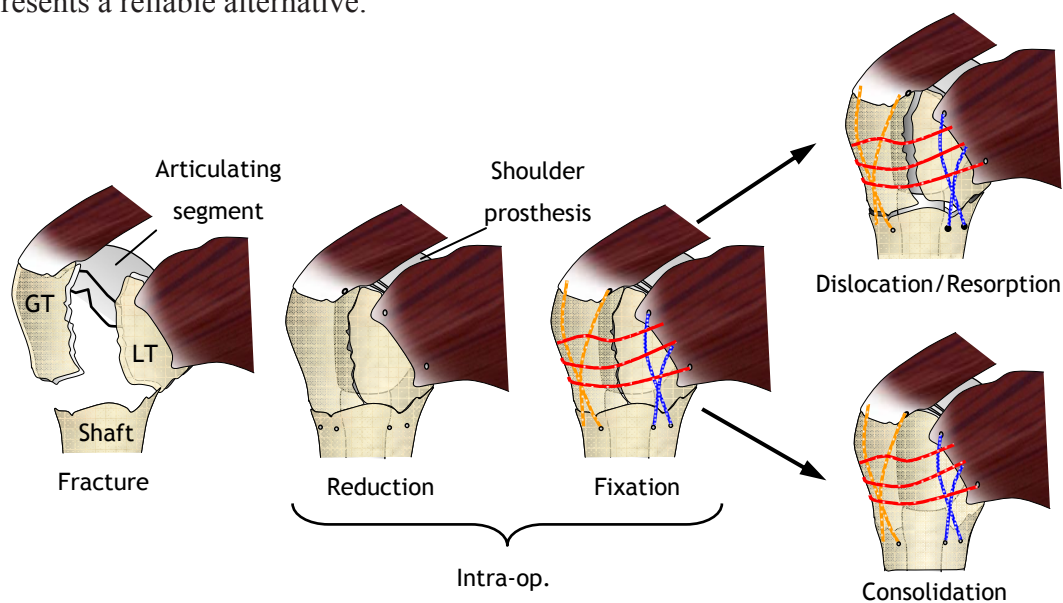


Figure 8: Initial state after fracture (left), intraoperative treatment procedure and postoperative outcome, either resulting in a consolidation of the bone, or fragment dislocation.

1.2.4 Postoperative rehabilitation

Assisted exercises in physiotherapy are usually performed shortly after surgery, where the arm is passively supported by a physiotherapist (Table 2). Active exercises by moving the total arm weight over the whole range of motion are initiated 4-6 weeks postoperatively. On the one hand, multidirectional pendulum exercises are performed; on the other hand, single plane movements are often described in Figure 9. It is postulated that an aggressive physiotherapeutic intervention already starting 3-4 weeks postoperatively reveals a better functional outcome than conventional treatment [47]. Risk of fracture dislocation by applying such a rehabilitation protocol is presumably increased, since the biological ingrowth process is completed after 8-12 weeks. Consequently, the fixation technique contributes to the primary stability in that initial phase of recovery, and is even more important.

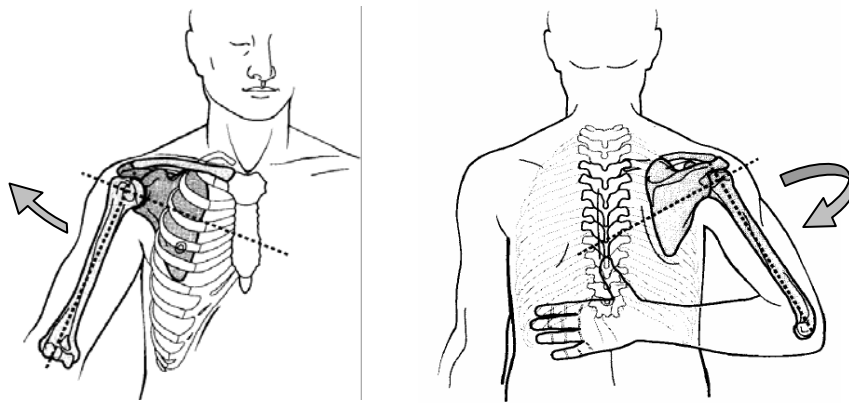


Figure 9: Movements in postoperative rehabilitation such as abduction (left) and rotation of the upper arm around the longitudinal humeral axis (right).

<i>Reference</i>	<i>Kinematics and Range of Motion</i>	<i>Remarks</i>
<i>Naranja [52]</i>	<i>Forward flexion 120°</i>	<i>passively assisted</i>
<i>Ambacher [37]</i>	<i>abduction 90°</i>	<i>partially active</i>
<i>Christoforakis [41]</i>	<i>passive flexion 140°, passive ext. rotation 30°</i>	<i>no active movement before 6 weeks</i>
<i>Brems [53]</i>	<i>elevation 140°, ext. rotation 40°</i>	<i>4 times/day, 5min/session</i>
<i>Ballmer [54]</i>	<i>Int. Rot. until abdomen, Ext. rot. 5° less than Int. Rot.</i>	-
<i>Krause [55]</i>	<i>Int. rotation until abdomen, external 15° less than healthy arm</i>	-

Table 2: Postoperative rehabilitation protocols with corresponding range of motion for the performed movement tasks.

1.2.4.1 Reasons for failed reconstructions after surgery

Until now, the initial failure mechanisms of a reconstructed proximal humerus can not be explained. On the one hand, it is assumed that tuberosity fragment displacement leads to missing vascular supply, consequently leading to resorption. Pilliar et al. postulated that a stable immediate (primary) fixation is a requirement for a successful osseous integration [56]. If that boundary condition is not fulfilled, oversized fracture gaps negatively influence the vascular system reorganisation [57, 58]. On the other hand, the absence of stresses and inadequate stimuli in the bone, in particular in the fragmented isolated bone, may lead as well to resorption of bone stock. The optimum interfragmentary motion and induced stresses are therefore in a specific range and represent a compromise to fulfil the requirements for healing.

1.3 Aim of the project

The aim of the project is the optimisation of existing fixation techniques for a fractured proximal humerus with respect to an improved primary stability.

To optimise the fore-mentioned fixation concepts, several requirements have to be fulfilled: First of all, state of the art fixation techniques have to be reviewed. Based on this analysis, improved, novel promising techniques will be determined. To assess the stability of the different techniques, a physiological testing procedure which reflects typical in-vivo movements and loading has to be evaluated and developed. The overall aim can be described more specifically by the following sub goals:

A) Literature review

A literature review is done with regard to two main topics: Existing fixation techniques are collected and analysed. Furthermore, a literature review of existing biomechanical testing strategies at the shoulder is performed to reveal the state of the art.

B) Performance of clinically established fixation techniques

An experimental testing method according to physiological loads is developed for a biomechanical analysis of clinically established fixation techniques.

C) Development and testing of a novel fixation technique

A novel fixation technique will be developed based on the requirements which result from the failure analysis of clinically established techniques.

D) Finite Element Analysis

Finite Element Analysis (FEA) is used to investigate implant-to-bone interactions, in particular maximum stresses applied to the bone and resulting displacements for the different fixation techniques.

2 Literature analysis

2.1 Detailed analysis of existing fixation techniques

A fundamental analysis of existing fixation techniques to treat four-part fractures demonstrates the state of the art of that surgical procedure. Such an overview provides the necessary information for the optimisation of fixation techniques. In this study, we have reviewed popular suture and wire orientation patterns for tuberosity fixation in the case of hemiarthroplasty for proximal humerus fractures.

2.1.1 Introduction

2.1.1.1 Clinical background

Due to limitations in osteosynthesis plating, hemiarthroplasty represents an established treatment method for displaced three- or four-part fractures of the proximal humerus. Pain relief can often be achieved by this surgical intervention, but the functional result is less predictable [59, 60]. Consequently, clinical outcome ranges from poor-satisfactory to good-excellent as shown in Table 1. Complications such as non-union or resorption of the tuberosity fragments occur in 30-70 % of all cases [32, 34, 44, 61-64]. Reasons for this poor outcome may be secondary displacement which negatively affects the muscular balance at the rotator cuff and predisposes the patient to worse outcome [40, 42, 43, 48, 65]. Tuberosity malposition also correlates with muscle atrophy and subsequent fatty infiltration into the rotator cuff [66]. Different patient specific factors such as health status or rehabilitation after surgery influence the result: Injury-related variables are predetermined such as the severity of fracture dislocation, neurological deficits or the type of fracture [67]. Although the optimisation of the implant design is often discussed, a significant correlation between a specific prosthesis type and patient satisfaction was not observed by Loew et al [45]. Nevertheless, a significantly better Constant Score for one specific fragment fixation technique (using an additional cable to the suture fixation) compared to the established technique of using only sutures was seen [47]. Others report that the fixation technique seems to be crucial for tuberosity union and apparently represents one of the most important factors in a good outcome [12, 31, 68, 69]. Furthermore, the grade of tuberosity dislocation directly correlates with clinical outcome, and the prevention of fragment dislocation by the fixation technique presumably has a direct impact on the clinical result [33].

2.1.1.2 History

The first operation of a shoulder replacement combined with reattachment of the tendons was performed 1893 by Dr. Péan [70]. Horse hairs were used to reattach the muscles to the predrilled holes in the prosthesis shaft. Themistocles Gluck published different prosthesis fixation methods at the bone [71]. However, he did not further analyse the fixation of the single fragments in particular. In the modern era, techniques for proximal humeral fragment fixation were established by Neer et al., focussing on the placement of the cables and sutures at the proximal humerus [24]. In present times, specific fixation techniques correspond to the appropriate prosthesis designs and are therefore primarily presented in detail in the operation manuals of the implant industry.

2.1.1.3 Objective

Summarising existing fixation techniques may help to identify advantageous techniques before complex biomechanical testing is carried out. By comparing the most frequently used techniques, promising features and innovative procedures may be combined and optimised. Existing publications focus primarily on one specific technique and therefore it is of interest to have a direct comparison, classifying the different strategies in distinct groups. The aim of present meta-analysis is therefore the review of existing fixation techniques for fracture treatment in order to obtain a broad overview.

2.1.1.4 Method

A review of different fixation techniques in the literature (Medline & Cochrane databases) was carried out for four-part proximal humerus fractures. Suture and wire placement was transferred qualitatively into a standardised image which shows the restored rotator cuff in an anterolateral view (Figure 10). Anatomical landmarks at the proximal humerus, such as the bicipital groove, the surgical neck fracture line, tendon insertions and the rotator cuff interval, were used as fixed points to localise the suture configurations. For simplicity, all left shoulders have been inverted to standardize all techniques to the right shoulder. In our opinion, this procedure represents a reliable method, as the mentioned anterolateral view is frequently used to present the fixation techniques for four-part fractures. Data recorded include:

- the number of strands connecting the humeral shaft to the greater tuberosity;
- the number of strands connecting the humeral shaft to the lesser tuberosity;
- the number of strands connecting the greater and lesser tuberosity to each other;

- the number of attachment points of the prosthesis to the greater tuberosity;
- the number of attachment points of the prosthesis to the lesser tuberosity;
- the design of the used middle part of the prosthesis including the number of holes and fins.

2.1.1.5 Conventions

Several conventions were defined that correspond to the frequently used terminology (Figure 10): The orientation of strands parallel to the shaft axis was defined as a longitudinal placement; leading from proximal-to-distal. Circular strands are perpendicular to the longitudinal axis of the humerus, placed circumferentially around the cuff in a horizontal plane. Transverse sutures represented a placement through the prosthesis. Diagonal sutures are guided from either the GT-LT fragment to the anterior-posterior diaphysis of the shaft.

Generally, dotted lines were used to illustrate transosseous sutures. Blue lines represent a tuberosity connection to the shaft, and green lines represent interfragmentary connections between the LT and the GT. Cerclages around the GT and LT guided through the prosthesis are magenta, and metallic braided cables are black. Sutures interconnecting all three fragments like GT, LT and shaft are red.

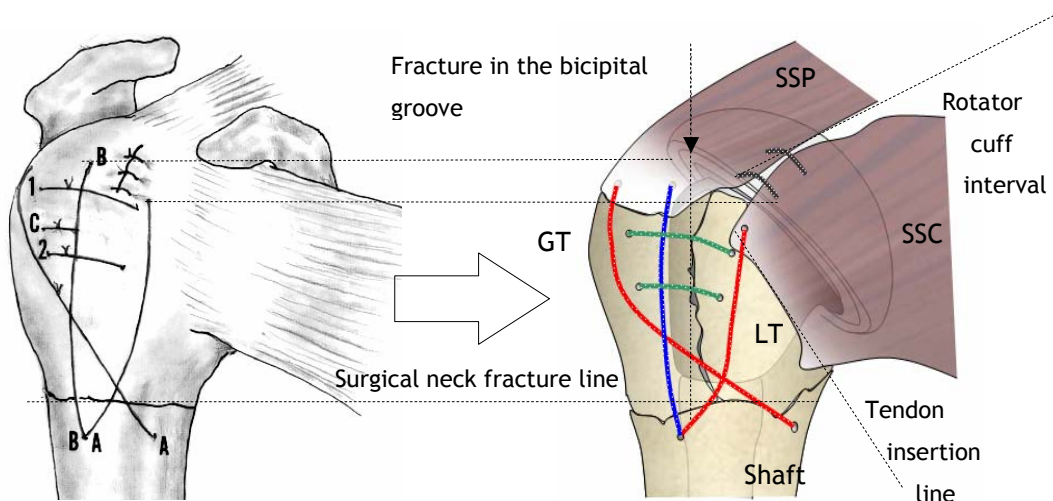


Figure 10: Transfer of one fixation technique based on the illustration in literature (left, Dines et al.) into a schematic representation (right) by using anatomical landmarks.

2.1.2 Results of the literature review

Elementary configurations of suture placement are often applied to reconstruct the fractured proximal humerus: The figure-of-eight tension band technique represents a standardised application that is often used to fix the proximal fragments to the humeral shaft: A first suture loop is attached in a fragment and a second loop in the adjacent fragment to compress both fragments together. This technique is documented in the AO-recommendations for internal fixation but can also be applied in case of hemiarthroplasty using braided polyester sutures. Several investigations have applied the figure-of-eight technique by interconnecting all three fragments such as the shaft, the GT and the LT, seen in [62-64]. Dines et al. recommended attachment of the tuberosities to the shaft, to each other, and to the fin of the prosthesis (Figure 11, left) [12]. First the GT is secured to the shaft and to the fin of the prosthesis using transverse sutures. Then the LT is fixed to the shaft and to the GT. With the tuberosities now secured to the shaft, a figure-of-eight tension band is placed through the rotator cuff tendons near their insertion into the tuberosities, and connected to the proximal shaft.

A longitudinal suture is used for an additional fixation of the GT to the shaft: The posterior longitudinal suture enters in the superior portion of the supraspinatus tendon and is connected to the shaft. Hence, the GT is secured to the shaft with a separate suture in addition to the figure-of-eight tension band.

Similar to the technique of Dines et al., the technique of Frankle et al. is based on using the same prosthesis design [12, 72]. Both tuberosity fragments are fixed to the middle part of the prosthesis. A circumferential oriented suture secures the tuberosities together: One end of this suture captures the GT by placing it through the posterior rotator cuff, whereas the opposite end captures the LT. The circumferential suture is tied first to fix the tuberosities together, similar to the technique mentioned previously. Drill holes are placed distal to the surgical neck for reattachment of the tuberosities to the shaft in a figure-of-eight technique. These longitudinal sutures are then finally tied to secure the tuberosities to the shaft.

The Aequalis fracture prosthesis is used in another current technique, described by Boileau et al. [31]. Two sutures are placed in the ISP tendon and two in the TM tendon. Reconstruction starts with the first two of totally four circular sutures positioned at the beginning. These are passed around the prosthetic neck to fix the GT. Then the LT is fixed by using the other two circular sutures. The two lower sutures are subsequently fixed to the tendon insertion to pull the rotator cuff distally and restore the resting tension on the rotator cuff tendons. Translational and rotational tests have been performed to assess strength of fixation. In all

cases of their series, large-diameter (no. 5 or 7) non-absorbable sutures were used to secure both tuberosities. Circular and longitudinal sutures secure fragment stability with respect to a multidirectional muscular loading.

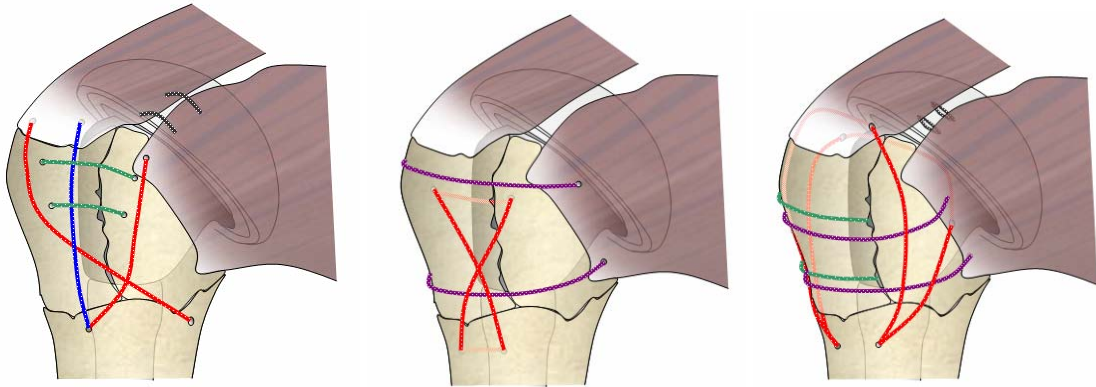


Figure 11: Cerclage suture (red) was used to reapproximate the three fragments of the GT, the LT and the proximal humeral shaft together. Dines (left), Mighell (middle) and Boileau (right).

Compared to the previously discussed techniques, both tuberosities may be fixed individually to the shaft by separate figure-of-eight tension bands [73]. In the description by Voigt and Lill (Figure 12, right), the Univers prosthesis is used which has lateral fins. Two holes are drilled in the posterior and anterior humeral shaft and are used for two sutures to reduce each of the tuberosities. Three circular sutures are initially positioned around the greater tuberosity and the prosthetic neck. The lesser tuberosity is held by two sutures passed through the anterior-medial holes of the prosthesis. The circular sutures are tied first to pull down both tuberosities into anatomical position realising a cross-over of the two longitudinal sutures.

A technique similar to that of Voigt and Lill has been performed by Gerber et al. [74] (Figure 12, left). In this technique using the Anatomical fracture prosthesis (Zimmer Ltd), sutures are placed in the tuberosities to bring the distal end of the greater and lesser tuberosities down to the shaft. In contrast to the prosthesis used by Voigt and Lill, the Zimmer fracture prosthesis does not have fins, which affords more room proximally for tuberosity positioning. First, the circular sutures connecting the tuberosity fragments together are tied, then they are tightened to the shaft. A suture is placed in a GT hole and a second one in the LT suture hole. A cerclage suture is passed through the SSC tendon, around the GT and the LT and ends up at the ISP and TM tendon insertion. A suture in the humeral shaft, medial to the bicipital groove, pulls the distal end of the lesser tuberosity back down to the shaft. Additional sutures in the

middle of the prosthesis are used for a further reduction and fragment compression to the middle part of the prosthesis.

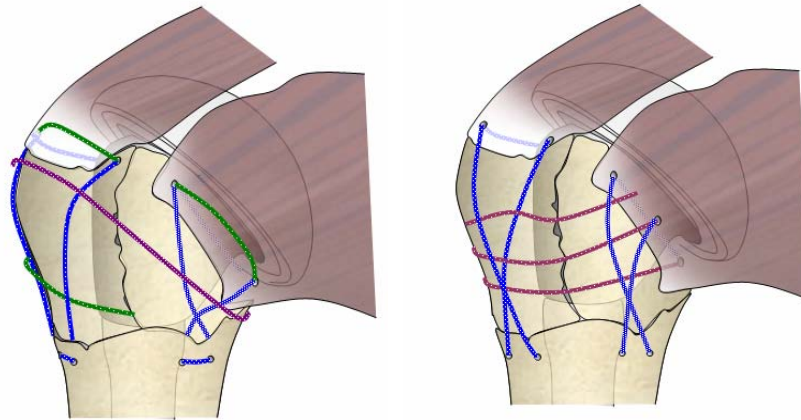


Figure 12: Connecting single fragments to the shaft by a figure-of-eight, Gerber (left) and Voigt (right).

Reuther et al. used the Affinis fracture prosthesis (Mathys Ltd) [30]. To achieve a better tuberosity fixation, the central part of the prosthesis is equipped with two holes to insert non-absorbable sutures or cables (Figure 13, left). The central part does not have any fins, and is covered by rough calcium phosphate coating (Bionit). After pulling through the sutures, the tuberosities are height-adjusted and fixed with retention stitches to the outer edge of the central part and over one another. Both tuberosities are fixed to the stem by circumferential wiring. Finally, a circular compression with a cerclage cable (grey) is placed through the cross holes of the central part of the prosthesis. In the technique of Krause et al., fixation consists only of metallic cables [55]. This method is applied with the Epoca prosthetic system (Synthes). This prosthesis has a rectangular shaft design including three anteroposterior holes, but no fins. Four metallic wires connect the fragments to the prosthesis and two transverse wires are used to attach the GT and the LT to the prosthesis. Two diagonal wires attach both tuberosities to the shaft. The titanium cables are pulled by a tensioner and closed by a clamp mechanism (Figure 13, right).

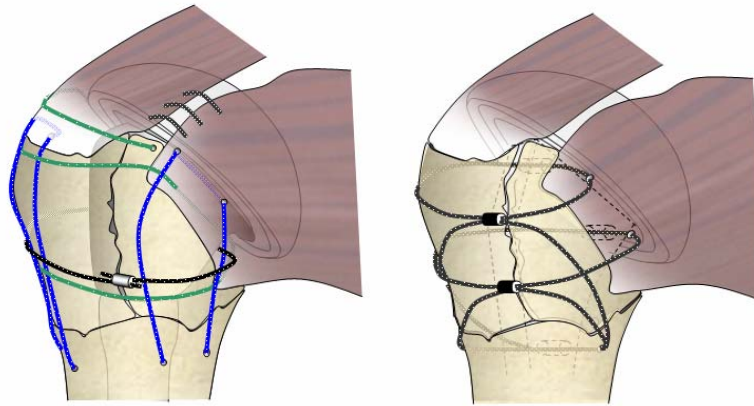
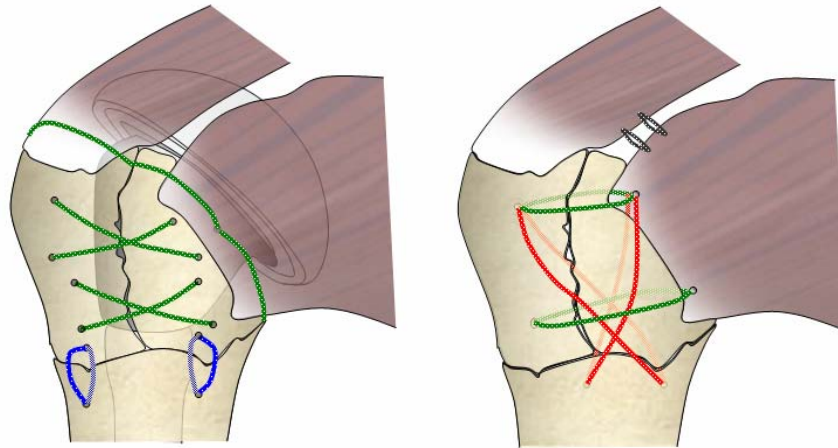


Figure 13: Reuther et al. (left) uses metallic cables and sutures whereas Krause et al. only use the cable technique (right).

A tension-band technique using 5-0 braided polyester sutures has been applied by De Wilde et al. [75]. Epoca prosthesis was used (Synthes GmbH, Switzerland). The tuberosities are fixed to the rim of the prosthetic head via sutures passed through the tendon-to-bone junction. In addition, the tuberosities are sutured to one another and to the humeral diaphysis. Circular placed transosseous sutures connect both tuberosities. The tuberosities are fixed to the diaphysis with longitudinal single-loop sutures at each tuberosity (Figure 14, left).

The refixation technique has also been applied without the implantation of a prosthesis, shown by Dimakopoulos et al. [76]. Although these techniques have to meet different requirements compared to the hemiarthroplasty, these configurations may show some advantages: The study showed a treatment for a four-part valgus-impacted fracture where the tuberosities are secured to each other and to the medial and lateral sides of the diaphysis in a cruciate fashion (Figure 14, right). Another two pairs of sutures are inserted laterally and medially through drill holes in the diaphysis. These sutures are guided into the opposite tuberosity, near the musculotendinous junction, and onto the adjacent area of the articular segment. Each suture is tied individually and then to one another in a cruciate arrangement.



**Figure 14: Secure fixation of the LT and GT by horizontally oriented sutures.
De Wilde et al. (left) and Dimakopoulos (right, without prosthesis)**

Three different fixation techniques were described by Abu Rajab et al. [77]. The monoblock-design Neer prosthesis was used, which contains two lateral fins and four suture-wire holes. In the first technique, both tuberosities were attached to the shaft and to each other, each with separate sutures. In the second technique, an additional cerclage is placed through the medial fin. Interestingly, the described novel concepts of tuberosity fixation were biomechanically tested. The results revealed that an additional cerclage does not enhance the stability with respect to tuberosity migration. The stability of one of the three techniques was significantly reduced, if the tuberosities were not fixed to one another.

Metallic wires were also used for the figure-of-eight tension band technique by Wijnman et al. [78]. The anterior wire fixes the lesser tuberosity and the attached subscapularis muscle, and the superior one passes through the supraspinatus tendon and around the greater tuberosity back to the shaft. Whereas Wijnman et al. placed the cerclage wires as close as possible to the tendon insertions, others prefer a transosseous placement of the cable through the tuberosities. [79, 80] [81], [82]. Wires presumably have a negative effect on the periosteal vascularisation and on the tendon insertions, particularly in a vascular watershed area such as the rotator cuff. Transosseous passage may decrease that vascular compromise.

A summary of published fixation techniques is presented in Table 3.

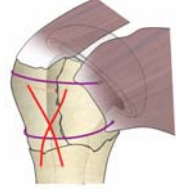

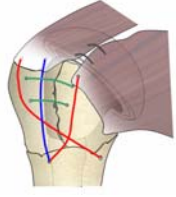
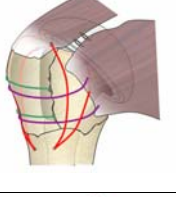

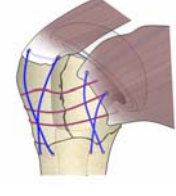

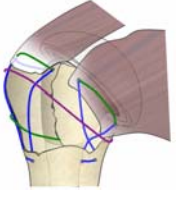

Reference	Graphics	Prosthesis	Fixation Technique					
			# of slings GT-shaft	# of slings LT-shaft	# of slings LT-GT	# of slings LT-GT Shaft		
Mighell 2005 [69]			2 fins	1 hole, 4 holes each in the fin.	1	1	2	0
			Neer III, Smith&Nephew Two internally placed augmentation sutures Vertical cross-stitches					
Dines 2002 Abrutyn 2003 [12],		-	-	-	2	1	2	0
			No remarks of the implant type					
Boileau 2002 [31]			No fins	One big hole	0	0	2	2
			Aequalis, Tornier					
Voigt 2007 [73]			2 fins	4 holes in each fin	1	1	3	0
			Two figures-of-eight tuberosities fixed at the head support. Univers, Arthrex					
Gerber OP- Manual [74]			No fins	2 holes	1	1	2	0
			Anatomical Fracture, Zimmer					
			Cable system for the entire fixation Epoca, Synthes					

Table 3, Part 1: Schematic overview of performed fixation techniques and corresponding implants.



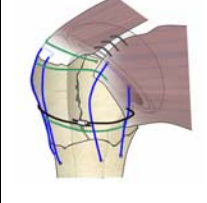

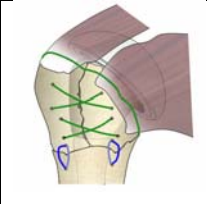

Krause 2007 [55]			No fins 2 holes	0	0	1	2
Reuther 2008 [30]			No fins 2 holes	1	1	2	0
				<i>Cable system around the GT-LT prosthesis Affinis Fracture, Mathys Medical</i>			
De Wilde 2006 [75]			No fins 3 holes	1	1	2	1
				<i>Epoca, Synthes</i>			

Table 3, Part 2: Schematic overview of performed fixation techniques and corresponding implants.

Recent developments have used different middle parts of the prosthesis compared to the standardised designs. Schittko et al. propose a middle part with multiple holes for an unconstrained placement of the tuberosities using the Ortra prosthesis [83]. A further method of tuberosity reconstruction was presented by Sosna et al. [84]. ProSpon and MMS prosthesis combine proximal humeral plating and hemiarthroplasty: A screw inserted into a proximal plate (fixed to the prosthesis middle part), through the tuberosities into the prosthesis middle shaft provides primary stability of the fracture.

2.1.3 Discussion and Conclusions

The literature provides a great variety of fixation techniques for the repair of four-part proximal humeral fractures. Some similarities can be found despite the great number of different techniques. The procedure of fixing the LT and GT fragments together, followed by reduction of the GT-LT construct to the humeral shaft is a standard part in all techniques. Further similarities in suture management can be found: Dines and Frankle/Mighell use a figure-of-eight tension band over the entire surface of the rotator cuff to connect all three fragments such as the humeral shaft, the GT and the LT. Unlike Voigt and Gerber et al. who use the figure-of-eight tension band to connect only single fragments without involving all three fragments. Voigt, Boileau and Reuther place several sutures ranging from the SSC to the

ISP tendon insertion and apply a tension-band technique between the LT and the GT in a horizontal orientation. Reuther and De Wilde et al. use metallic cables whereas Reuther places the cables orthogonally to the longitudinal axis of the humeral shaft. Hertel et al. use a diagonal placement to connect the shaft and both tuberosities.

Optimisation of suture orientation should be performed with respect to the typical in vivo loading directions. It is generally assumed that forces of the SSP and the ISP pull the GT proximally; the LT is pulled medially by the SSC, while the Pectoralis Major (PM) adducts the shaft medially. Nevertheless, since the exact circumstances that lead to secondary displacement of the fragment are not well understood, the reconstruction has to be configured with regard to a multidirectional loading. Security against proximal fragment migration seems to be crucial for a successful outcome, as a good clinical result directly correlates with anatomical tuberosity-to-shaft healing. Enhancing the stiffness of the fixation in the proximal-to-distal direction may reduce the migration of the GT and increase the healing rate. Existing circular cable tensioning around the proximal humerus is performed to secure towards a medial migration of the fragments. A stiff and stable cable system preventing a fragment migration in proximal direction would be of interest. This is difficult to achieve because no anchor points for cables can be installed at the bone surface.

Over reducing the fragments down to the shaft may lead to a tuberosity overlapping with the shaft. This telescoping effect occurs when the fragment in the form of a partial hollow cylinder glides into the shaft while tensioning the suture from proximal-to-distal. This can be prevented by “self-locking” stitches where an alignment of the fragments relative to the shaft prevents any further displacement beyond the fragment border (Figure 15). Recent designs use a circular suture anchoring around the shaft, as presented in Figure 16.

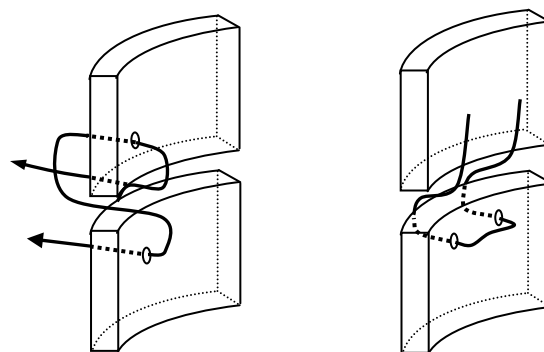


Figure 15: Using a self-locking stitch aligns the superior fragment to the lower one (left) in comparison to the commonly applied stitches (right).

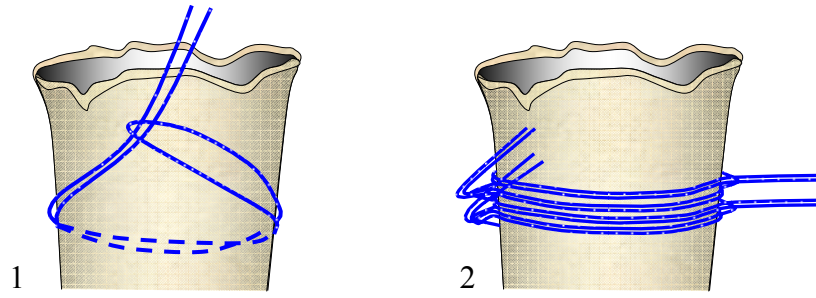


Figure 16: Anchoring multiple suture loops circumferentially placed around the shaft [85].

2.2 Existing experimental shoulder testing devices

This chapter summarises existing experimental shoulder testing devices in literature. In order to perform an optimisation of fixation techniques, the application of a reproducible biomechanical testing is essential. If a test does match physiologic boundary conditions, the results and conclusions are presumably adaptable to in-vivo situations. On the one hand, the own measurements can be compared to existing investigations. On the other hand, such a database supports the realisation of a novel testing device, because technical details are well documented.

2.2.1 Introduction

2.2.1.1 Biomechanical characteristics of the shoulder

The shoulder joint, with its large range of motion (ROM) and high number of acting muscles, represents one of the most complex joints in the human body. Developing an experimental shoulder model reproducing kinematic and kinetic conditions of the glenohumeral joint is a challenging task. Generally, the human shoulder is characterised by three biomechanical attributes distinctive from other joints in the skeletal system: An unconstrained geometry of the glenohumeral (GH) joint with a small articulating surface enabling a high range of motion. It is stabilised by a capsular system and the rotator cuff muscles to provide the so-called “concavity compression”. The “wrapping mechanism” of the tendons around the spherical proximal humerus allows extensive rotations in spatial direction. The humeral and the scapular kinematics during arm abduction are directly linked by a specific ratio which is expressed by the “shoulder rhythm”. The consideration of these specific boundary conditions is necessary to build a physiological shoulder model. Due to that biomechanical complexity, up till now no experimental testing method has been considered as an approved standardised model.

2.2.1.2 History of biomechanical shoulder models

Throughout history, a variety of experimental shoulder models have been presented in literature: The first efforts to build a mechanical shoulder model were made by Fick and Weber in 1877, using hemp threads to apply muscular tensional forces. By means of the tendon excursion method, the change in length of individual muscles was determined in respect to the corresponding position. Additionally, moment arms and potential torque were calculated. In 1899, Mollier et al. built a model prototype allowing a scapulothoracal

movement. The resulting change in position by variation of the muscular forces was analysed for different moment arms. Muscular forces were resolved in 1913 in Shiino's model, which correlated change in muscular length with the applied loads. An entire upper arm model, in which muscles were replaced with wires, was designed by Hvorslev in 1927. The thorax, spine and pelvis were attached to a rib cage frame, allowing for free scapular movement. The necessary torque to maintain a specific arm position was evaluated. Further to these muscular tension measurements, the contribution of single muscles to specific arm movements became a popular field of research with the advent of the new electromyography technology [86].

In the last decades, shoulder models were not only used to explain basic biomechanics and general functionality. Specific questions on instability or luxation were also addressed to explain such functional abnormalities by means of shoulder models. Surgical interventions like tendon transfers or the implantation of orthopaedic implants were evaluated before clinical in-vivo trials. Prosthesis design optimisation was tested such as effects of humeral prosthesis shaft placement on the joints' range of motion [87], or articulating head component sizes on GH-translation effects [88]. In case of shoulder fracture, the stability of fragment fixation is of great interest to avoid secondary dislocation. The primary stability of fragment fixation is evident for a good clinical outcome and was analysed by different experimental tests [75, 77, 79, 89, 90]. Although the experiment is important element to analyse the implants, results gained by computer simulation become more and more realistic [91].

2.2.1.3 Motivation and tasks studied

Existing experimental shoulder models an important knowledge repository of applied techniques and chosen boundary conditions. Due to a high variation of load scenarios and kinematic protocols, it is difficult to directly compare the results between the different studies. An overview of the broad range of the existing testing strategies is, therefore, important to get an insight into the limitations and possibilities. In particular, allocating related types of shoulder models into specific groups allows a classification of the testing type. Favourable installations, which implement kinetic and kinematic boundary conditions according to physiology, are detected; advantageous methods may be combined.

2.2.2 Material & Methods

A computer-aided search was done to retrieve the literature in PubMed (MEDLINE), ScienceDirect (EMBASE) and COCHRANE database. The search included experimental in-vitro shoulder models applying muscular loading to the proximal humerus. In particular, the analysis included a combination of the search terms: “shoulder” and “experimental” and “model or testing”. The references of the literature found were additionally analysed for leads of further interest. A graphical description of the searching procedure to include and exclude distinct studies is shown in Figure 17.

The collected references were categorised with respect to specific biomechanical boundary conditions and allocated to specific groups. The type of muscular loading was analysed in detail as well as the mechanism of humeral stabilisation during movement. Individual muscular loading was summarised in respect to the individually acting muscles. Single muscle forces of supraspinatus (SSP), infraspinatus (ISP), subscapularis (SSC) were summarised. Further muscles like teres minor (TMin), teres major (TMaj), latissimus dorsi (LD), anterior deltoideus (a.DELT), middle deltoideus (m.DELT), posterior deltoideus (p.DELT) and pectoralis major (PM) were additionally analysed regarding their load magnitudes. The corresponding kinematic boundary conditions were summarised in a table for a direct comparison (Table 4). Studies were excluded, if the following criteria were matched:

- Studies performing the tendon excursion method (similar to the “tendon travel method”, chapter 3.1.4.3) to analyse the muscular moment arms. By measuring the increment of the joint angle and corresponding tendon length, the moment arm is determined; the force-to-angle relation isn't in the focus [92-98].
- If the GH-contact force was introduced by a direct compressive load onto the proximal humeral head without simulating any muscular tension, the study was then not included.

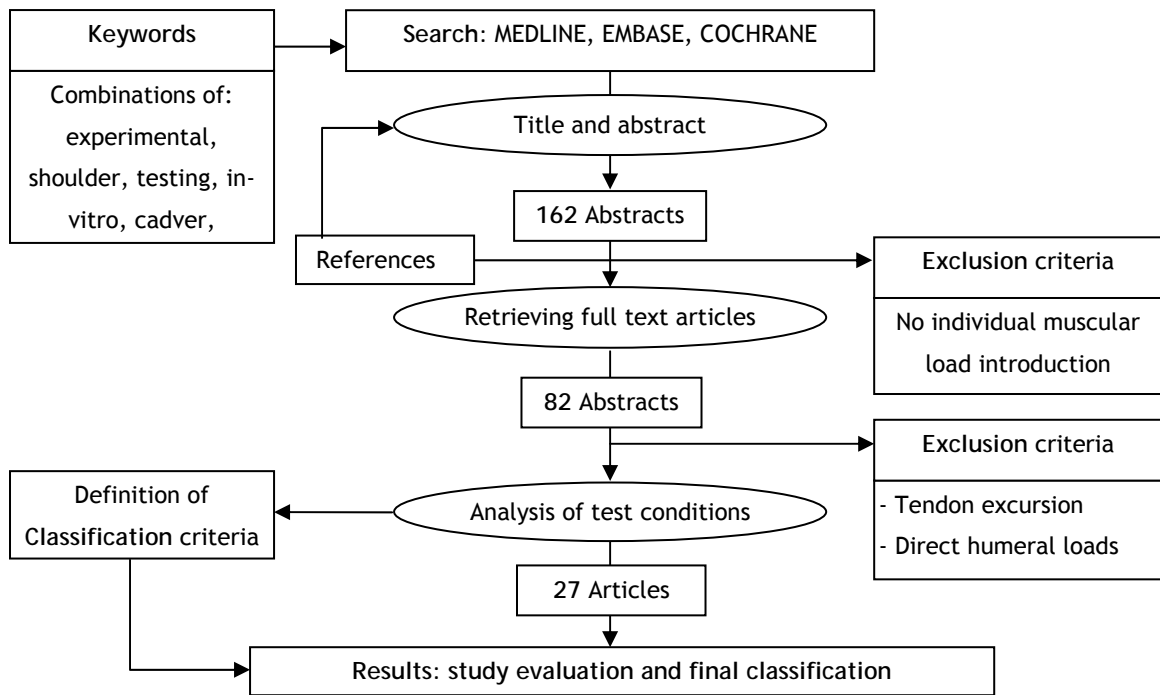


Figure 17: Search and evaluation procedure following a systematic process.

2.2.3 Results of the literature review

All references were allocated to one specific group which characterised the test strategy type. Similar to existing definitions by Kedgley et al., differentiation between active and passive muscle force recruitment was done [99]. An active loading scenario was used if an increasing, progressive force profile resulted in a change of the humeral position. Passive loads were applied by static weights where individual muscular loading for different humerus positions remained constant.

A further parameter for a more detailed description represented the mechanism of humeral guidance in the testing device. Such a bearing mechanism which constrains the humeral bone around the rotational axis, reduces the degree of freedom. This additional parameter of how the testing device restricted the motion of the humerus refined the classification and resulted in sub-groups. By combining the principles of muscular loading (active vs. passive) and the type of humeral guidance (unconstrained vs. constrained), all experimental shoulder tests could be referred to one of the four groups (Figure 18).

In group A, the humeral 3-D position of free-hanging active models is directly dependent on the individual muscular loading. The individual muscular force, therefore, represents a

function of the abduction angle. These models are mostly used in the investigation of the basic biomechanical functions of a healthy shoulder joint and the rotator cuff load distribution. In group B, passive loading by static weights stabilises the joint, keeping the humerus in a constrained position. In group C, internal and external rotation around a fixed longitudinal shaft axis of the humerus is realized by applying pure moments directly on the bone, which in turn effects passive tension. In group D, muscular loading is applied for a fixed humeral position.

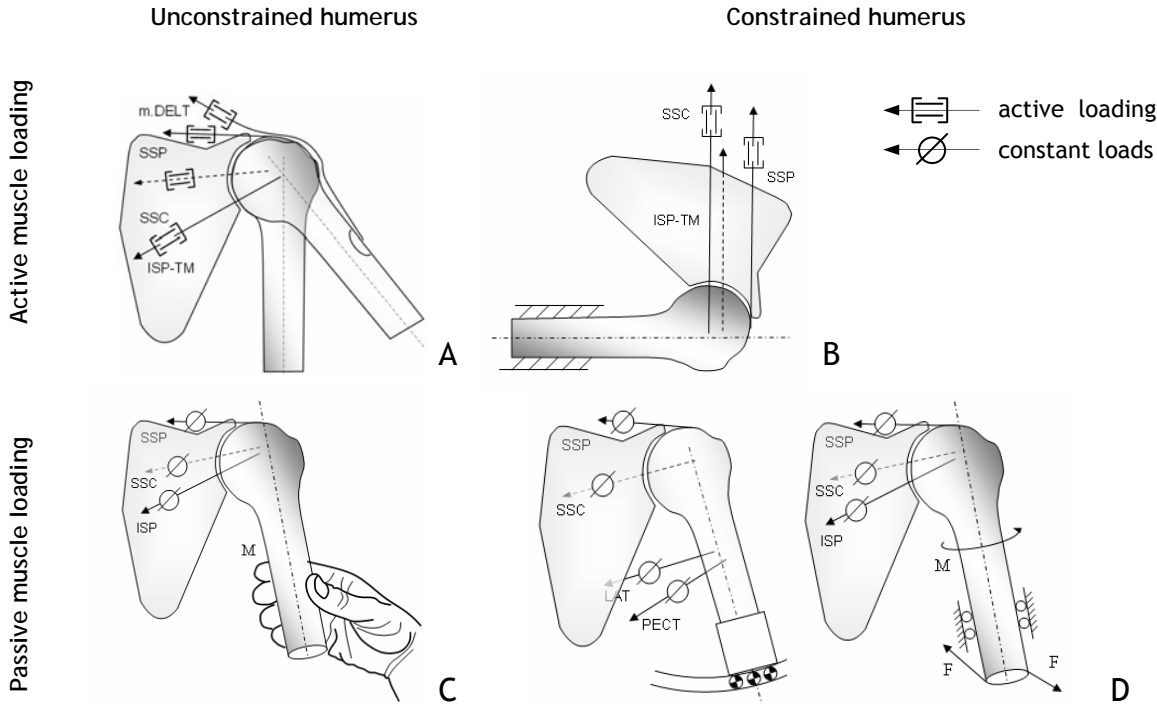
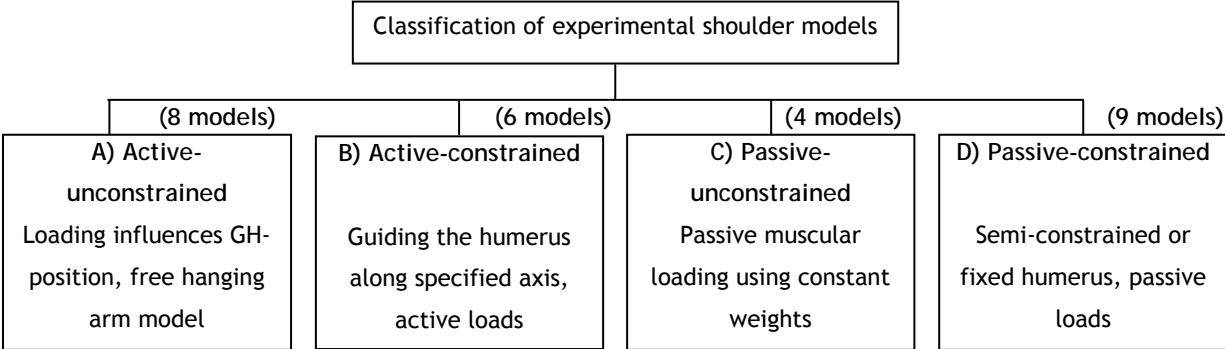
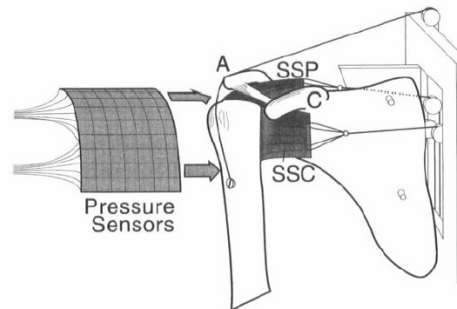


Figure 18: Classification of the analysed studies in respect of the muscle recruitment. The scapula is assumed to be fixed.

A) Active muscular loading

The first group with similar testing conditions can be characterised by activation of individual muscles which directly influence the arm kinematics. The GH-joint position is directly related to the introduced muscle force. Thus, increasing muscle forces result in an abducted humeral position. The muscle force represents the reference variable, by which the abduction angle is measured as output. In the following, the characteristic parameters of the single testing setups within that group are addressed in detail.

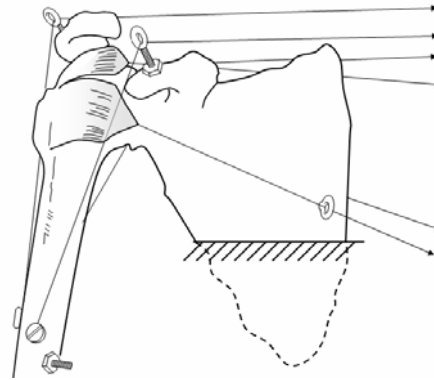
A free hanging shoulder model, including one deltoid segment, was developed by Wuelker et al. to determine the rotator cuff muscle force distribution [100]. The effect of rotator cuff forces on GH-joint stability was assessed by performing scapular plane abduction up to 90° of elevation. The forces were linearly increased as an input parameter, until a distinct abduction angle was achieved. The magnitude of muscular forces with respect to the abduction angle was resolved based on the ratio of the muscular cross-sectional area [101]. A maximum flexion/extension angle of 8.5° was detected out of the scapular plane during abduction with this free hanging model (Figure 19). Mean deltoid force reached 241 N, at a nominal elevation angle of 90°, and was, therefore, consistent with other measured data. Klages et al. determined the muscle efficiency with respect to the position of the prosthesis head by using the same shoulder model [102]. Muscle activation was chosen according to Veeger et al. [103].



**Figure 19: Representative drawing with four active muscles and a middle DELT segment [100].
(With permission of The Journal of Shoulder Elbow Surgery. Elsevier)**

To determine the GH-contact area through a large range of abduction motion, a cadaver test setup was realised by Soslowsky et al. [104]. The deltoideus (DELT) was segmented into posterior, anterior and middle parts, with the scapular plane positioned with a 20° anterior tilt (Figure 20). Loads were derived from Perry et al., based on clinical, anatomical and EMG data [105]. Arm elevation was performed until a GH-joint force of 180 N was reached. An arm weight of 3.2 kg was chosen, representing 5 % of whole body weight. Humeral head

translation during abduction was investigated in a similar testing setup, applying identical loading conditions [106]. Thoracohumeral (TH) scapular plane abduction was performed between 0° - 180° for neutral rotation, and subsequently for 20° internal rotation. A similar model was also used by Karduna et al. [107] to measure the influence of articular geometry on the GH-joint forces.



**Figure 20: Model considering three segments of the deltoideus [104] .
(Adapted with permission of the author, Prof. Soslowsky)**

Kedgley et al. evaluated resultant motion pathways for different muscle loading protocols, simulating subscapularis, supraspinatus, infraspinatus/teres minor and the segmented deltoideus as shown by Kedgley et al. [99]. The simulator is built similarly to the model of Soslowsky et al., comprising the same muscles, but varying muscle force ratios, which were selected on the basis of empirical and clinically derived force distribution. Muscle forces were defined from equal load application to every single muscle [108, 109], loads with respect to muscular cross-sections [110-113], and from the product of PCSA (Physiological Cross Sectional Area) and EMG-values. DELT and SSP were aligned in the scapular plane. The internal/external rotation remained unconstrained in abduction.

Six servo-actuated hydraulic cylinders were used to apply muscle forces through tendon clamp-cable-pulley systems in the model of Debsky et al. [109]. The four tendons were loaded equally by a linear force increase until a specified position was achieved. According to Apreleva et al. [108], a maximum arm abduction angle of 90° resulted in a 117 N tensional loading in both SSP and DELT. Debsky's study used the so-called "DSTA simulator", a device to test entire cadaveric arms, which is also mentioned in other studies from McMahon et al. [114] and Konrad et al. [115].

Bono et al. [89] used a defined muscular force distribution. The rotator cuff loads were serially adjusted to reflect 16 % (SSP), 28 % (ISP-TM), and 38 % (SSC) of the measured (100 %) DELT muscle force respectively [116]. The active DELT was applied by a servo hydraulic

actuator. The test-setup was adapted from previously validated systems [100, 104, 107]. A static external weight of 22 N was applied 4 cm distally to the insertion of the DELT to reproduce an external arm weight.

Sharkey et al. created a set-up to simulate both glenohumeral and scapulothoracic rotation within a single model (Figure 21). The contribution of the rotator cuff muscles for abduction, as opposed to the force of the deltoideus muscles was analysed [112], [117]. Nylon webbing, transmitting the forces to a cable-to-pulley arrangement was applied to simulate the deltoid load transmission to the humerus. Contraction of the DELT was simulated by a computer-controlled linear stepper motor. Scapulothoracic motion was executed with a rotational stepper motor. A relationship of 3:2 between the glenohumeral and scapulothoracic abduction angle was maintained throughout the experiment. Four configurations of muscle activity were simulated by independently controlling SSP, ISP-TM and SSC. Unlike all previously described models, only the DELT was active, while other structures were stabilising the joint.

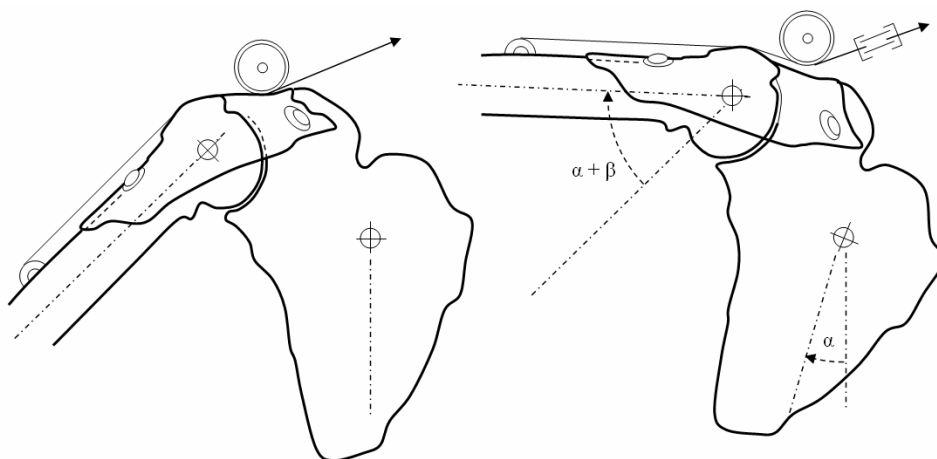


Figure 21: The deltoideus is simulated by nylon webbing around the rotator cuff.
 (Adapted and modified with permission of the author, Prof. Sharkey)

B) Active forces applied to a constrained or fixed humerus

This group covers an increasing muscular loading profile to a constrained or even fixed humerus, which is often seen in load-to-failure testing. The humerus is fixed at a specific abduction angle in all tests, ranging from 20° - 30°. Abu Rajab et al. performed a testing of the tuberosity displacement at the fractured proximal humerus during muscular loading by SSC and ISP [77]. The movement of the tuberosities relative to the axis of the humeral shaft was investigated. Displacement at maximum load was detected for an abduction angle of 20°, whereas symmetric loading was applied to each tuberosity to prevent torsion of the humerus. A similar study by De Wilde et al. tested tuberosity reconstruction strength by using a tension test [75]. An increasing tendon force was applied for a fixed abduction angle of 20°. The force

line of action remained constant during loading. SSC and ISP, fixed at the tuberosity fragments, were loaded until failure. Similar loading conditions were applied by Halder et al. [118]. In this study, SSC tendon strength was investigated in a load-to-failure test by direct application of the force at a 0° abduction angle. Smith et al., on the other hand, performed a testing of arthroscopic rotator cuff repair (single row vs. double row) in a cyclic tensile test [119]. Each sample was initially preloaded with 40 N; increasing the loading steps after a defined amount of cycles. Force introduction was done for a fixed position of 30° GH-abduction to the rotator cuff tendons of SSP, SSC and ISP-TM, whereas the load was distributed in respect to the muscle cross sectional areas.

C) Passive muscular loads applied to a free hanging humerus

In an effort to simulate a shoulder rehabilitation program, manual passive movement of a free hanging shoulder was performed by a surgeon in the investigation by Blevins et al. [88]. Constant muscular forces were determined to hold the GH-joint stabilised, in particular 27 N for the SSP, 18 N for ISP-TM, and 22 N for the SSC. A routine shoulder examination was done by applying rotations and translations to the humerus. In the procedure all subjects were tested in the same sequence (maximum elevation, total rotation, anteroposterior (ap-) translation, inferior translation). The maximum elevation in the scapular plane was performed five times by an unconstrained rotation.

Nyffeler et al. considered the influence of the anteversion/retroversion of the glenoid component position and ap-humeral head displacement [87, 120]. Application of a force of 20 N to each rotator cuff tendon was performed during elevation. All measurements were done in neutral rotation. Harryman et al. also applied a manual GH-elevation up to a maximum torque of 3 Nm [121]. During that passive motion, the humeral head translation was analysed. Novotny et al. investigated motion patterns of the GH-joint for an unconstrained movement [122]. This technical solution is unique in the field of experimental shoulder testing. In the set-up, a force couple, produced by air jets, induced free floating coupled moments (Figure 22). Three coupled moments were introduced simultaneously, reaching a maximum moment of 3 Nm along each axis. The resulting range of motion was detected as a function of the applied moments. One of the notable conclusions of the study was that rotations are coupled with translations.

D) Passive muscular loads applied to a constrained humerus

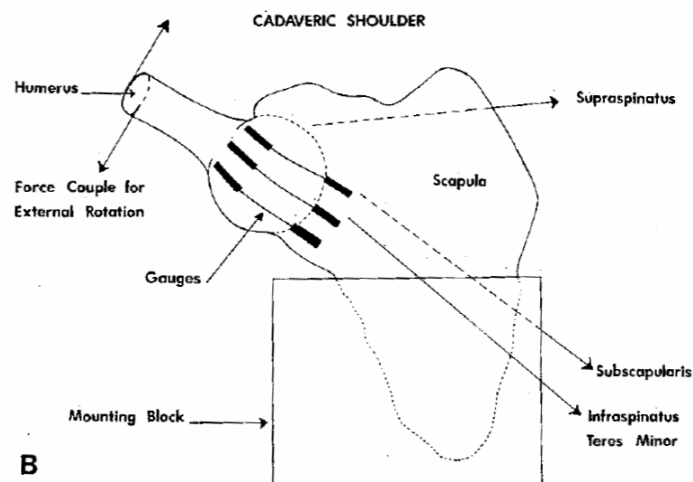
Passive stability provided by static weights guided over pulley-systems is the subject of the following discussion. In such set-ups, the upper arm position is not dependent on the amount

of applied forces, instead it is semi- constrained with a pivot-mounted jig; allowing rotation or translation only in predefined directions. The humerus is therefore guided along a predetermined motion pathway such as rotation around the longitudinal axis or is free to abduct in the scapular plane.

Constraining the humerus along its longitudinal axis

In some testing devices, the humerus is guided along the longitudinal axis. Pure moments are introduced directly to the distal end of the humeral bone which affects passive tension to the capsular system at the GH-joint.

Anatomical versus non-anatomical reconstruction, in the case of hemiarthroplasty was performed in one of the experimental tests by Frankle et al. [90]. A robot applied angular controlled internal/external rotation done at a constant rate of 10° per second, until a maximum angle of 50° was reached, at which point the resulting torque was measured. Angular controlled rotation showed higher resulting torques for a non-anatomical fragment fixation at the prosthesis shaft. Similar to a previous study, Werner et al. applied 1 Nm step-wise loading to a maximum value of 4 Nm [123]. Testing was done for predetermined fixed abduction angles of 0° , 30° and 60° . The measurement of strains at the inferior GH-ligament by combining constant muscular tension with a force couple at the distal humerus was taken by Cain et al. [124]. Muscle forces were randomly varied by different loading step increments, resulting in a total of 64 combinations. Loading directions were derived as well from the study of Perry et al. [105], aligning the SSP 15° superior to the plane, and the SSC 45° inferior to the plane of the glenoid.



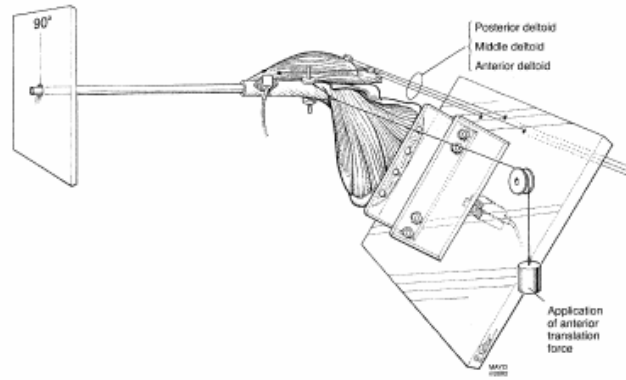
**Figure 22: Test setup developed by Cain [124]
(With permission of Am Journal of Sports Med.)**

Similar conditions were used in a study by Williams et al. [125], where 30 N force was applied at each rotator cuff tendon at 90° scapular plane elevation. By increasing and decreasing a force couple of SSC/ISP, internal and external rotations were performed until a maximum torque of 1.5 Nm was reached, which can be referred to 60 N tensional force at a moment arm of 2.5 cm.

Constraining the humerus in the scapular plane

The function of the SSC muscle during anterior subluxation of the humeral head was evaluated by Werner et al., by measuring the resulting humeral head displacement [126]. Lines of action of the SSC segments were evaluated during an anterior-inferior displacement for three arm positions: neutral rotation, 60° elevation in the scapular plane (corresponded to 90° clinical abduction), and 90° axial external rotation. 30 N of a constant tensile force (10 N per muscle segment) was applied, while two repetitions of each cycle were performed. Yu et al. determined the inferior shift of the humeral head in a healthy condition, and with a full-thickness supraspinatus tear, using the following kinematic input: 10° GH-abduction and 60° TH-abduction, both applied in neutral rotation [127]. Loading conditions were taken according to a previously published simulator [114]. In each position, the load was applied to the single tendons, while a ratio of 3:2 between the DELT and SSP was maintained. The influence of the tuberosity displacement on the glenohumeral force was analysed by Huffman et al. [128]. The scapula was abducted 30° to replicate an anatomic scapulothoracic relationship for 90° of shoulder elevation. At each position, muscles were preloaded to 20 N before loading the DELT with a constant force of 80 N, and the rotator cuff muscles, PM and LD, with 40 N, using a pneumatic muscular loading. A study discusses a similar model, where pectoralis and latissimus dorsi are also simulated [129]. Biomechanical effects of glenoid retroversion on the resulting GH-joint load were analysed. Total shoulder abduction of 90° is performed (30° of scapular inclination and 60° of GH-abduction), resulting in a horizontal arm position. 120 N of DELT force and 60 N of all other muscles were applied. The second study tested posterior subluxation by additionally simulating the latissimus and pectoralis muscles. A minimum of 40 N was applied to each rotator cuff muscle. To simulate the arm weight, a 25 N load was applied to the humerus at the centre of gravity of the upper limb.

Itoi et al. determined the contribution of single muscles to anterior shoulder stability. Muscles were loaded proportionally to their cross-sectional area [111]. Constant forces, introduced by static weights hanging from pulleys, were used to load single muscles. Maintaining that position, an exterior anterior force was introduced to the humerus, resulting in a GH-displacement (Figure 23).



**Figure 23: Passively loaded rotator cuff [111, 130].
(With permission of Am. Journal of Sports Medicine)**

An overview of the discussed experimental testing devices is presented in Table 4.

		Reference	Aim of the investigation	# muscles	Simulated muscle forces and load distribution for specific arm positions	Kinematic protocol of the upper arm	
Active	A) Unconstrained, free hanging humerus	Wuelker [100]	GH-stability testing, measuring humeral head displacement relative to the scapula	4	DELTA 43 %, SSP 9 %, SSC 26 %, ISP-TM 22 %, linear increase of all muscles	Starting position at 29°, until 90° of elevation	
		Klages [102]	Evaluation of muscle forces with respect to the position of the prosthesis head	6	Lin. Increase proportional to DELTA 45.4 %, SSP 9.1 %, ISP-TM 21.8 %, SSC 23.7 % [103]	0°, 30°, 60°, 90°, 110° GH-elevation	
		Soslowky [104], [106]	Analysis of GH-contact area and humeral head translation for different abduction angles	6	ISP-TM, SSP, SSC, (ant., mid., post.) DELTA, force ratio according [105]	Elevation angle up to 180°	
		Kedgley [99]	Evaluation of glenohumeral motion pathways for different muscular loading protocols	6	SSP, DELTA (ant., mid., post.), ISP, SSC, four different muscle force ratios.	Scap. Plane abduction until 50°	
		Debsky [109]	Application of different force distribution profiles and its influence on the arm position	4	DELTA max. 128 N, ISP, SSC acting as stabilisers	Max. arm abd. angle of 90°	
		Bono [89]	Measurement of the deltoid force with respect to greater tuberosity fragment position	6	Linear increase of DELTA force constant loading of SSP, ISP, SSC	Force distrib. acc. [116], GH-abd 90°	
		Karduna [107]	Determination of three-dimensional glenohumeral translations	4	DELTA, SSC, SSP, ISP/TM, force ratio according [105]	post. ant. and scap. plane, 0°, 30°, 60° elevation	
		Sharkey [112]	Contribution of ISP, TM, SSC for glenohumeral joint elevation	4	Four different configurations of muscle activation.	0°, 30°, 60°, 90°, 120° scapular plane abduction, 1.5:1 ration of GH-to-scapulothoracal motion	
	B) Constrained	Abu Rajab [77]	Tuberosity displacement of a fracture during loading for different fixation techniques	2	Load-to-failure: max. tensile force, SSC, ISP, 1188-2424 N	20° abduction (fixed)	
		Smith [119]	Analysis of rotator cuff repair technique (single row vs. double row), cyclic loading to failure	4	SSP 40N, TM 10N, ISP 20N, SSC 50N, increasing load steps after 10 cycles.	30° of scapular abduction	
		De Wilde [75]	Stability of tuberosity fixation techniques for a fractured proximal humerus	2	Load-to-failure test, SSC, upper part of ISP. Testing speed of 0.5 mm/ sec 117-822 N	Static Position of 20° abduction	
	Passive	C) unconstrained humerus	Novotny [122]	range of motion for specific preloading of the glenohumeral joint	Rotator cuff	rotator cuff intact External moment introduction of 3Nm each plane,	Resulting abduction angles of approx. 90° @ 3 Nm torque.
			Blevins [88]	Influence of the prosthetic head diameter of the shoulder joint range of motion	3	SSP 27N, ISP-TM 18N, SSC 22N, constant forces	Max. int/ext. rotation, elevation, controlled by surgeon's hand
Nyffeler [120]			Influence of glenoid retroversion/ anteversion on anteroposterior humeral head displacement	4	m. DELTA 20 N, 3x SSC segments 20 N each	Elevation of the arm controlled by surgeon's hand	
Harryman [121]			Humeral head translation during passive motion	Rotator cuff	3 Nm max., manually applied	Motions manually performed until desired moment controlled by surgeon's hand	
D) constrained humerus		Free rotation	Frankle [90]	Fragment displacement of a fixed humeral head fracture in case of hemiarthroplasty	Rotator cuff	rotator cuff muscles (intact)	50°max rotation @ 0° of abduction, 10°/sec
			Shapiro [131]	Biomechanical effects of glenoid retroversion on joint position	5	DELTA 120N, SSP, ISP, PECT maj, LD, 60N each	Int./Ext. rotation out of GH-plane in 90°abducted position
			Cain [124]	Inferior GH-ligament strain measurements for different loading scenarios	4	ISP-TM, SSP, SSC, DELTA Variation of muscle force 5-20 lbs. 10 to 50 lbs. external rot. torque	Abduction of 90°, ext. rotated, cooking or throwing phase
		Free abduction	Williams [125]	Influence of prosthesis malposition on GH-joint kinematics	2	Force couple of 30 N at ISP, SSC resulting in a torque 1.5 Nm	90° of total elevation in scap. plane, max. int./ext. Rotation
			Yu [127]	Humeral head shifting before and after supraspinatus tear	7	DELTA 90 N, SSP, SSC, ISP-TM, PM, LD, TMaj 60 N each	Acc. [114] 10° / 60° Abduction in neutral rotation
			Huffman [128]	Influence of the tuberosity displacement on the GH-force	6	DELTA 80N, PM 40N, LD, Rotator cuff muscles as stabilisers	Static loading of rotator cuff muscles in various positions
			Itoi [111]	Evaluation of GH-displacement due to introduction of an exterior load	4	SSP 2.0 kg, ISP 4.8 kg, SSC 5.7 kg, biceps 1.5 kg	Scapula inclined 30°, humerus horizontal
			Werner [123]	Influence of capsular tightening on humeral head translation	Rotator cuff	Abduction and flexural torque up to 4 Nm	Scap. Plane abduction, 30° / 60° GH-abduction
			Blasier [129]	In-vitro simulation of the "jerk test" for patients in post-operative rehabilitation	7	ant. DELTA 65N, mDELTA 72N, SSP 62N, SSC 45N, ISP-TM 61N, PM 36N, LHB 31N.	TH forward flexion of 90° at 90° abduction
Halder [92]	Evaluation of the depressor function of single muscle forces, measuring GH-translation	8	SSP, ISP, LAT, LHB, TM, ISP, PM, SSC sup., TMin, SSP, 20 N each muscle	0°, 30°, 60°, 90° GH-abduction			

Table 4: Overview of the different shoulder testing models in literature.

2.2.4 Discussion and Conclusions

The presented literature review covers the design of biomechanical shoulder models for experimentally testing the glenohumeral joint. Testing devices throughout history represent a valuable database in which the applied loading scenario and the kinematics are well documented. The wide spread of applied boundary conditions shows that no standardised shoulder joint model has been established. The number of simulated actuators, the muscular load distribution and the applied upper arm motions in particular were analysed to get an overview on the testing procedures. Independently of the specific biomechanical questions in the study, a categorisation into four different testing characteristics was done.

All types of testing could be clearly allocated to one of the four defined groups, each considering the type of load activation and humeral degrees of freedom. On one hand, an active force profile influences the humeral motion as it is realised in Group A) and B). These groups are considered to be closer to a physiologic behaviour. On the other, constant forces are acting passively to stabilise the joint, represented by groups C) and D). As a refined categorisation, the constraints and fixation of the humerus in the testing device were analysed. If the proximal humerus is additionally restrained by predefined guidances and pathways, the GH-joint is no longer free to accommodate physiological changes during the movement. Unpredictable GH-joint reaction forces may therefore be the result, if the humerus is for example guided at the distal end.

Validation of the measured data by comparing GH-joint loads enables to prove the reliability of the testing sequences. Acquisition of these data has been done only in few studies. Measuring the GH-contact force in the experiment would help to validate the model against the recently performed in vivo measurements by Bergmann et al. [132]. These acquired data would facilitate a better proof of the implemented experimental conditions.

A further option for inter-individual comparison is the analysis of individual muscle forces. In some experiments, the deltoideus force curve is displayed in respect to an increasing abduction angle. Similar force characteristics are detected by a direct comparison of mathematically calculated data and measured data up to 90° of GH-abduction. The cadaver models are incapable of reaching the range of motion compared to the mathematical simulation models for higher abduction angles. This can be justified due to the instability of the experiments for higher abduction angles.

The simulation of the deltoideus, in particular the wrapping mechanism, is frequently realised by cable guidance along predetermined pathways on the bone surface. Obviously, this

simulation by cables is somewhat in contrast to the large segments adjacent to the bone structure, due to punctual load transmission through the hooks. The system devised by Sharkey et al., which uses nylon webbing, approximates the physiological behaviour more accurately by an even load distribution on the subjacent structures compared to the cables. Generally, there is still some uncertainty concerning the biomechanical function of the deltoideus. Contradicting statements are postulated by Gagey et al. on whether the deltoideus acts as a depressor or as an abductor, or even a combination of both [133]. Until the exact effects of the deltoideus are determined, a precise reproduction of the anatomical structures is therefore of importance.

Considering the performed kinematics, a single plane movement is often realised, including the abduction movement in the scapular plane or an internal/external rotation for a given abduction angle. Combined motions around two or even three axes simultaneously have not yet been established.

Historically, complex biomechanical testing such as that in group A was done in the 1990s, whereas studies about implant component testing strongly increased in recent years. The forerunning knowledge which has been attained in earlier years should be transferred to the present and applied to physiologically designed shoulder simulators. It is obvious that a multiple sample testing of implants is time intensive by using a complex testing setup. Nevertheless, efforts have to be made in a future shoulder model design to achieve reliable results for implant functionality.

2.3 Conclusion based on the literature review

The unsatisfactory clinical results of the surgically treated four-part fractures call for a comprehensive overview of current knowledge. The fixation technique has to be optimised to enhance the primary stability of the fracture reconstruction. Such a better stability leads to a reduced fragment migration. The preservation of the postoperative, anatomical reattachment of the tuberosities directly correlates with a better clinical outcome. To be able to quantify that primary stability of fixation techniques, appropriate characteristic values have to be defined to assess their biomechanical performance.

The biomechanical evaluation of novel fixation techniques has to be done based on the state of the art techniques: Numerous publications discuss the available fixation techniques at present. A summary of the existing knowledge represents a fundamental database to highlight promising and advantageous technical details. Furthermore, present models may be taken as a baseline to perform the optimisation process in comparison with novel techniques.

Parameters for optimisation of the fixation technique are the materials used and the placement of the wires and cables around the proximal humerus [31]. More specifically we hypothesize that a placement of stiff connections, collinear to the lines of muscular action, prevents proximal migration of the tuberosities. This assumption is taken based on the analysis of the literature analysis of existing fixation techniques.

To achieve biomechanical analysis of the stability of a reconstructed fracture, a testing device according to in-vivo conditions is needed. Therefore, the second part of the literature review about experimental shoulder testing was done to derive a testing device for fixation techniques. The simulation of postoperative, muscular loading has to be consistent with the biomechanical boundary conditions in the patient. If such kinetic and kinematic conditions match the in-vivo boundary conditions, a reliable behaviour according to physiology is expected.

The analysis of existing shoulder testing devices is therefore helpful to develop a novel testing strategy. A detailed analysis of applied boundary conditions such as simulated muscles and applied range of motion is fundamental. Additionally, a summary of the technical installations (used actuators, bone models, prosthesis types) is important for an efficient realisation of an improved testing device.

3 Material & Methods

3.1 Experimental testing of fixation techniques

3.1.1 Existing testing strategies for fracture reconstructions

Different strategies in literature are documented which experimentally assess the stability of proximal humeral fracture reconstructions. Load-to-failure testing was applied to analyse the maximum strength of the fixation techniques. In this particular case, the humerus was embedded at the distal end. Unidirectional muscular tension forces were applied to the fragments. A fixed humerus which is loaded by a constant force line of action only partially reproduces the in vivo loading. The maximum load can be acquired and compared in several fixation designs, but the interpretation of failure mechanisms may lead to contradicting conclusions in regard to an improved design. Consequently, the biomechanical behaviour of fixation techniques under physiological loading is of great interest for analysing bone-to-implant interactions. The reproducible simulation of in-vivo conditions by a testing device may compare different fixations under the same conditions. Reasons of poor stability may be determined and improved with a performed failure analysis. The reproduction of in vivo conditions by an experimental testing device is therefore of great interest for loaded fixation techniques. If an improved primary stability is equivalent with a smaller fragment migration, optimisation of the fixation techniques may be achieved by preventing oversized interfragmentary gaps. In particular, the knowledge of acting forces and the corresponding muscular line of actions are taken as a basis to define the boundary conditions for improved fixation techniques. The use of novel materials or an innovative placement of sutures and cables may enhance the stability of the reconstruction.

3.1.1.1 Results of existing biomechanical testing

The primary stability of a reconstructed humerus has been analysed by using different testing devices. Generally, loads are applied to the fragments, simulating a muscular tension which displaces them. In the investigation of Frankle et al., a rotation about the longitudinal humeral axis was performed, applying a passive muscular tension [134]. Consequently, muscles in the cadaver model were wrapped around the proximal humerus until a predetermined torque was reached. However, if the humerus is passively rotated, the rotator cuff muscles are not tensioned, which does not simulate active muscular contraction. Dietz et al. simulated an abducted humerus at a fixed position of 25°, applying an alternating loading of the shoulder

muscles subscapularis and infraspinatus. Parameters like the intertubercular motion, the motion of the lesser tuberosity relative to the shaft, and the motion of the greater tuberosity relative to the shaft were investigated. Failure of the reconstructed humerus was detected in one sample by a wire cutting through the bone, wire slippage and subsequent instability. A mean displacement of the lesser tuberosity relative to the shaft was around 0.19 mm for cable fixation and 0.63 mm using sutures. Higher displacements were detected for the greater tuberosity such as 0.25 mm for cable fixation and 0.83 mm for the suture fixation. It must be taken into account that physiological muscular loads are normally in a higher range. Higher displacements are therefore expected by applying a physiological loading. Abu Rajab et al. and De Wilde et al. performed a load-to-failure testing to the rigidly fixed humerus. Unidirectional muscle forces were introduced to the rotator cuff by maintaining a constant line of action [75, 77]. In contrast to that testing, the direction of the muscular loads at the rotator cuff changes during arm rotation. The dynamic characteristics of wrapping muscles around the humerus while performing abduction have not been tested yet, although abduction represents a movement frequently performed during daily life [135, 136]. A summary of in-vitro tested fragment fixations and corresponding testing conditions is shown in Table 5.

<i>Frankle [134]</i> <i>Application of 50° external rotation, resulting in a passive muscular tension.</i>	<i>Measured Parameters</i>	<i>Control</i>	<i>Non-cerclage</i>	<i>cerclage</i>	
	<i>Tuberosity-Shaft Displacement [mm]</i>	<i>GT-humerus</i>	0.9 +/- 0.6	0.63 +/- 0.39	0.14 +/- 0.07
		<i>LT-humerus</i>	0.94 +/- 0.49	0.72 +/- 0.47	-0.002 +/- 0.05
		<i>LT-GT</i>	0.75 +/- 0.64	0.44 +/- 0.41	0.09 +/- 0.14
<i>Abu Rajab [77]</i> <i>Applied 680, 1200, 1500 N for a fixed abduction to the SSC and ISP</i>	<i>Measured Parameters</i>	<i>Fixation A</i>	<i>Fixation B</i>	<i>Fixation C</i>	
	<i>Tuberosity-Shaft Displacement [mm]</i>	<i>GT-shaft</i>	1.95 (0.9-2.8)	1.47 (1 - 2.05)	1.47 (1.3-1.5)
		<i>LT-shaft</i>	0.86 (0.6-1.5)	0.98 (0.7-1.5)	0.94 (0.5-2)

Table 5, Part 1: Resultant fragment displacements of analysed studies in literature.

<i>De Wilde [75]</i> applied 100, 200, 300 N to the SSC, ISP until load-to-failure, 20° of abduction	<i>Measured Parameters</i>		<i>A (suture)</i>	<i>B (wire)</i>
	Rotation [°]	GT-LT @ 100 N	0.52° (0.15-0.9)	0.58° (0.18-0.95)
	(distal opening of the fracture between the tuberosities GT and LT)	GT-LT @ 200 N	1.9° (0.8-3)	2.2° (0-4.7)
		GT-LT @ 300 N	5° (2.7-7.5)	4.8° (0-9)
<i>Dietz [137]</i> 40 N acting at the SSP, alternating load of 40 N of SSP ISP, application of 20 cycles for a fixed 25° abduction angle	<i>Measured Parameters</i>		<i>Cable</i>	<i>no cable</i>
	Intertubercular Displacement [mm]	LT-GT	0.04 (0.02-0.1)	0.14 (0.08-0.28)
	Tuberosity-Shaft Displacement [mm]	LT-shaft	0.19 (0.04-0.35)	0.63 (0.12-3.30)
		GT-shaft	0.25 (0.06-0.37)	0.83 (0.3-4.79)

Table 5, Part 2: Resultant fragment displacements of analysed studies in literature.

3.1.1.2 Objective

The aim in this study is the development of an experimental, reproducible shoulder testing device according to physiological, muscular loading. The use of artificial tendon and bone components allow a reproducible testing procedure for a reconstructed proximal humerus in respect of an improved primary stability. Additionally, the artificial bone model is validated by testing human humeral bone samples.

The following output parameters are defined and acquired to quantify the kinematic behaviour of a loaded, reconstructed fracture:

- **Failure mechanism of the fixation technique:** the analysis of the failure mechanism is essential to optimise existing fixation techniques.
- **Fragment kinematics during loading:** the displacement of the fragments (interfragmentary distance and angulation) during cyclic loading is analysed.
- The “**migration rate**” represents the progression in the displacement per loading step and is a characteristic value to quantify the biomechanical behaviour under load.
- **Cycles-to-failure:** the amount of loading cycles-to-failure is counted, representing a value for the survival rate of fixation techniques during a dynamic loading.

Comparison of different fixation techniques

The analysis of the failure mechanisms and fragment kinematics of the reconstruction during cyclic, physiological loading allows an optimisation of the clinically established fixation techniques.

Comparison of the artificial bone model with the human samples

Additionally, a comparison of human samples with the artificial bone model is made with respect to the fragment kinematics during cyclic loading, in particular in respect to the quantifiable “migration rate”. A similar migration rate between artificial and human bone model would justify the artificial bone model for a further use.

3.1.2 Four-part fracture model

A four-part fracture model was chosen for the experiments according to Neers classification. The displaced four-part fracture with a detached articular head segment represents an indication to perform hemiarthroplasty. That type of fracture is often detected and represents almost half of all proximal humeral fracture types (Figure 24).

3.1.2.1 Geometry of the proximal humerus

The humeral proximal bone shape was reconstructed based on CT scans of the shoulder complex of healthy subjects [138]. The bone geometry was standardised by using spherical, cylindrical and conical shapes in order to create a body of revolution. Concave parts like the bicipital groove and the local elevations of both tuberosities were not taken into account. A coordinate system on the humerus was set according to the ISB recommendations [139]: The z-axis of the coordinate system was collinear to the longitudinal central axis of the humerus, pointing cranially. The x-axis was oriented at the frontal scapular plane and pointed medially. As a result, the y-axis was chosen versus dorsal direction. The defined fracture borderlines were built by planes which cut the proximal humerus in multiple segments.

The vertical fracture line was built by a plane through the central longitudinal axis (z-axis), 30° internally rotated out of the scapula plane along the positive z-axis. The vertical fracture line matches approximately the biceps groove. The plane defining the surgical neck fracture was tilted 15° around the positive y-axis relative to the horizontal xy-plane. These predefined straight fracture planes represent a simplified fracture scenario, but have been used as well by Frankle et al. [134].

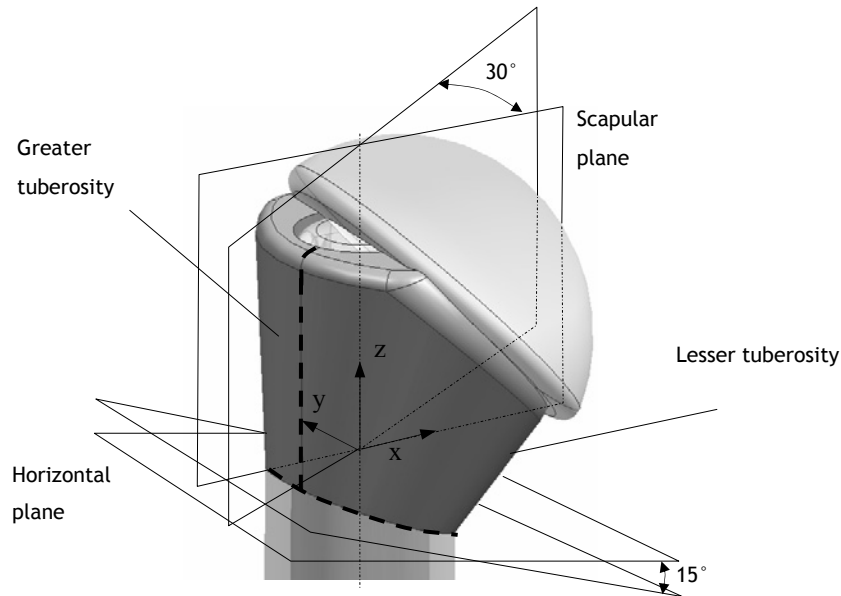


Figure 24: Schematic view of a four-part fractured humerus with visible fracture planes which build the shaft fragment, the greater and lesser tuberosity. A detailed sketch is shown in Appendix 8.1.

3.1.2.2 Used bone material

Artificial bone samples were manufactured and used for the tests. Additionally, a small series of human bone samples were tested under the same conditions. The use of human samples allows a comparison with the artificial bone with respect to the resulting fragment kinematics.

Artificial bone model

Artificial bones made of commercially available polyurethane foam with specified density, strength and stiffness were used to simulate the four-part fractured humerus (Last-a-foam® FR6715, General Plastics Manufacturing Company, Tacoma, US). The mechanical properties of the artificial bone were defined according to ASTM F1839-97 (Table 6), a standard specification of a rigid polyurethane foam. This material is used as a standard for the testing of orthopaedic devices and instruments [140-144]. The artificial bone is specified by a very low structural variation and homogeneously distributed pores. The density of the material is around 0.24 g/cm³, which is in the range of human cancellous bone (0.1–1.4 g/cm³), shown by Zhu et al. [145].

Last-A-Foam Data for: - Parallel to Rise of Foam - closed cell PUR foam	Density		Compressive material properties		Tensile material properties	
	[lbs/ft ³]	[g/cm ³]	Strength [MPa]	Modulus [MPa]	Strength [MPa]	Modulus [MPa]
FR6708 (osteoporotic)	8	0.13	1.7	54.3	1.8	48.2

Table 6: Artificial bone material properties.

Human samples

A total of 9 humeri were excised from human shoulders and prepared by an experienced surgeon. Thiel-fixed samples were used for the tests. The procedure of storing the samples and the composition of the liquid is described by Fuchs et al. [146]. Three samples had to be excluded, two of them due to rotator-cuff tendon lesions and one because of a not anatomically healed fracture. Therefore, six samples could be used for the tests including 4 female (3 left, 1 right) and 2 male (1 left, 1 right). The tendon attachments were left intact including a minimum tendon length of 30 mm, to be able to fix them to the actuators of the testing device. The capsule and the surrounding tissue were removed in order to simulate comparable conditions to the artificial bone model. Additionally, a free view on the fragment borderlines allowed the control of the fragment distances. The humeral long bone was cut distally to the tendon insertion of the deltoideus, including an approximate length of $\frac{3}{4}$ of the total humeral length. The diameter of the articulating surface (caput humeri) was determined by lateral photographs. The mean radius of the articulating surface was $r = 29.5 \text{ mm} \pm 1.6 \text{ mm}$. Left shoulder were mirrored and considered as right shoulders in order to keep uniform coordinate system for fragment migration measurements.

3.1.2.3 Prosthesis design

Implant geometry was chosen according to the Affinis Fracture Prosthesis (Mathys Ltd. Bettlach) [30]. The prosthesis was made of titanium alloy, comprising a stem, a middle part and a ceramic cup with a head diameter of 35 mm (Figure 25). The middle part of the prosthesis had a cylindrical shape with 3 holes in the anteroposterior direction for suture and cable insertion to fix the fragments. The surface of the prosthesis middle part comprised a macrostructure made of pyramide pins. The exact prosthesis dimensions are shown in Appendix B.

In the patient, the part of the glenoid is not replaced during clinical intervention, the ceramic cup articulates directly onto the chondral tissue. However, an artificial glenoid made of polyethylene (Affinis Prosthesis, Mathys Ltd.) was used in our test setup to simulate the concave glenosphere. Frictional parameters of a dry polyethylene-to-ceramics articulation are around $\mu = 0.1$. Consequently, frictional effects do only marginally influence the necessary muscular loading for arm abduction.

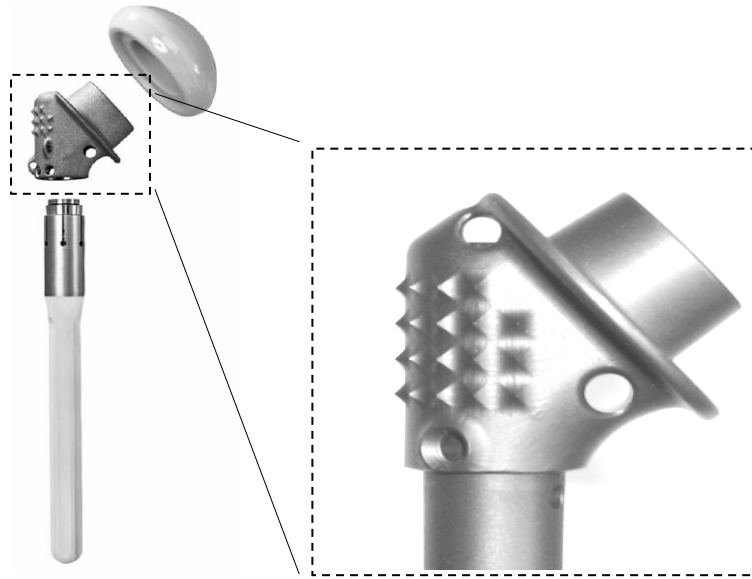


Figure 25: Assemblies of the Affinis Fracture prosthesis (Mathys Medical Ltd.).

3.1.2.4 Prosthesis implantation

The prosthesis is implanted in congruency to the bone by using a rasp for a proper adjustment of the inner cavity. The form-fit of the embedded shaft is proved before implantation by trial prosthesis (without any macrostructure on the implants' surface) in order to preserve the inner surface of the bone cavity.

The distal end of the prosthesis stem was in direct contact to the end of the bone cavity. Movement of the prosthesis stem relative to the humeral shaft was then additionally prevented by fixing the humeral stem to the prosthesis by using screws. This reproduces the conditions of a cemented stem, as it is common in most cases of prosthesis implantation. Consequently, a rigid connection between the prosthesis stem and the humeral shaft prevented a relative rotation or a proximal movement of the prosthesis stem relative to the humeral shaft.

3.1.2.5 Tendon insertions (footprints)

A high variation of the geometry of the tendon insertions (footprints) is found in literature. In present investigation, the anatomic location of the footprints was taken from the investigation of Curtis et al. [147]. The graphs of the footprints based on the anatomic model were transferred to the artificial model of the humerus using a technical sketch (Figure 26). The subscapularis was represented by two tendons, whereas infraspinatus and teres minor were described by one footprint each. As previously described, the biceps groove represents the fracture line between the greater and lesser tuberosity. The coordinate system is placed in the centre of the prosthesis head.

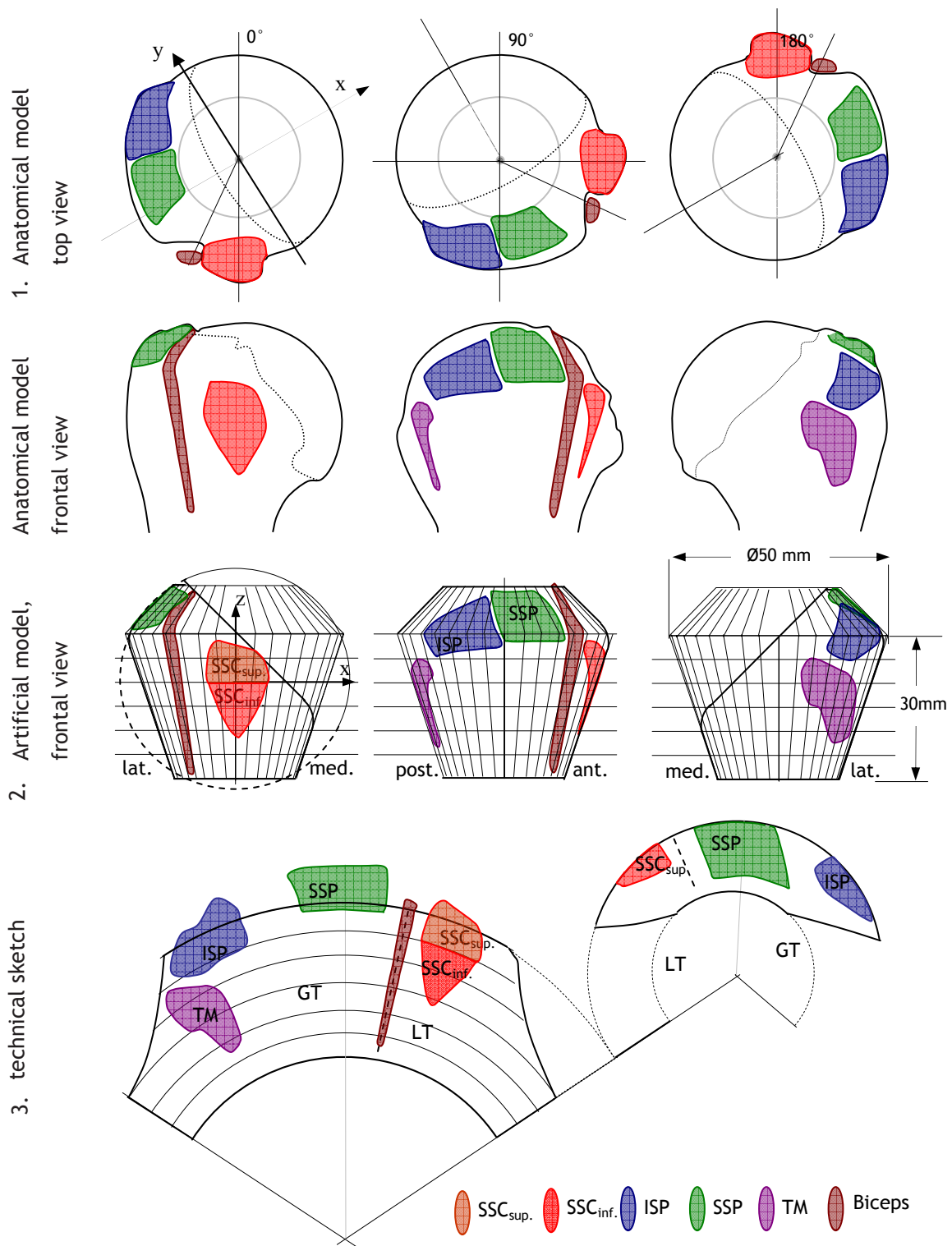


Figure 26: Technical sketch of the tendon insertions derived from the anatomical model and transferred to the artificial model. (A detailed sketch of the humerus is found in the Appendix 8). As a reference length, the width and the height of the artificial humeral head is shown.

3.1.2.6 Artificial tendons

Artificial tendons made of a 100 % polyester webbing (Tobby GmbH, Austria) were used to introduce the muscle forces to the proximal humerus at the specified tendon insertions. The width of the tendons was 12 mm in the unloaded condition, whereby a reduction in the width occurred during tensioning. Tendon-to-bone fixation was realised with instant adhesive (Loctite 406, Henkel & Cie. AG, Switzerland). The area of the footprints was coated with a 1 mm thick layer of the adhesive before the unloaded tendons were pressed against the bone surface. Pre-tests revealed maximum shear strength of the tendon-to-bone connection of approximately 250 N. The flexible tendon material allows a transmission of an evenly distributed force to the entire insertion area. The arm abduction affects a rotation of the footprints with a subsequent buckling of the tendons (Figure 27). This buckling effect is reduced due to the contractile properties of the tendons at the unloaded border. However, the loads are primarily transferred through the lower border of the tendon for higher abduction angles.

3.1.2.7 Lines of action of the muscle forces

The tendon directions were aligned with the lines of actions of the corresponding muscular forces. According to the investigation of Van der Helm et al., the segment of the infraspinatus was horizontally placed, as well as the proximal segment of the subscapularis [148]. The distal segments of teres minor and the inferior subscapularis segment (SSC 2) were inclined by an angle of 8° , whereas the deltoideus segment had an angle of 16° relative to the horizontal plane. The supraspinatus pointed horizontally, parallel to the infraspinatus segment.

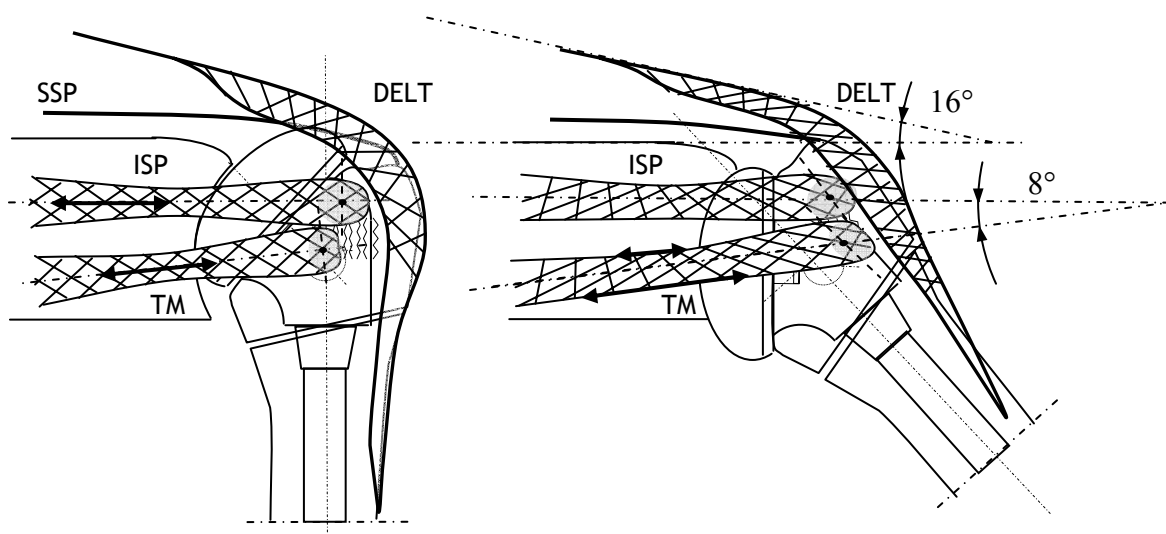


Figure 27: Abduction of the humerus causes rotation of the footprints (red) and subsequent buckling of the artificial tendon which shifts the force line of actions.

3.1.2.8 Applied fracture fixation techniques

The two clinically established fixation techniques were tested in order to gain experience on biomechanical behaviour during loading (Figure 28). Type A represents the clinical standard suture technique including two longitudinal slings connecting the LT and the GT to the shaft. Additionally, a circular sling connects both tuberosities to each other. Type B is designed similarly to technique A but includes an additional circular cable through the prosthesis and around both tuberosities [30]. The fixations have been prepared by an experienced surgeon; sutures have been knotted by the clinically applied knot technique known as the “surgical’s knot”. Pretension was applied manually to tighten the knots. The used holes in the bone to guide the cable were predrilled by a diameter of $\varnothing = 1.5$ mm, rectangular to the bone surface. The sutures were pulled through the bone by means of a sharp needle, which was pre-assembled with the suture end. The placement of the sutures was predefined by using the straight fracture lines as landmarks. Obviously, a higher strength of the reconstruction of type B is expected due to the additional cable cerclage around both tuberosities.

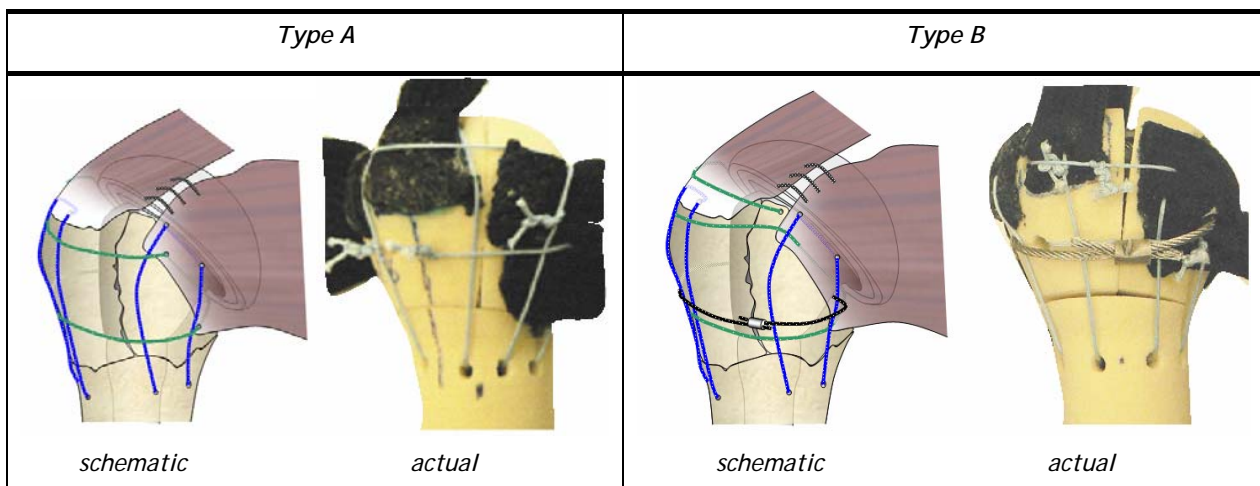


Figure 28: Fixation techniques of Type A and B for the fractured proximal humerus.

A reproducible placement of the fixation technique was enabled by a defined pre-drilling of the suture and cable holes. The suture holes which connected the greater tuberosity to the shaft were placed in a distance of 20 mm from the humeral shaft (Figure 29).

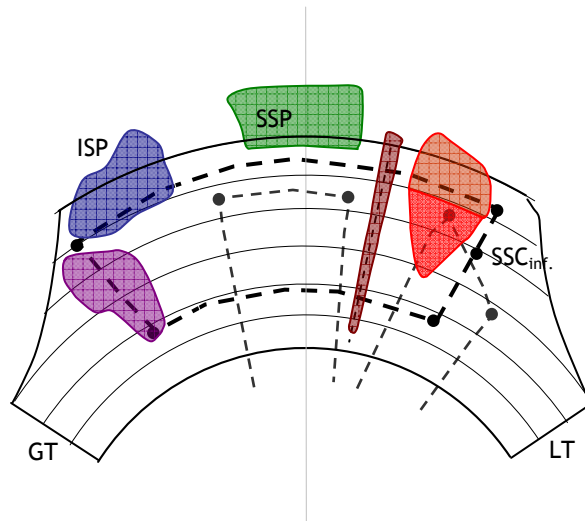


Figure 29: Suture placement on the projected proximal humeral surface. The suture connecting both tuberosities is shown (black dotted); sutures connecting the tuberosities to the shaft are grey dotted.

3.1.3 Experimental testing device

3.1.3.1 General concept

The kinematic boundary conditions for the test setup are defined based on postoperative rehabilitation exercises of the patients 3-4 weeks postoperatively (Chapter 1.2.4). Single plane abduction is chosen as a kinematic boundary condition due to the standardised and reproducible movement during the functional assessment of the shoulder.

The design of the testing device comprises a fixed scapula relative to the humerus, according to previous testing concepts (Chapter 2.2.3). Graichen et al. showed that the movement of the humerus relative to the scapula contributes to 50 % to the overall arm abduction, whereas the other 50 % are provided by the scapular rotation relative to the thorax [149]. Consequently, the 70° humeral abduction relative to the scapula may be considered as 140° total arm abduction. A free hanging arm is stabilised in the glenoid by muscular tension of the simulated rotator cuff muscles.

The muscles which connect the scapular part with the humerus have been considered for the testing device: As a result, the middle deltoideus, supraspinatus, infraspinatus/teres minor and two segments of the subscapularis are simulated. Active elements in form of actuators were used to simulate a muscular tensional load (Figure 30).

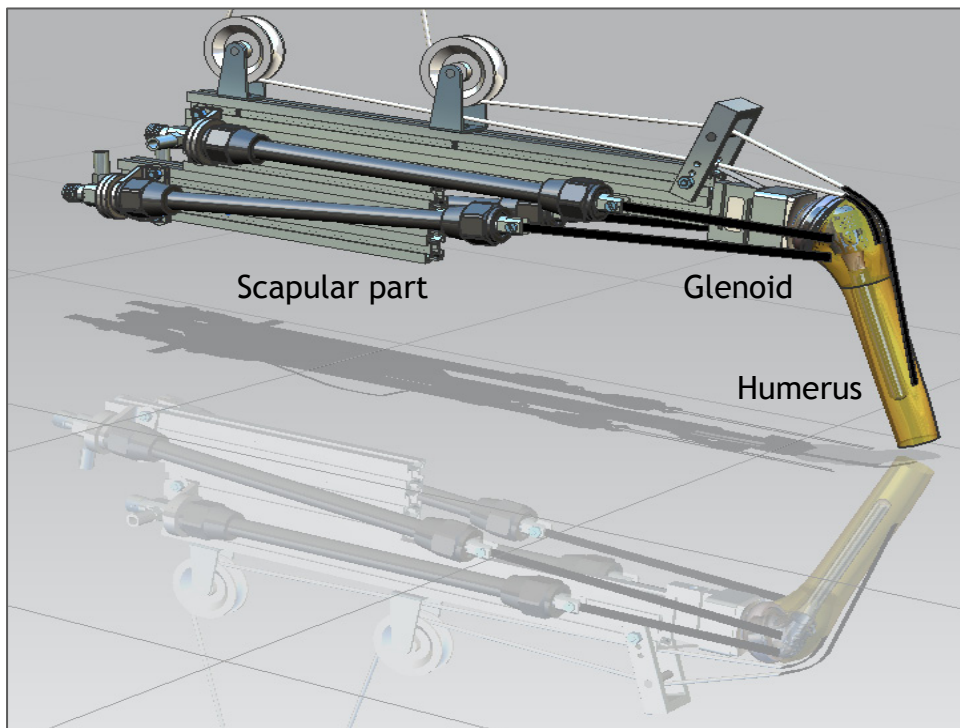


Figure 30: Anteriolateral view on the shoulder testing device with a fixed scapular part built by metallic profiles and the humerus which is connected by two segments of the SSC, ISP/TM on the contra lateral side and the pulley system simulating the m. DELT and the SSP.

The dynamic principle of the testing machine is described in a frontal view (Figure 31). The abduction angle of the humerus is actively increased with a simultaneous increase of the muscular tension. The magnitude of the acting muscular loads is therefore dependent on the position of the proximal humerus and by the arm weight at the end of the humeral bone. During abduction, the humerus is stabilised by the tensioned rotator cuff muscles which prevent a rotation along the longitudinal humeral axis.

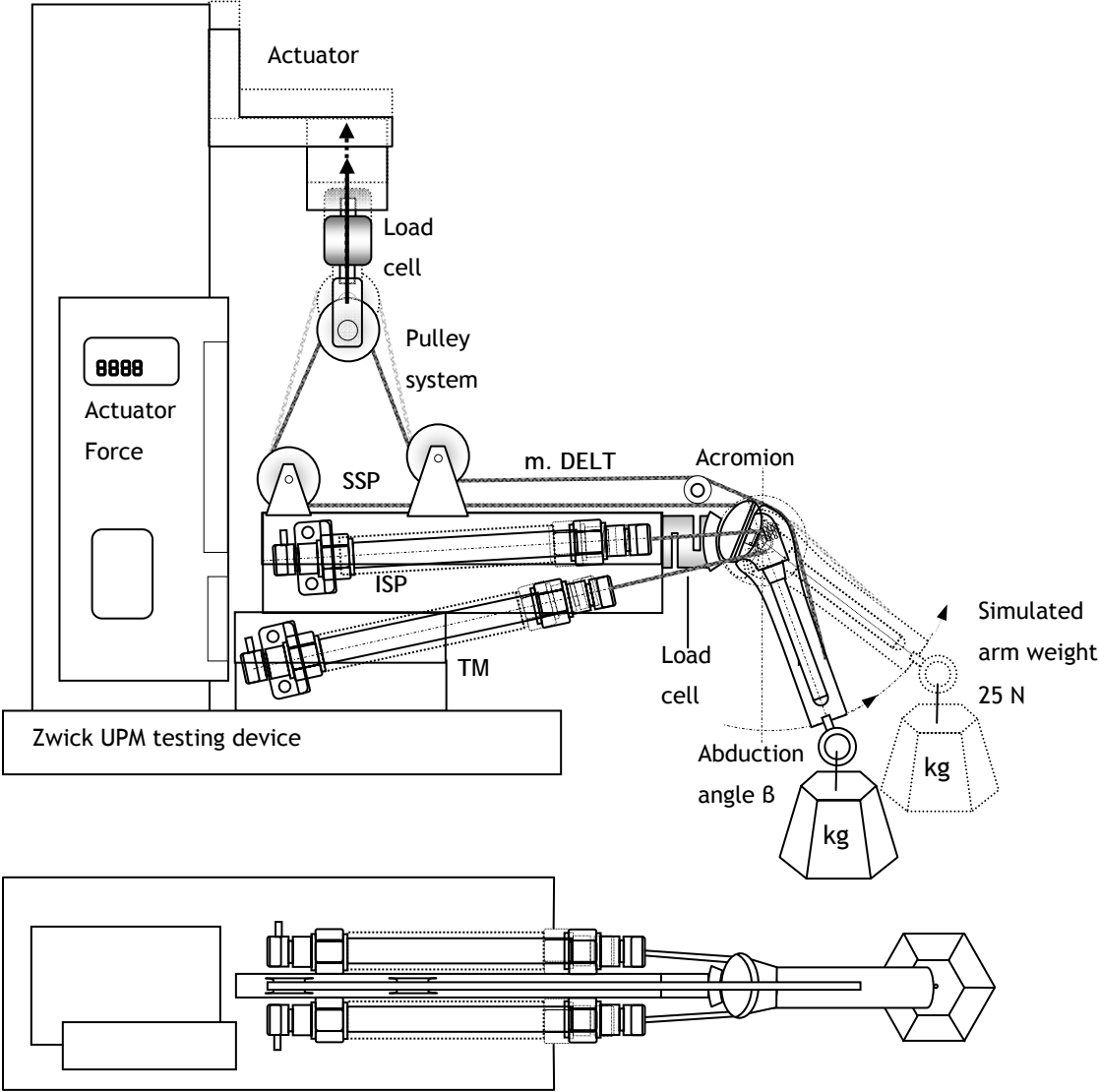


Figure 31: Schematic function of the testing device in a frontal view (top) and in a top view (bottom). Active forces of the deltoideus and supraspinatus, two segments of the subscapularis and infraspinatus / teres minor apply an active abduction.

3.1.3.2 Application of muscular forces

Middle deltoideus and supraspinatus

A Zwick tensile testing device UPM 1475 was used to simulate the increasing force profile of the middle deltoideus and the supraspinatus muscle during abduction. As a result of a pulley-system connecting both SSC and m. DELT tendons to the same machine actuator, each muscle contributed to 50 % to the necessary force to abduct the arm. The movement of the arm was therefore angle controlled, measuring the forces at the corresponding abduction angles of 15°, 30°, 45°, 60° and 70°. A controlled speed of 100 mm/s of the machine actuator was applied, resulting in an arm rotational speed of approx. 3°/sec at lower abduction angles but increased with higher abduction angles due to a sinusoidal ratio between the muscular shortening and the arm angle. A total of 40s is therefore needed to apply a full abduction cycle.

Subscapularis and infraspinatus/teres minor

Two actuators represented the superior and inferior segment of the subscapularis on the frontal view of the shoulder, whereas infraspinatus and teres minor were each simulated by an actuator dorsally. Contractile pneumatic actuators called “fluidic muscles” (Festo GmbH, Germany) were used to simulate the muscle forces. The actuators applied a tensile load by contracting their elastoplastic body due to an increase of air pressure (Figure 32). These actuators have been already used for biomechanical shoulder testing in previous study by Lilly et al. [150]. The initial length of each muscle was 200 mm, allowing full function over the necessary contraction length. The air pressure was predetermined to apply an increasing force profile from 10 N at 15° of abduction to 50 N at 70° of abduction. The actuators were laterally fixed at the scapular part by screws. Due to the flexible bending properties of the deformable cylinder tube, slight variations in the muscular force lines of action did not constrained.

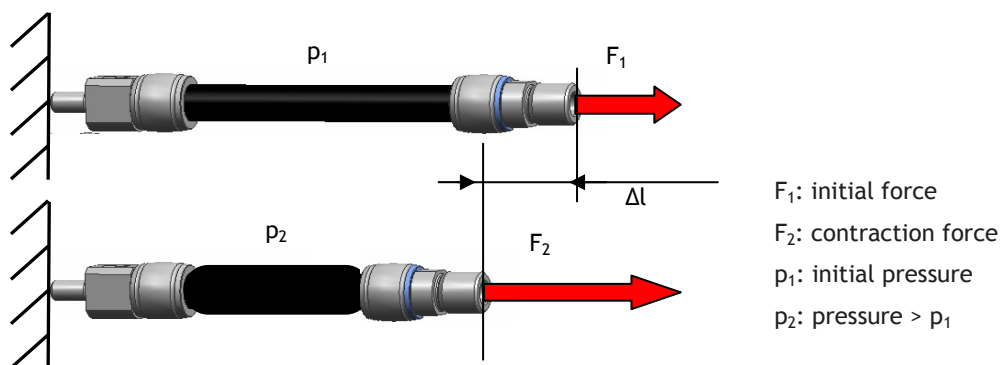


Figure 32: An increase in pressure contracts the pneumatic actuator and applies a tension force.

A photograph highlights the used measurement tools to acquire the needed output variables (Figure 33).

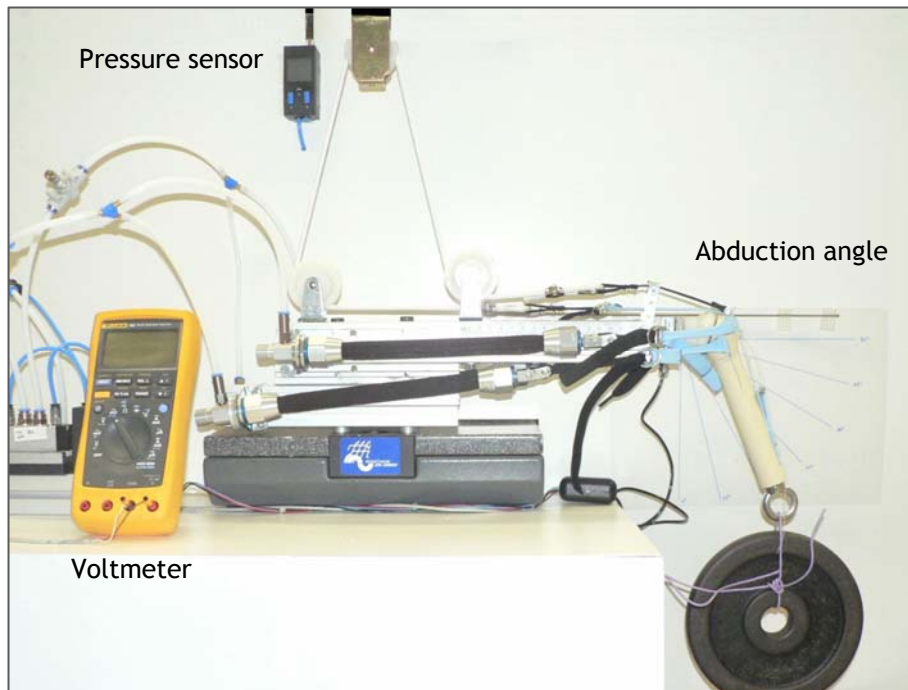


Figure 33: Photograph of the testing device and the measurement equipment of the pressure sensor and the voltmeter to acquire the GH-joint forces.

3.1.3.3 Sample mounting and conditioning

After the reconstruction of the fracture by the fixation techniques, the artificial tendons at the proximal humerus were connected to the actuators by a clamping mechanism. The single artificial tendon bands were then tightened manually, until a defined contact force in the range of 5 – 15 N was achieved. The humerus was visually aligned in the scapular plane by pretensioning the individual tendon-to-actuator connection. After initial fixation of the sample by loading infraspinatus, teres minor and the two segments of the subscapularis, the humerus was unloaded, and tightened again to prevent any relaxation effects. The pretensioning caused an initial abduction angle of about 5-10°. The initial starting condition was finally achieved by attaching a simulated arm weight of 25 N to the middle of the humerus shaft.

Preconditioning of the sample

1. Reset the machine force (DELT and SSP) equal to „zero“
2. Reset the joint load cell equal to zero (pretension is zeroed)
3. Connect the tendons to the actuators
4. Manually tighten the rotator cuff muscles (SSC1/SSC2, ISP, TM)
5. Adjustment of a GH-contact force of approximately 5 – 15 N during tightening
6. Apply a pressure of 2 bar to the rotator cuff muscle actuators for 1 min
7. Unload the actuators, retighten the tendons, readjust the GH-contact force
8. Alignment of the humeral rotation visually to the longitudinal axis
9. Set the abduction to initial starting position of approx. 5° by tensioning DELT/SSP muscles

Initial loading of the sample

After sample mounting, the abduction movement was initiated by increasing the tension forces of the active muscles DELT and SSP by the machine actuator. At visually controlled abduction angles of 15°, 30°, 45°, 60° and 70°, the humerus was stopped and held statically in fixed position. A simultaneous, stepwise increase of the corresponding loading profiles of SSP, ISP/TM by increasing the air pressure was performed.

3.1.3.4 Testing procedure and loading sequences

Abduction from 15° to 70°

After sample fixation, the testing was started by applying repeatable cycles up to 70° glenohumeral position (Figure 34). Photographs were taken at 15°, 30°, 45°, 60° and 70° during the applied loading cycles. A maximum of 10 cycles was applied; the first, second, third and 10th cycle were analysed and documented.

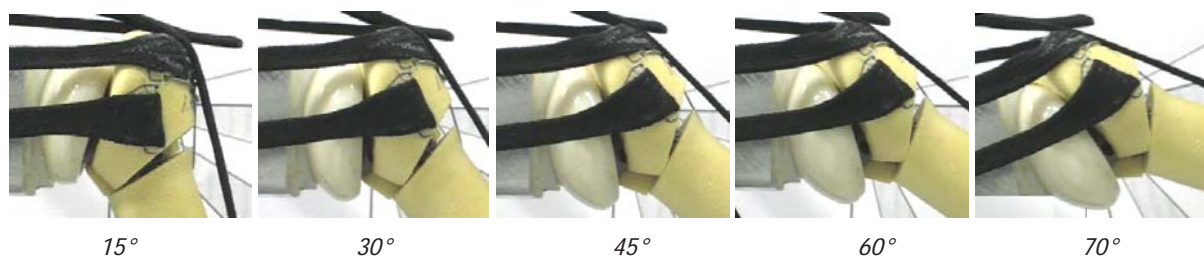


Figure 34: Sequence of images taken at different abduction angles ranging from 15° to 70° (The fragments are already in a displaced position; a 3rd cycle is shown).

Internal/external rotation

Internal/external rotation from $+30^\circ$ to -30° was performed with respect to neutral rotation at a fixed abduction angle of 45° (Figure 35). The longitudinal axis of the humerus remained at a fixed position in the space.

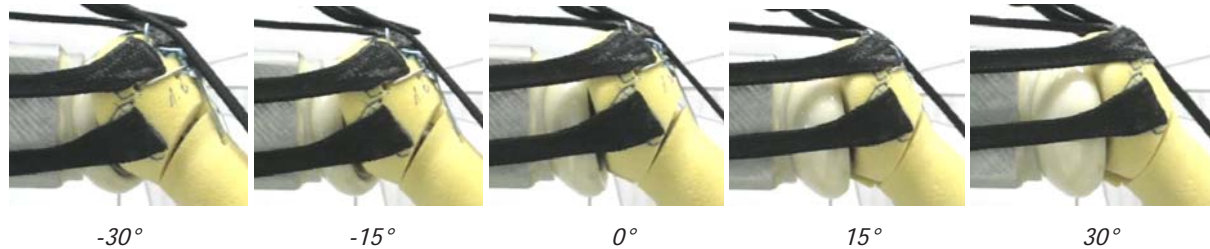


Figure 35: Internal/external rotation from -30° to $+30^\circ$ with regard to neutral rotation.

3.1.4 Data acquisition during testing

3.1.4.1 Glenohumeral contact forces

The glenohumeral contact force was measured in the glenoid by an s-shaped, one-dimensional load cell (KD40s, 5000 N, Transmetra Haltec GmbH, Switzerland) perpendicular to the glenoid in y-direction. The results were compared with recently acquired in vivo measurements by Bergmann et al. [132]. Bergmann et al. measured the contact forces in the prosthesis head and not in the glenoid. To be able to transfer the contact force data from the prosthesis to the glenoid, a frictionless articulation must be assumed.

3.1.4.2 Muscle forces

Supraspinatus and middle deltoideus

The muscular tensile forces of the supraspinatus and middle deltoideus were acquired at every loading step, measured by the load cell of the testing machine (Angewandte System Technik GmbH, Germany) and displayed by the software Test-Expert V10.0. An even load transmission to each muscle was assumed, although frictional effects of the pulley system may slightly differ from the theoretical 50:50 force distribution of the machine actuator.

Subscapularis and infraspinatus/teres minor

The muscle forces of the SSC and ISP/TM were applied passively and provided no real-time force feedback. Applied muscle forces were determined by measuring the present contraction

length of the fluidic muscle and the applied air pressure during testing. By means of these two variables, the resulting force was read out from the muscle force-length diagram. This diagram resulted from a pre-evaluation by calibrating every single muscle before the tests. The acquired isobaric curves allowed the determination of the forces (Figure 36).

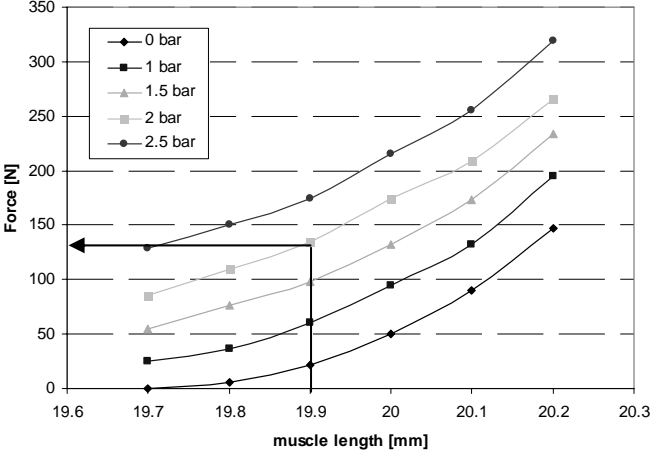


Figure 36: Experimentally acquired calibration data of the fluidic muscles to extract the resulting muscle force for the corresponding muscle length.

3.1.4.3 Analysis of the muscle moment arms

The moment arms of the supraspinatus and deltoideus during abduction were acquired using the tendon travel method (Figure 37). The tendon travel method (also known as “the tendon excursion method”) is well described by Werner et al. [123]. In total three samples were tested by acquiring full abduction cycles, the mean values were taken and compared with literature.

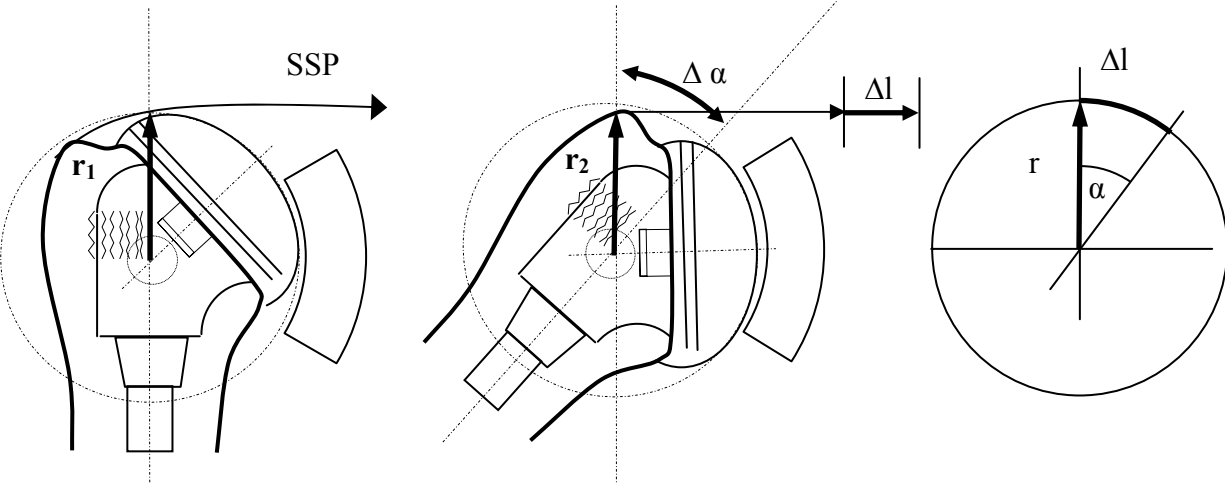


Figure 37: Tendon travel method and the relation between joint angle and muscular moment arm.

3.1.5 Reproducibility of the applied joint and muscle forces

3.1.5.1 Introduction

To prove the reliability of the experimental results, the use of standardised samples and the application of equal boundary conditions during repetitive testing are crucial. In the present testing, the fracture model consists of uniformly manufactured artificial bone, standardised procedure of prosthesis implantation and defined tendon insertion sites (“footprints”). Nevertheless, the variability of the samples due to manufacturing tolerance can not be excluded completely. In our particular case, the prosthesis height relative to the humerus and the tendon line of action influences the loading scenario: A variable muscular moment arm, which is predetermined by the shape of the bone, has a direct influence on the applied forces to reach a distinct arm deflection. In particular, the longer the supraspinatus moment arm, the smaller is the needed muscle force to abduct the arm. To determine the influence of the testing samples’ variability on the loading scenario, a sensitivity analysis was done.

- A) The prosthesis position in the bone was considered as a potential source to influence the applied muscular loads and thus the resulting GH-joint force.
- B) The tendons were slightly displaced from normal position (towards proximally) to estimate the influence on the resulting force.
- C) The reproducibility of repetitive loading cycles for the same sample, and the initial loading cycles for different samples, were compared.

3.1.5.2 Method

Specific test setup

An intact, not fractured, artificial humerus sample was used as validation setup. Three subsequent cycles were analysed, the mean curve and the standard deviation were displayed. Data acquisition was performed according to chapter 3.1.3.4 for abduction.

A) Influence of the prosthesis position

The influence of the prosthesis position on the supraspinatus & deltoideus muscle force was analysed (Figure 38). According to existing study of Nyffeler et al. [87], proximal displacements of 2.5 mm and 5 mm relative to normal position in the humerus were chosen. The proper prosthesis position was guaranteed by distance holders with the corresponding thickness between the rear of the prosthesis and the bone.

It is to mention that the superior prosthesis position increased the humeral arm length. This length was not adjusted to uniform length. As an effect, the weight at the end of the humerus had an increased distance of 3 % to the rotation centre.

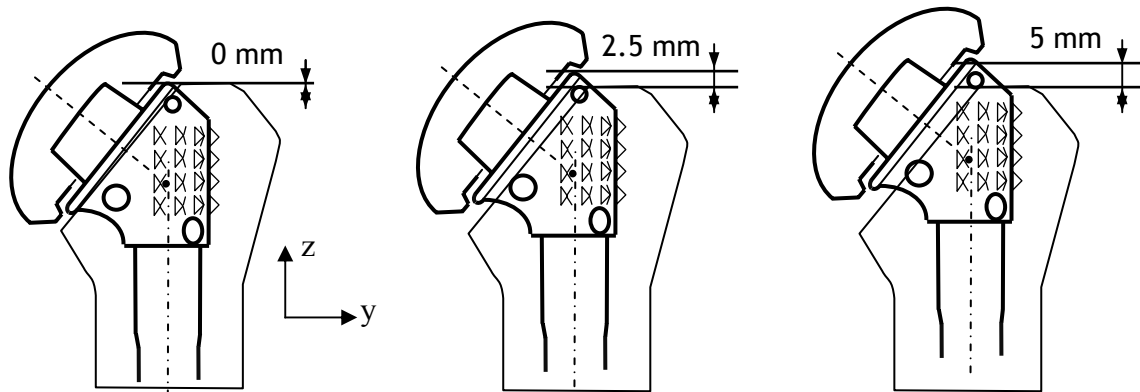


Figure 38: Variation of the prosthesis position in z-direction. Normal position (left), 2.5 mm superior position (middle) and 5 mm superior position (right).

B) Influence of the tendon insertion placement

A standardised attachment of the tendons is important for a reproducible testing of multiple specimens. The choice of the tendon placement is sensitive with respect to resulting muscular loading, as it directly affects the muscular moment arms.

A large variation of the anatomic localisation of tendon insertions are found in literature [151-156]. In present study, the artificial tendons which transfer the muscular loads were attached according to the investigation of Curtis et al. [151]. The infraspinatus/teres minor and subscapularis muscle were each subdivided in two functional segments. On the contralateral side, the subscapularis is divided into a superior part (SSC 1) and a inferior part (SSC 2), as previously described in chapter 3.1.2.5. The lower border of the superior subscapularis tendon is placed on the same height such as the rotation centre of the prosthesis. The superior border of the lower segment is placed adjacent to the first segment (Figure 39).

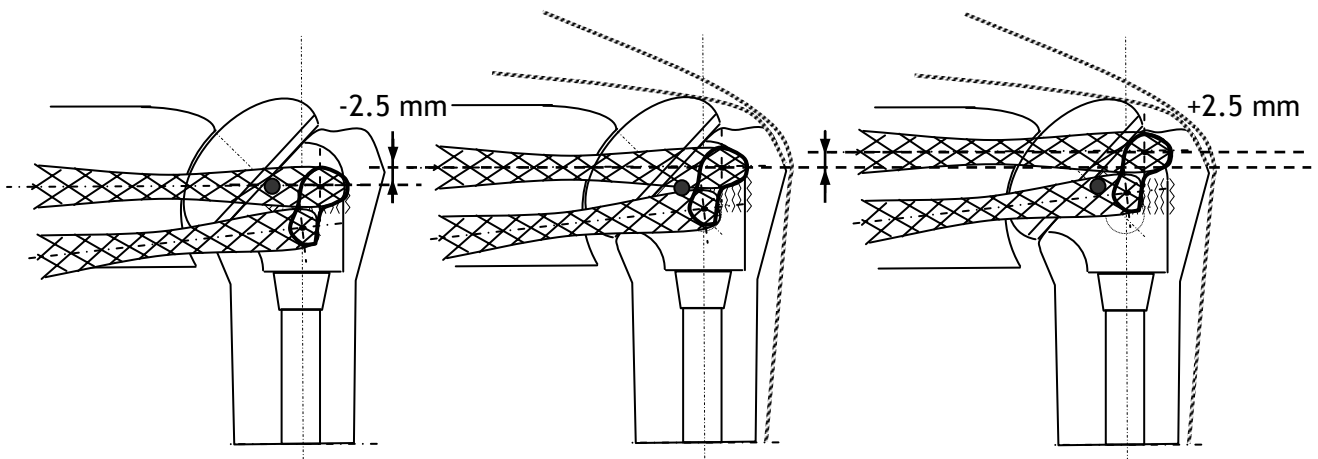


Figure 39: Variation of the tendon insertion position. Inferior (left), normal (middle) and superior position (right).

C) Influence of the initial fixation on the required forces

A small variation of the forces with respect to the initial clamping of the specimen is evident for a reproducible testing. By means of that investigation, the influence of the initial tendon fixation method on the acting muscle forces was achieved. The samples were initially fixed according to the defined conditioning procedure described in chapter 3.1.3.3. In total three samples have been tested, required muscle forces and resulting GH-contact forces were acquired.

3.1.5.3 Results

A) Prosthesis position

Generally, a higher prosthesis position results in an increased glenohumeral joint and muscle force in comparison to the normal prosthesis position (Figure 40). No further increase of the muscle force is seen from abduction angle of 60° to 70° for a superior prosthesis position of 5mm. Due to an increasing muscular moment arm of the DELT between 60° and 70° , the necessary muscle force to maintain an abducted arm position does not increase. DELT&SSP forces are influenced by a superior prosthesis position to the same magnitude as the GH-joint forces.

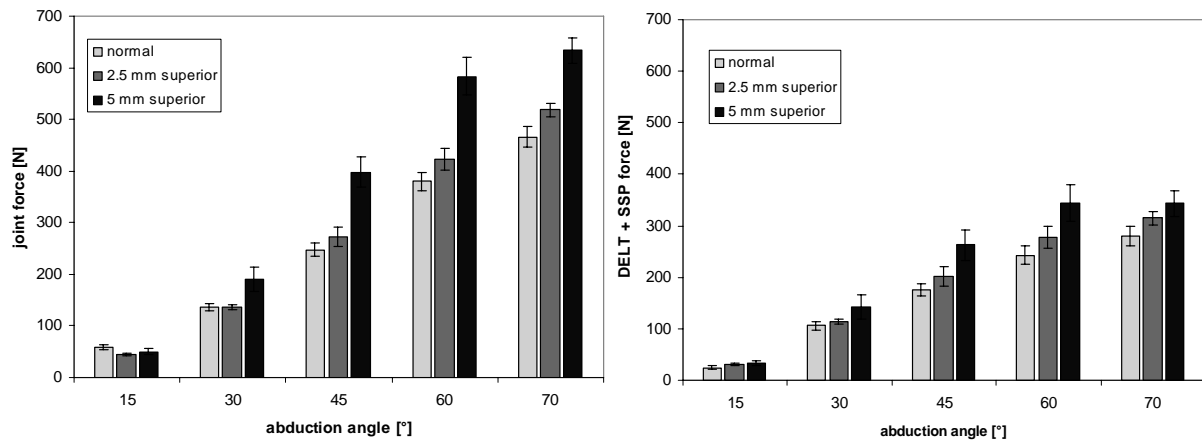


Figure 40: The prosthesis height influences the GH-joint force and the muscle forces.

B) Tendon placement

Superior tendon placement of SSC and ISP/TM results in lower joint forces, whereas an inferior tendon placement (in distal direction to the humerus) increases the applied GH-joint forces (Figure 41). An inferior or superior placement of the tendon insertion does not significantly influence the muscle forces.

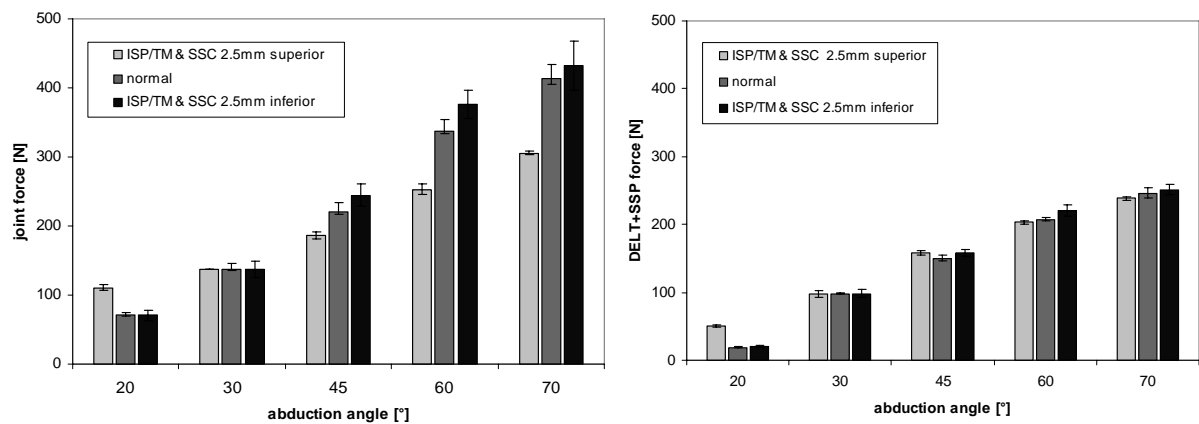


Figure 41: Effect of tendon placement on the resulting joint forces and muscle forces.

C) Variability of the 1st cycle of three samples

Variability of the first cycles (initial cycles of each single sample, n = 3 testing samples) does not differ more than 10 % with respect to the maximum joint and muscle forces (Figure 42). A systematic decrease of the muscle forces is detected with additional cycle number.

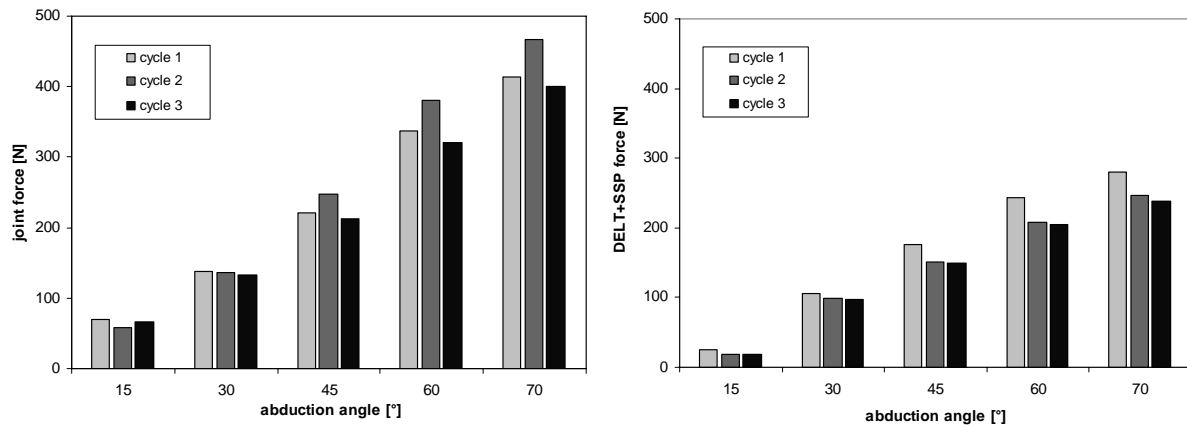


Figure 42: Initial cycle of three different samples with respect to the joint and muscle forces.

3.1.5.4 Discussion

A) Prosthesis position

A proximal prosthesis shift does simultaneously induce an inferior placement of the lateral tendons. These distally placed tendons counteract the proximal muscle forces which contribute to abduction. This circumstance explains the higher muscle and joint forces of up to 25 %.

As an additional effect, an increased moment arm of the arm weight (distance from the rotation centre to the arm weight) as an effect of a superior prosthesis position requires to increased muscle and joint forces.

Nyffeler et al. showed a reduction of the supraspinatus moment arm of approximately 5 % for an elevated prosthesis of 5 mm. Present investigation is therefore in a similar range, if an indirect proportional correlation between supraspinatus / deltoideus moment arms and the necessary muscle force is assumed.

B) Tendon attachment

The comparison of a normal tendon placement with superiorly placed ISP/TM and SSC tendons results in smaller muscle forces, if the superior tendons contribute to a higher extent to abduction. The counteracting effect mentioned under A) is reduced. Superior prosthesis position of 2.5 mm increases the joint force to a higher magnitude than a 2.5 mm inferior placement of the tendon.

C) Variability of the 1st cycle

Reproducibility of each initial fixation of different samples has a variation of approximately 10 % with respect to the loading scenario. Subsequent cycles with the same sample have a smaller variation vs. each first cycle for different samples. Generally, a systematic decrease of the necessary forces is detected for subsequent cycles for one sample. This behaviour can be explained by an optimised positioning of the prosthesis head after the initial cycles.

3.1.5.5 Conclusion

The loading cycles simulated by the testing machine can be reproducibly applied. The sensitivity analysis revealed significant influence of the tendon placement and prosthesis position on the resulting muscle forces. Assuming a higher prosthesis malposition of 1 mm and a simultaneous inferior tendon placement of 1 mm, an increase of the applied loading of about 10 % is expected. The muscular loading profile is therefore strongly dependent on an accurate positioning of the tendons on the bone surface. Slight variations of the tendon placement lead to significant differences in the needed muscle forces to abduct the arm. The small muscle lever arms at the rotator cuff call therefore for a sensitive control of the chosen tendon insertions to balance the glenohumeral joint.

The preparation of the testing samples has therefore to be handled with care; an improvement of the reproducibility could be achieved by an accurate and automated manufacturing of each sample. Additionally, quality control of each sample after prosthesis insertion and exclusion of not sufficient samples would enhance the accuracy.

3.1.6 Analysis of the fragment kinematics

3.1.6.1 General considerations

The clinical evaluation of the fragment displacement after accident is important to define the surgical treatment. Generally, the quantification of the fragment dislocations is done according to the clinical evaluation. In the work of Greiner et al., the relative position of the greater tuberosity is measured in respect to the already inserted prosthesis [66] (Figure 43). The greater tuberosity displacement was detected two-dimensionally by the distance “a” in the frontal view. Two horizontal tangents to the prosthesis head and to the superior tuberosity edge were placed, the distance “a” is determined. This distance is called as well “HTD”; Head-to-tuberosity distance. To determine the displacement of the lesser tuberosity, the medial shift is analysed in a top view, by measuring the interfragmentary distance “c”.

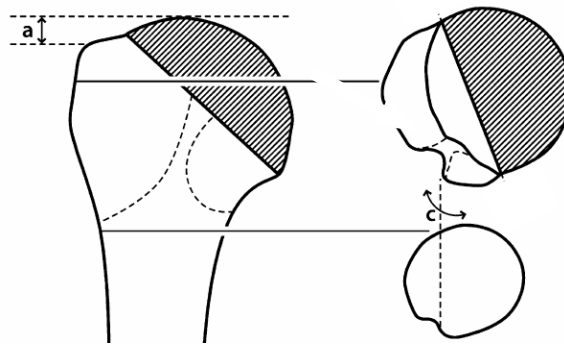


Figure 43: Tuberosity positions relative to the prosthesis [66].

The analysis of a secondary displacement of the tuberosities after surgery is difficult. Fragment displacement is superimposed by the effect of a simultaneous bone resorption, as described by Pijls et al. [85]. Missing landmarks make it difficult to determine resulting fragment distances relative to a fix-point. Plausinis et al. documented a superior shift of the greater tuberosity fragment for single cases [157].

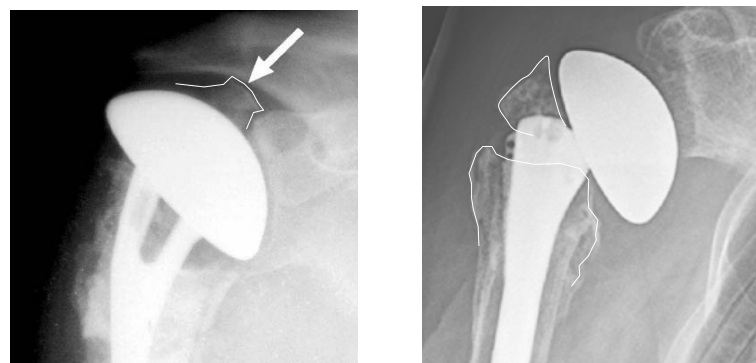


Figure 44: Proximal fragment displacement of the tuberosities (left, Pijls et al. [85]) and fragment resorption (right, Plausinis et al. [157]).

3.1.6.2 Measurement of the fragment displacement

The fragment migration of the greater and lesser tuberosity relative to the humeral shaft was evaluated by a planar projection. Photographs were taken at a distance of 500 mm perpendicular to the scapular plane. An additional medial photograph in the scapular plane was taken perpendicular to the humeral shaft axis at a defined distance to the fracture. The focus of the camera was horizontally aligned with the humeral head rotation centre. The distal fragment borderlines of the tuberosities were used as a reference to evaluate the angulation and the distance relative to the humeral shaft. Since the titanium prosthesis and the humeral stem were rigidly fixed together, the stem-to-prosthesis assembly was used as reference system. The photographs were analysed after testing by a contour mapping done in Adobe Photoshop (Figure 45). The fragment borderlines in the surgical neck were manually traced by thin lines in order to determine their exact position. The rotation of the humeral shaft around its longitudinal axis, or the tilting out of the scapular plane were in a small range and had only a minor influence on the projected fragment distances. The present method was justified according to the error analysis (chapter 3.1.7).

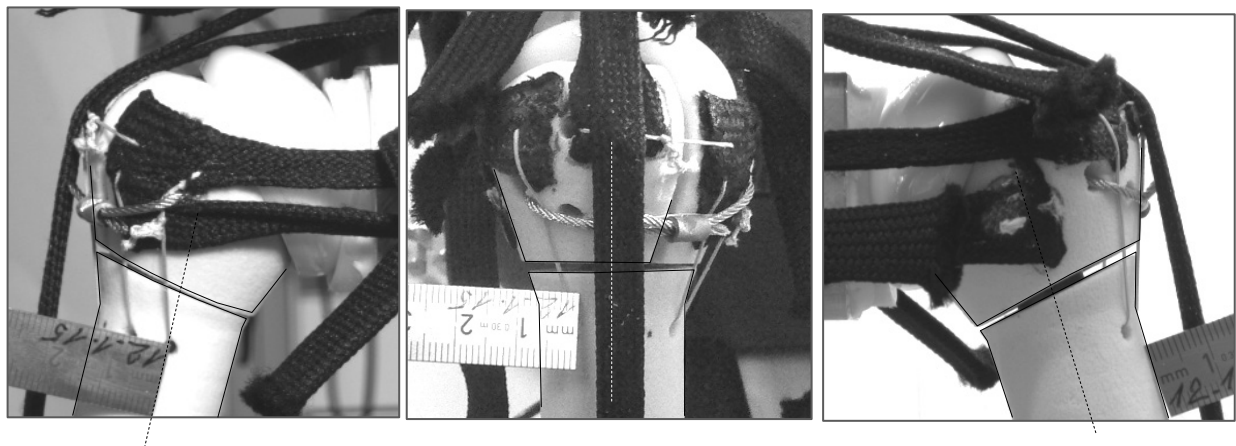


Figure 45: Contour mapping of the samples based on the photographs in three different planes at the humeral bone.

Fragment distance

The resulting interfragmentary distances were defined as the distance between two intersection points Q1 and Q2: Q1 was defined as the intersection between the central axis of the shaft and the distal border of the tuberosity. Q2 represented the intersection point between the central axis of the humerus and the proximal border of the humeral shaft (Figure 46). The uniform humeral shaft diameter of 25 mm was taken as a reference length to estimate the distances.

Angular displacement

The angular displacement of the fragments was defined as the angle between the first line (connecting medial and lateral edge of the tuberosity) and the second line (connecting medial and lateral edge of the shaft). An overview of the investigated variables is shown in Figure 47. The variables have been acquired in all three planes of the humeral coordinate system.

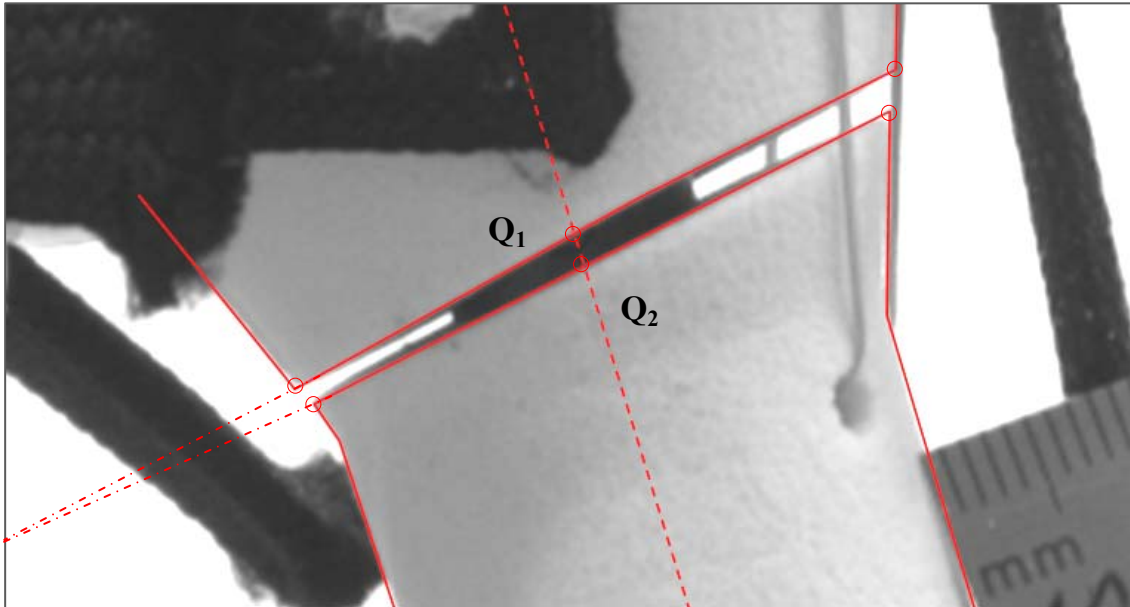


Figure 46: Magnification of the fracture line in the surgical neck.

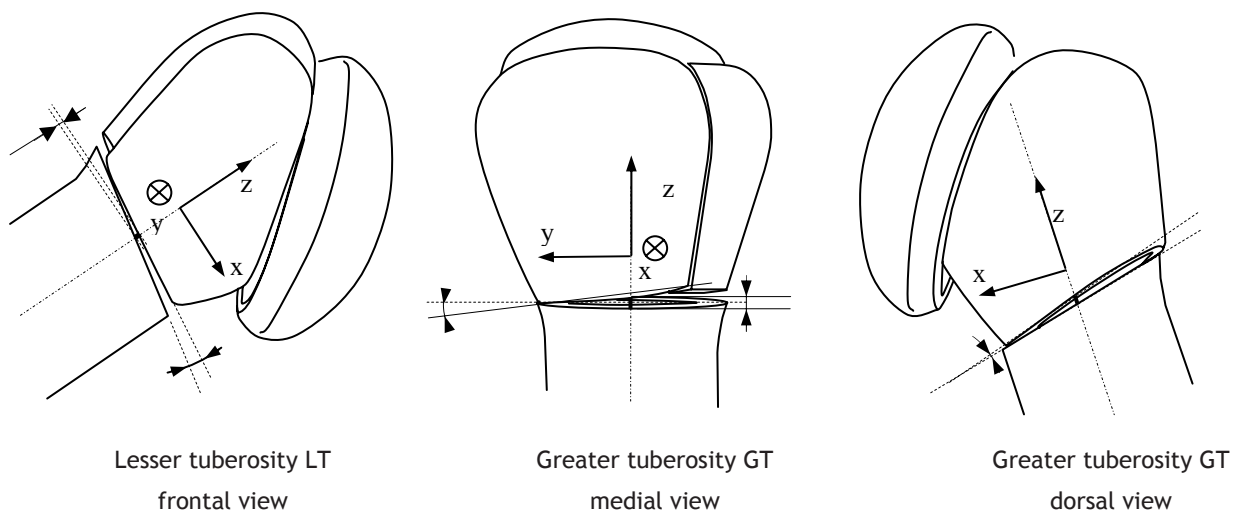


Figure 47: Scapular plane projection of the lesser tuberosity (left), medial view on the greater tuberosity perpendicular to the shaft (middle) and rear view on the greater tuberosity (right).

3.1.6.3 The migration rate

The fragment displacements were analysed for the first three cycles and the tenth cycle and displayed in a diagram. The slope of the line connecting the two maximum displacements after the first and the second cycle was taken as a reference for the increase in the fragment displacement. The slope of the linear regression of each single sample was displayed in a diagram (Figure 48). This characteristic value was defined as the “migration rate”, representing a value for the increment of the fragment displacement with subsequent loading cycles. The artificial bone model was compared with the human specimens by analysing the resulting migration rate for the same fixation techniques.

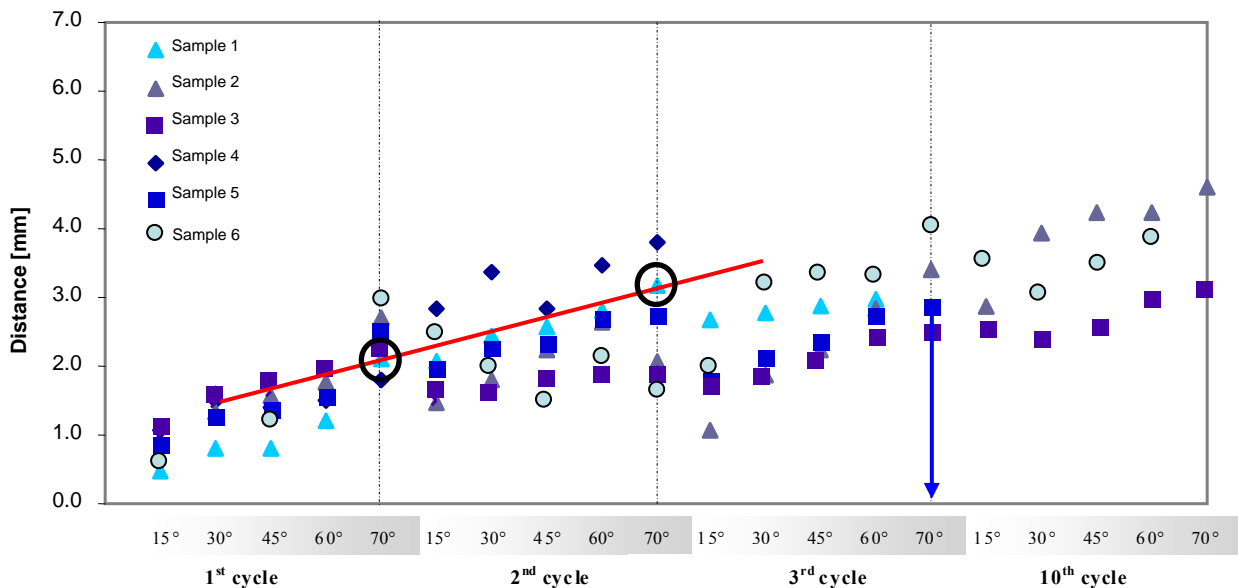


Figure 48: The migration rate is defined by the increase of the fragment distance per loading cycle, shown by the red line.

3.1.6.4 Failure criterion and loading cycles-to-failure

The described examination of the fragment distance is only valid if the humerus is positioned in the scapular plane. A humeral position which is tilted out of the projection plane leads to a distortion of the measured distances. A failure criterion was therefore defined to exclude tilted humeral out of plane positions. Failure of the reconstructed humerus was defined at a humeral tilt out of scapular plane of more than 10°. That position simultaneously reflected the abort criterion, by which the test was stopped. The accomplishment of the abort criterion was detected visually by means of a mounted, transparent slide.

The number of sustained loading cycles-to-failure was counted. Statistical analysis was performed by correlating the sustained loading cycles with each type of fixation technique using the Mann-Whitney-U-test.

3.1.6.5 Failure assessment of the fixation techniques

The failure assessment was performed by a visual observation of the examiner during the loading of the reconstructed proximal humerus. Additionally, video recording was analysed retrospectively to detect the initial sources of failure and subsequent failure mechanisms of the fixation technique.

3.1.7 Error estimation and reproducibility of fragment displacement measurements

The accuracy of the measured variables such as fragment distance and angulation is limited. Several errors influence the accuracy of the results; a combination of different error sources may lead to an error accumulation. First of all, a repetitive examination of the same observer, called the intraobserver variability, may negatively influence the accuracy. Furthermore, the comparison of two different observers may lead to contradicting results. A tilting of the fragments from the scapular plane has an influence on the measured fragment distance, if the described projection method is applied. All these errors may lead to high standard deviations. It is therefore important to quantify the single sources of error and estimate a total error.

3.1.7.1 Reproducibility of the fragment distance measurement

Intraobserver variability

The reproducible placement of the contour lines around the fragment edges has a limited accuracy. Measuring the corresponding distance with the Adobe Photoshop measurement tool influences the accuracy of the result. The total following assumptions were taken to estimate the total error:

- The placement of the fragment borderline varies due to the not sharp contours of the subject on the photograph. The thickness of the contour line is approximately 0.1 mm. This value does simultaneously reflect the inaccuracy of this method.
- The manual measurement of the distance using the Adobe Photoshop measurement tool negatively influences the correct result. Although the area of interest is magnified 5 times, the transition in the area of the not sharp contour cannot be accurately detected. An inaccuracy of approximately 0.1 mm has to be taken therefore into account.

Overall, the total intraobserver variability of data evaluation by the examiner is around 0.2mm (sum of both error sources). For an average fragment distance of 3 mm, a relative error of 6 % has to be expected.

Interobserver variability

Two different examiners evaluated two sequences of 20 different images each, measuring the fragment distance and angulation. A larger absolute fragment distance resulted in a smaller

relative difference between the examiners (Table 7). Furthermore, measured distances show less difference between the examiners in comparison to the values of fragment angulations. The results are as well displayed in diagrams in Figure 49.

#		15°	30°	45°	60°	70°	15°	30°	45°	60°	70°	15°	30°	45°	60°	70°	15°	30°	45°	60°	70°	Mean Diff. [%]
examiner 1	dist. [mm]	0.7	1.2	1.5	1.7	2.0	1.5	1.6	2.1	2.5	2.0	0.9	1.7	2.2	2.7	3.4	2.9	4.1	4.3	4.3	4.6	
	angle [°]	3.0	6.0	6.0	6.0	7.0	6.0	6.0	8.0	9.0	9.0	5.5	6.0	10.0	10.0	12.0	13.0	13.0	14.0	17.0	15.0	
examiner 2	dist. [mm]	0.9	1.3	1.6	1.8	2.1	1.5	1.8	2.2	2.7	2.1	1.1	1.9	2.2	2.9	3.4	2.6	3.4	4.2	4.2	4.6	0.14
	angle [°]	2.0	5.0	5.0	5.0	5.0	4.5	5.5	10.0	10.0	7.5	3.5	7.0	8.0	8.5	12.0	11.0	14.0	15.0	16.5	16.0	

#		15°	30°	45°	60°	70°	15°	30°	45°	60°	70°	15°	30°	45°	60°	70°	15°	30°	45°	60°	70°	Mean Diff. [%]
examiner 1	dist. [mm]	1.0	1.5	1.6	1.8	2.1	1.5	1.5	1.7	1.8	1.9	1.6	1.7	2.0	2.3	2.4	2.4	2.3	2.4	2.9	2.9	
	angle [°]	2.0	3.0	1.0	1.0	3.0	1.0	3.0	5.0	5.0	7.0	4.0	6.5	6.0	7.5	7.5	5.0	7.5	8.0	8.5	8.5	
examiner 2	dist. [mm]	1.50	1.80	1.30	1.60	1.90	1.20	1.20	1.70	1.70	1.70	1.50	1.50	1.60	2.30	2.40	2.00	2.30	2.00	2.60	2.60	0.14
	angle [°]	0.50	2.00	1.00	1.00	1.00	2.00	2.00	3.00	4.00	5.00	3.00	4.00	4.00	5.50	5.50	5.00	5.00	6.00	6.00	7.00	

Difference 1-2 [%]		15°	30°	45°	60°	70°	15°	30°	45°	60°	70°	15°	30°	45°	60°	70°	15°	30°	45°	60°	70°	Mean Diff. [%]
dist. [mm]		0.20	0.09	0.05	0.03	0.05	0.00	0.12	0.06	0.06	0.03	0.16	0.09	0.01	0.05	0.00	0.12	0.21	0.02	0.02	0.00	
	angle [°]	0.3	0.2	0.3	0.1	0.1	0.2	0.2	0.0	0.1	0.1	0.1	0.2	0.2	0.0	0.0	0.2	0.0	0.2	0.1	0.1	

Table 7: Comparison of two displacement sequences, analysed by the two examiners.

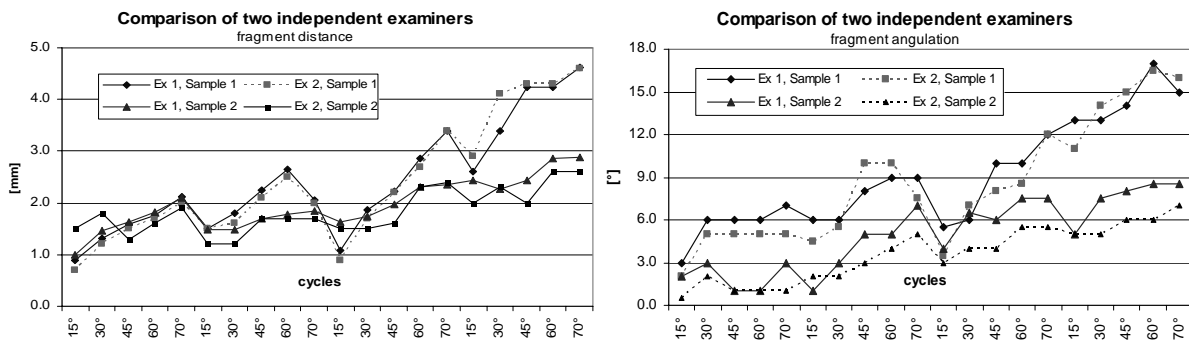


Figure 49: Comparison of the two measurements by different examiners comparing the results of the distance (left) and angulation (right).

The mean difference of the examined fragment distances lies in a range of 7 %, whereas an overall difference of 14 % is detected for the fragment angulation measurements. No statistical analysis has been performed for this analysis.

3.1.7.2 Projection error of the distances

By capturing photographs of the humerus, the fragment displacements can be measured reliably as long as the longitudinal axis of the humerus remains in the scapular plane and the camera is focused perpendicularly to the humeral axis. If this is not the case, distortion of the real lengths may negatively influence the correct distance measurements.

Measurement error due to displaced camera position

The measured fragment distance does not represent the real length, if the horizontal alignment of the camera is not perpendicular to the area of the fragment distance (Figure 50). During testing of a 15° to 70° abduction angle, the region of interest where the distance is determined rotates around the head centre and at the same time shifts approximately 20 mm superiorly. The effect of this rotation onto the projected fragment distance can be calculated by a trigonometric equation. With a camera distance of 500 mm, the projected distance after abduction is 6 % smaller in comparison to the real fragment distance.

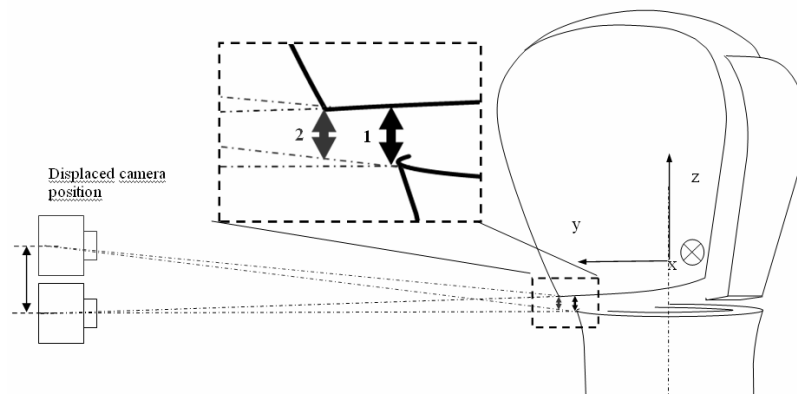


Figure 50: Camera position out of the horizontal plane. Distance 1 represents the real fragment distance; distance 2 (shown in red) is the projected distance.

Measurement error due to out of plane position of the humerus

The maximum humeral deflection out of the scapular plane is 10° at the point of the stop criterion. This maximum tilting angle was taken as a basis to determine the projection error (Figure 51). Trigonometric calculations give a resulting relative error of 6 % of the measured fragment distance.

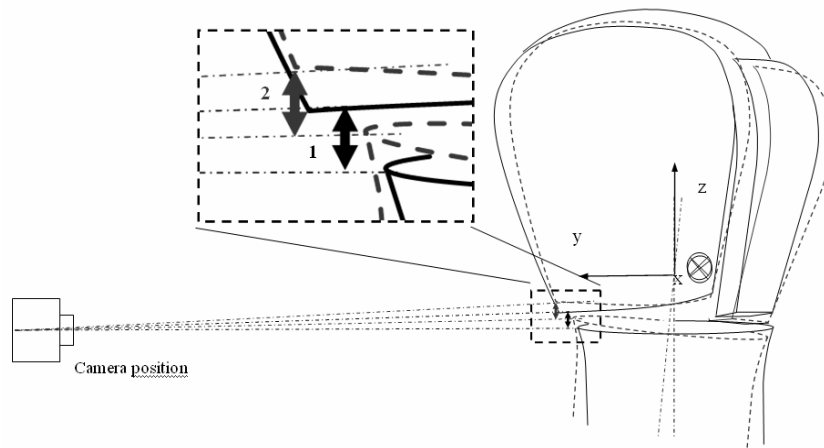


Figure 51: Humeral tilting out of the scapular plane. Distance 1 represents the real fragment distance; distance 2 (shown in red) is the projected distance.

3.1.7.3 Total error according to Gaussian error estimation

To calculate the total error with the single independent errors, a Gaussian error estimation was performed. For independent relative errors, the overall error according to Gauss is defined as:

$$u_y = \sqrt{\left(\frac{dy}{dx_1} \cdot u_1\right)^2 + \left(\frac{dy}{dx_2} \cdot u_2\right)^2 + \dots}$$

u_y : total error

y : calculated end value

x_1, x_2 : measurement values

Assuming a linear correlation between the measurement value and the calculated value, the formula can be simplified:

$$u_y = \sqrt{u_1^2 + u_2^2 + u_3^2 + u_4^2}$$

u_1 : intraobserver variability (10 %)

u_2 : interobserver variability (10 %)

u_3 : projection error (camera position) 6 %

u_4 : projection error (humeral tilt) 6 %

$$u_y = \sqrt{2 \cdot 0.06^2 + 2 \cdot 0.1^2} = 0.13 \sim \mathbf{13 \%}$$

In summary, the estimated error of the projection and of the reproducibility results in an estimated total error of 13 %.

3.1.7.4 Comparison with calliper measurements

The projection method was compared to manually performed calliper measurements (Figure 52). The calliper was held parallel to the longitudinal axis of the humerus. It was not possible to measure interfragmentary distances below a value of 0.5 mm.

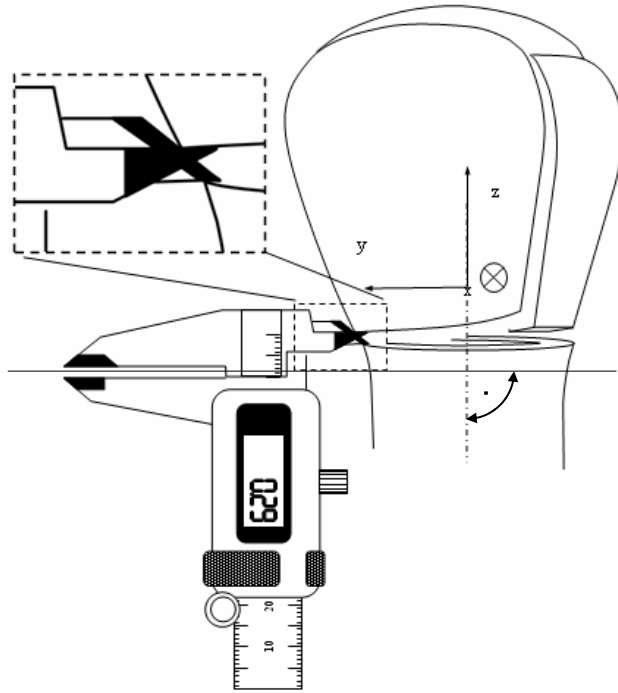


Figure 52: Calliper measurements analysed the distance between the fragments in z-direction.

The results for the calliper measurements show similar curve progression and differ from the projection method in Chapter 3.1.6.2 by around 15% in average.

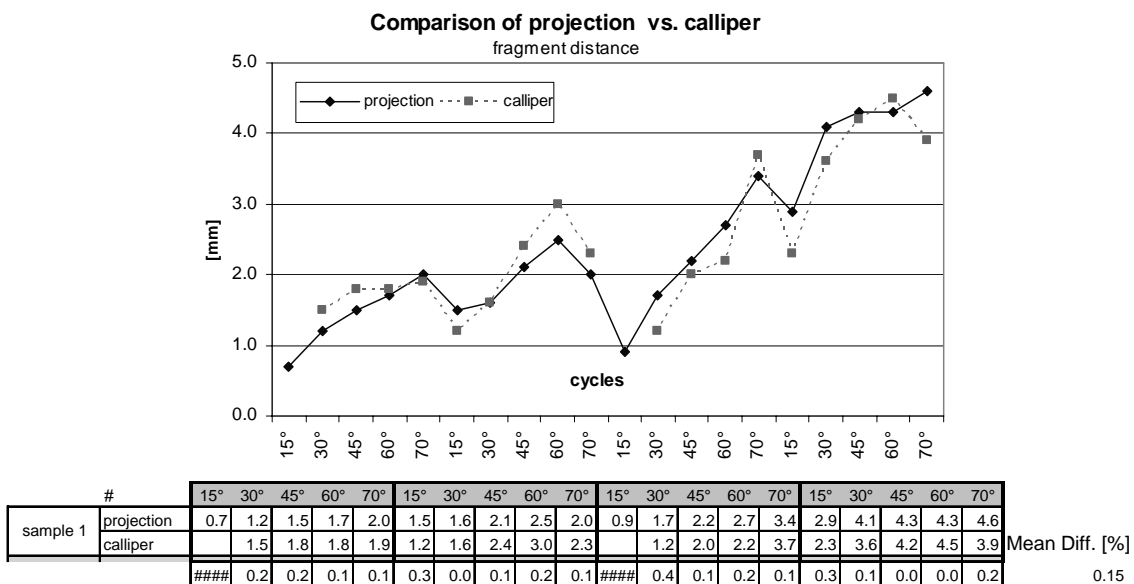


Figure 53: Comparison of projection method with calliper measurements for one series of measurements.

The data, however, have finally been acquired by the projection method for all measurements and not by the calliper method.

3.2 Finite Element Analysis of proximal humeral fixation

3.2.1 Introduction

The Finite Element Analysis (FEA) allows visualising the physical behaviour for a given geometry under predetermined loading conditions. This information is helpful to investigate implant-to-bone interactions and is able to visualise local stresses and deformations during loading. Few studies have used Finite Element Analysis to analyse the fractured proximal humerus during loading. Maldonado et al. considered the reconstruction of the fractured proximal humerus by osteosynthesis plates and screws in comparison to intramedullary nailing [158, 159]. The fracture was modelled in the surgical neck; the reconstructed humerus was loaded by a compressive force. In another study by Gupta et al. and Buchler et al., the glenohumeral load transfer to the articulating surface during abduction was analysed by FEA [160, 161]. To our knowledge, no study exists up to now which investigates different fixation techniques at the proximal humerus by using muscular load introduction.

One of the goals of the present investigation is the development of an FEA model that allows optimisation of existing fixation techniques in respect to enhanced fragment stability. In particular, FEA highlights the bone-to-implant interactions at specific regions of interest. In particular, the design of fixation techniques is optimised in order to reduce maximum stresses applied to the bone.

3.2.2 Material & Methods

The present FE study is based on a four-part fracture model of the proximal humerus. The four fragments comprise the greater and the lesser tuberosity, the humeral shaft and the humeral head (caput humeri). The caput humeri is replaced by the artificial surface of the artificial implant, whereas the GT and LT fragments were attached to the prosthesis. Three fixation techniques were studied and evaluated with respect to the displacements during loading and resultant stresses at the bone surface. The following assumptions were made for the calculations:

3.2.2.1 Implant and bone geometry

The implant geometry was built based on the Affinis Fracture Prosthesis (Mathys Ltd., Switzerland) [30]. The overall shape of the prosthesis middle shaft, the stem and the head were considered as one uniform rigid body model. The microstructure coating was not

simulated. The humeral proximal bone shape was chosen similar as described for the experimentally modelled humerus in chapter 3.1.2. A global coordinate system was set to define the orientation in the space: the z-axis of the coordinate system is collinear to the centreline of the cylindrical prosthesis shaft in cranial direction. The x-axis was medially directed in the frontal plane. As a result, the y-axis points dorsally.

An idealised four-part fracture model was simulated and built in CAD Unigraphics NX 4.0 according to Frankle et al. [162]. The humeral head fragment including the articulating surface is replaced by the prosthesis surface, whereas the greater and the lesser tuberosity fragment were attached by the fixation techniques. The fracture borderlines that divide the proximal humerus into the single fragments were designed using planes: The plane that defines the fracture through the bicipital groove, intersects with the central vertical axis of the prosthesis shaft and was rotated 30° around the positive z-axis. The plane defining the surgical neck fracture of the humeral head was rotated 15° around the positive y-axis (Figure 54). As a consequence, the fragments are not interlocked by a rough and uneven fracture zone.

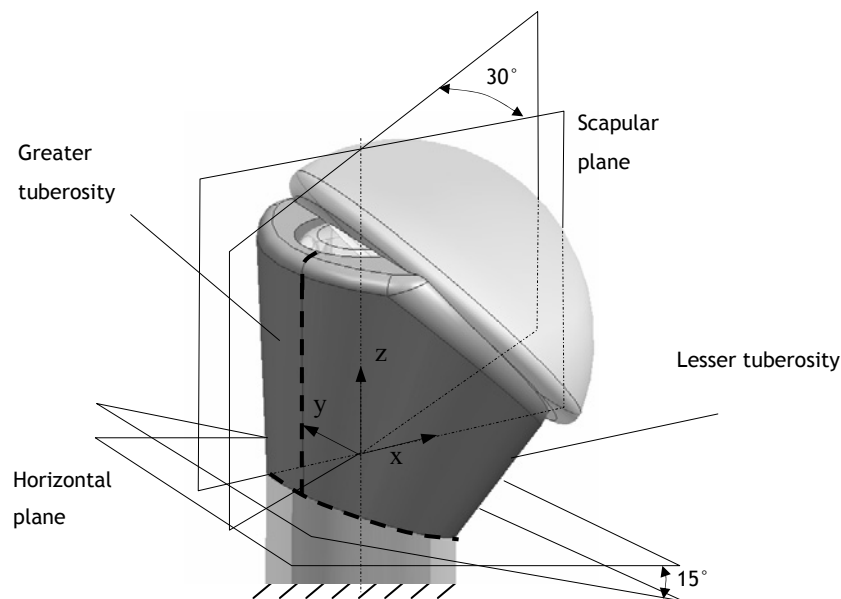


Figure 54: Geometry of the four-part fracture model on a left humerus according to Frankle et al. [162]

3.2.2.2 Fixation techniques

Three different fixation techniques were tested: Type A' consists of two horizontal cables around the greater and the lesser tuberosity, surrounding the whole fractured proximal humerus. Type B' comprises two cables, guided through anteroposterior holes of the prosthesis, located in the middle part. Type C' represents the novel design mentioned in Chapter 4.1.4 (Figure 55). It has been taken into account that the total cable length of each of

the fixation types did not vary in a great extent; total cable length was 220 mm for type A', 163 mm for type B' and 183 mm for type C'.

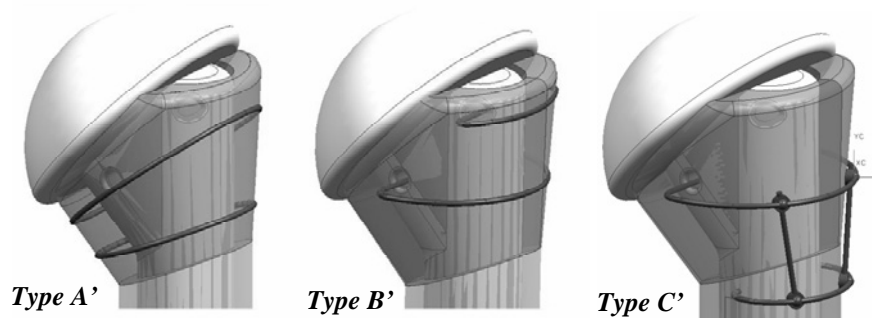


Figure 55: Fixation techniques around the fractured humerus: Type A': circumferential cables around the whole fractured proximal humerus, type B': cable guidance through the prosthesis middle part, type C': fixation of the tuberosities down to the shaft³.

These three models were compared with a control sample of a healed hemiarthroplasty. An ideal situation without fracture gap and with no cables around the bone was simulated. This circumstance represents an already integrated bone, which refers to an ideal postoperative result. A comparison of the healed sample was compared to the fractured samples with respect to displacements and stresses in the bone. To simulate the cable guidance on the bone surface, predefined grooves were modelled which did not allow a lateral shifting. The grooves had a depth of 0.5 mm which represented half the cable diameter (Figure 56). The concavity of the groove corresponds to the cylindrical shape of the cable; a perfect form fit was therefore defined between the cable and the bone interface.

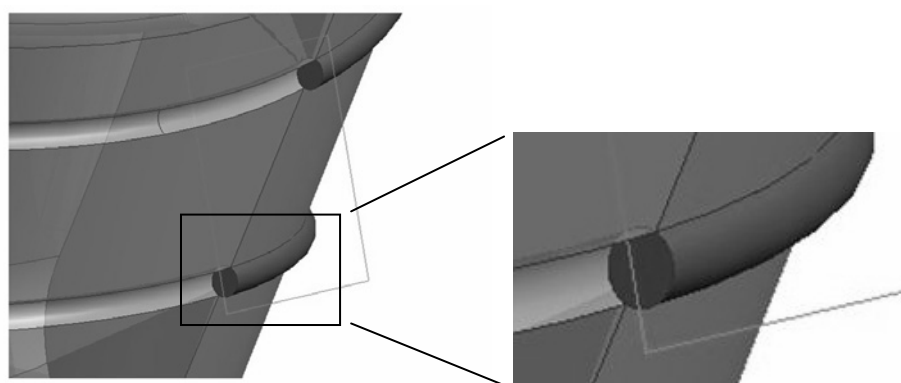


Figure 56: Cross section orthogonal to the cable direction. The cable guidance is shaped by a groove with a depth of half the cable diameter to prevent lateral shifting.

³ Fixation techniques B' and C' refer to the used fixation techniques B and C mentioned in the experiment in chapter 3.1.2.8 and 4.1.4. Fixation technique A' used in FEA does not correspond with technique A.

3.2.2.3 Material properties

The implant's middle part made of titanium and the ceramic head were considered as one rigid body. A cylindrical shape with a constant cross section was used for the humeral shaft. Cortical and cancellous bone material properties were taken from Orr et al. [163]; the elastic modulus of cortical bone $E = 6.0$ GPa, cancellous bone $E = 0.7$ GPa, the poisson's ratio was homogenously defined as $\nu = 0.3$. Neither subchondral bone layer nor articular cartilage and ligament structure were modelled. The steel cables were modelled according to the existing biomechanical experiments [75]. Although the used flexible cables consist of several filaments, a fully homogenous cross section was assumed. No pretension was applied. The assumptions were considered to be realistic, provided that no tissue adaptation occurs after tightening of the cable. No cerclage closing technique like knots or cable ends were simulated; the closed loop of the cable was simulated as a smooth transition. Therefore, relaxation effects induced by knots were not taken into account.

3.2.2.4 Loading conditions

The model represents a static arm position for a 30° glenohumeral abduction angle. The rotator cuff muscle supraspinatus (SSP) contributes to an abduction movement, whereas subscapularis (SSC) and infraspinatus (ISP) control an in-plane scapular movement and therefore act as lateral stabilisers. The absolute forces of 24 N for the SSC, 12 N for the SSP and 6 N for the ISP were applied to the fragments. They are consistent with calculated tensile forces at the rotator cuff by Van der Helm et al. [164]. All muscular forces pointed in positive x-axis. This assumption was made according to existing models such as by De Wilde et al. [75]. These data correspond to muscle forces of a free hanging, unloaded arm. Individual muscular forces were evenly distributed over the lateral surface of the greater and lesser tuberosities and introduced on all surface nodes. The prosthesis shaft and the head as an entire rigid body was fixed by defining the displacements equal to zero. Therefore, it was not necessary to introduce a counteracting glenohumeral joint force at the prosthesis head to hold the system in equilibrium.

3.2.2.5 Finite Element calculations

Calculations for the continuum Finite Element Model were done by the MSC Nastran Solver. Cosmos Design Star v4.5 (Dassault Systèmes SolidWorks Corp.) was used as the pre- and postprocessor. The implant-to-fragment and cable-to-bone interactions were modelled

frictionless. These conditions refer to an initial postoperative situation, where no osseous bonding on the prosthesis surface is generated. As a consequence, the only parameters that prevent a tuberosity dislocation are the cerclages around the fragments and the geometric form fit at the prosthesis-to-fragment interface. Due to the fact that the greater tuberosity embraces the prosthesis to a greater extent, the displacement is expected to be less in comparison to the lesser tuberosity.

A tetrahedral mesh was used with a total number of approximately 50'000 linear elements and 80'000 nodes. The influence of a refinement of the mesh (increase of the amount of elements by about 20 %) on the resulting stresses was calculated for one case (Type A') and showed a negligible change.

As output parameters, von Mises stresses were calculated as well as the resultant displacements of the specified points P1 and P2 on the lesser tuberosity and P3 and P4 on the greater tuberosity surface (Figure 57). P1 and P2 were located 5 mm and 25 mm below the proximal end of the humerus, both in a distance of 10 mm anterior to the frontal plane. P3 and P4 had the same vertical distance to the proximal end of the humerus and were located in the intersection line between the frontal plane and the greater tuberosity fragment. Additional points located at the inner bone interface to the implant were analysed: P1' – P4' represent the projected Points P1 – P4 on the inner bone surface.

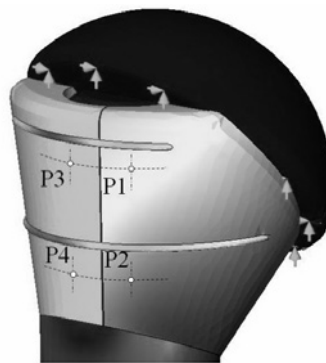


Figure 57: Illustration of the specific locations of data acquisition.

3.2.3 FE validation study using speckle interferometry

To validate our FE results, a strain mapping on the lateral bone surface using speckle interferometry was done (Limess Ltd, Germany). The same geometry as described in the FE model was chosen for the artificial bone model made of polyurethane foam (FR 6715, last-a-foam, General Plastics, Tacoma US, 0.24g/cm^3 , specified in ASTM F1839-97). A commercially available two-camera system (Figure 58) was used to carry out surface speckle interferometry.



Figure 58: Two-camera system (Limess GmbH, Germany).

The speckles were applied on the surface of the artificial bone with a black paint brushing (Figure 59). Local displacements were calculated with the Vic-3D-Software that calculates a vector displacement field of the single speckle dots using an iterative algorithm. In a post processing, strain values were calculated for the predefined locations P1-P4. Total $n = 3$ measurements were done with the fractured and with the healthy humerus.

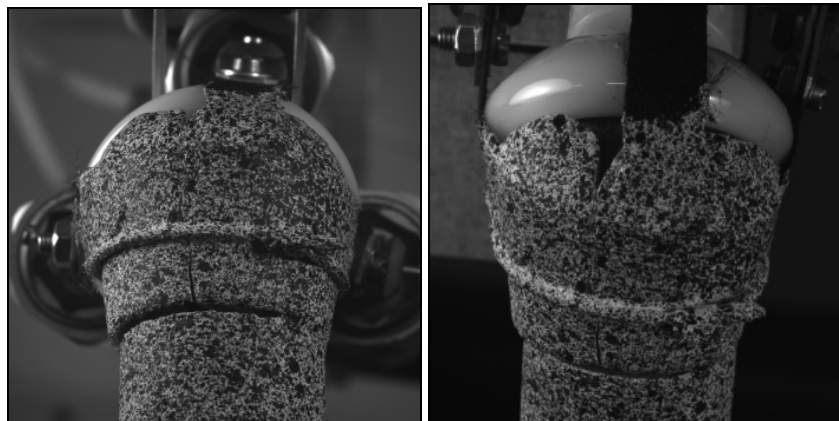


Figure 59: Speckles on the bone surface at the bone surface in a lateral view. Two different camera views (bottom and top view) are superimposed to visualise displacement on the surface.

The accuracy of measured strains is highly dependent on the size of the speckles. If refined speckles with smaller diameters are used, the accuracy of the strain distribution is improved.

4 Results

4.1 Results of the experimental testing

4.1.1 Applied muscle and contact forces

4.1.1.1 Muscle forces

The supraspinatus and deltoideus forces show a linear increase up to a force of 150 N at a maximum abduction angle of 70°. The infraspinatus and subscapularis/teres minor loading profile linearly increases up to a maximum force of 100 N at 70° of abduction (Figure 60 and Figure 61, red coloured lines).

In our testing, an initial glenohumeral contact force of 10 – 20 N at 15° starting position was measured for stability reasons. A complete unloading of the muscles would lead to luxation of the humeral head in the glenoid, because missing ligament structures and joint capsule do not provide additional stability.

4.1.1.2 Glenohumeral contact force

The glenohumeral contact force shows an overall linear increase up to a maximum force of 500 N at an abduction angle of 70°, seen in Figure 62. All maximum muscle forces of deltoideus, supraspinatus (2 x 150 N each) and infraspinatus/subscapularis (2 x 100 N), acting together, result in a maximum force application of 500 N which equals the maximal glenohumeral contact force.

4.1.1.3 Comparison with literature data

The comparison with existing data in literature covers a broad range of results. Mathematically calculated forces by simulation models and experimentally determined force progression curves are summarised in one diagram (mathematical calculations are shown in black, experiments in blue). The experimental models are already discussed in Chapter 2.2. Resulting muscular forces are dependent on the arm weight and the number of simulated muscles. The broad range of resulting forces is therefore explained by the variation of these variables.

Favre et al. used an iterative algorithm to equilibrate given external forces [148]. In total 27 muscles were simulated whereby supraspinatus, subscapularis and infraspinatus were divided into three main segments. Loading scenario was moment controlled with defined moments of 9 Nm in medial and lateral rotation for 30° of abduction angle. For an abduction angle of 30°, supraspinatus showed a total force of 85 N, the infraspinatus was approximately 50 N.

Karlsson et al. investigated static load sharing of muscles forces at 45° of abduction angle in the scapular plane [165]. Optimisation technique minimising the sum of squared muscle stresses was done. The simulation was done according to an existing model of Högfors [166]. In the model, the muscle elements followed the shortest path between the attachment points.

The analytical model of Oizumi et al. was based on anatomical data of a volunteer with a weight of 65 kg [167]. The muscular loads were defined as a percentage of the entire body weight. Primary active muscle fibres were approximated to a straight-line vector, which changed its direction in each abduction angle. Totally eleven muscle forces were rebuilt in a 3-D model. Supraspinatus was loaded with 10.9% BW at 60° of abduction in the coronar plane. Infraspinatus showed maximum values at 70° and 130° abduction of 8% BW, which refers to a force of 52 N. Subscapularis was loaded only with a BW of 1%, Teres minor showed 2.5 % BW at 130°. Totally 16 Muscles were considered in the inverse dynamic model of Van der Helm et al. [164]. Supraspinatus consisted of 6 elements; the subscapularis was as well divided up into 6 elements. No arm weight was applied during abduction.

Scepi et al. used a Solid Dynamics System SDM, a simplified ball and socket joint including a reversed dynamic algorithm to evaluate muscle forces [168]. At an abduction angle of 60°, a force of 160 N was measured for the infraspinatus, 165 N for the deltoideus and 125 N for the supraspinatus muscle. An overview is of all summarised studies in the diagrams is listed in Table 8.

Reference	Method	Lever arm and external weight	Number muscles	Muscular segments	GH-contact forces	General remarks
Favre 2005	Optimisation	0.3 m, 35 N	27 muscles	SSP 2,SSC 3 ISP 3,DELT 6	450 N @ 30°	Tendon excursion method
Karlsson 1992	Optimisation	1 kg hand load [Pheasant 1986]	19 muscles	SSC 2 ISP 3	550 N @ 45° 650 N @ 60°	Based on model of Högfors
Oizumi 2006	Static equilibrium equations	0.55m arm length, 65 kg, 3.38 kg	11 muscles	3 DELT,1 SSC 1 SSP,1 ISP	367N @ 95°	Lever arms based on anatomical data
Van der Helm 1994	Minimising sum of squared stresses	Van der Helm 1992	20 muscles	2 DELT,1 SSC 1 SSP,1 ISP	-	
Scepi 2006	Reverse dynamics	Arm weight 2.5 kg	7 Muscles	1 SSP, SSC, ISP, 3xDELT	165 N @ 60°	Program: Solid dynamics
Yanagawa 2008	Minimising sum of squared stresses	(Visible human male dataset)	11 Muscles	1 SSP, SSC, ISP, 3xDELT	575 N @ 112°	
Debsky 1995	Cadaver Study	3.5 kg	4 Muscles	m. DELT SSP, SSC, ISP	-	
Sharkey 1994	Cadaver Study	25 N, end of humerus	4 Muscles	m. DELT, SSP, ISP, SSC	-	Active deltoideus
Wuelker 1995	Cadaver Study	2.25 kg (3.2% BW),	4 Muscles	m. DELT, SSP, ISP, SSC	-	0.3 m arm lever arm
Present study	Cadaver/artificial bone	25 N	6 Muscles	m. DELT, SSP, ISP, SSC	350 N @ 60°	m. DELT : SSP 50:50%

Table 8: Shoulder models and boundary conditions from existing studies⁴.

Comparison of literature data with the present measurements revealed higher supraspinatus forces in present measurements, whereas the deltoideus is apparently below the range of the literature. The measured GH-contact force is as well smaller the mean values from literature, specifically at the beginning of arm abduction. These data are presented in Figure 62.

⁴ To display the results of different studies uniformly in one diagram, body weight data were converted into Newtons. Absolute values were considered because of the different orientation of the coordinate system in space.

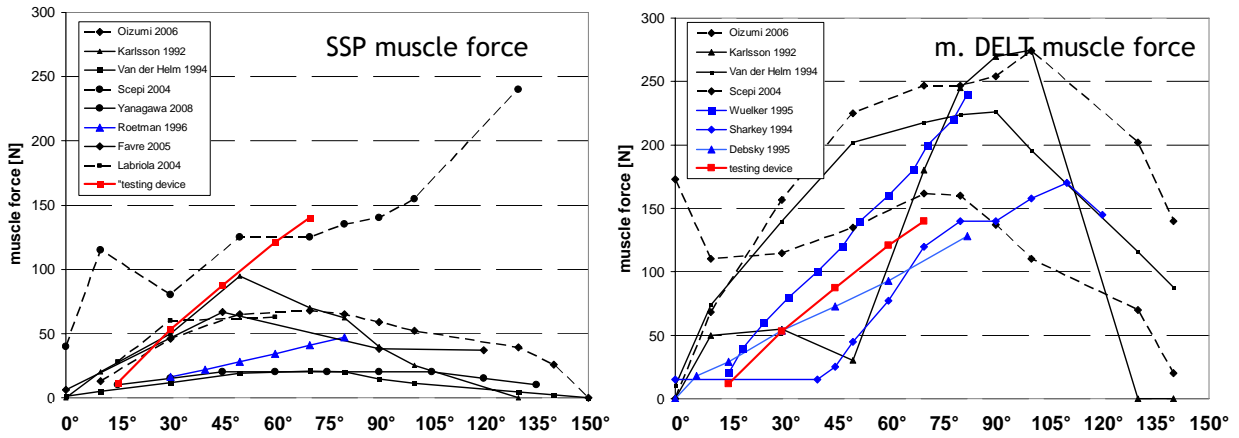


Figure 60: Force progression of the supraspinatus force (left) and deltoideus force (right) in comparison to the literature.

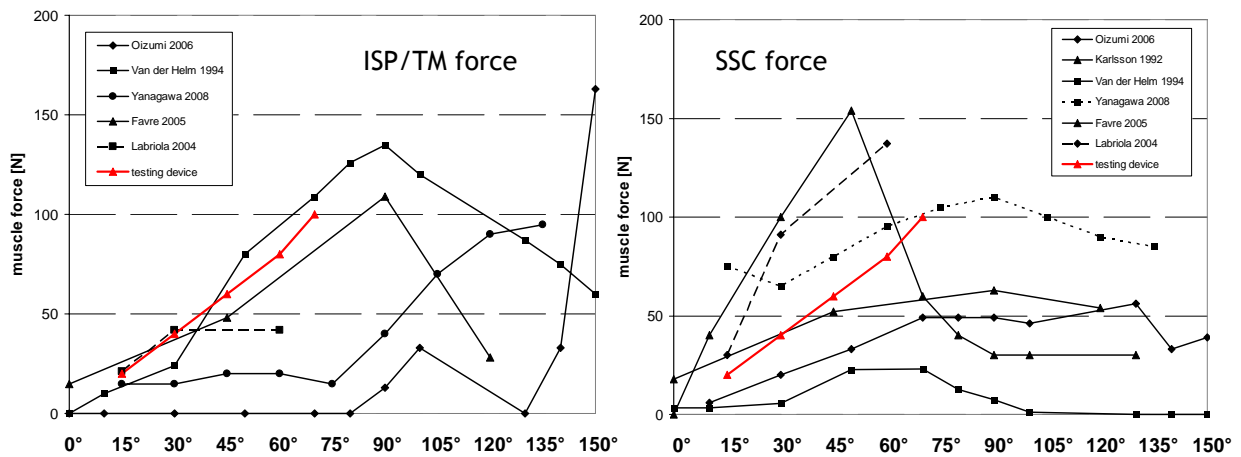


Figure 61: Force progression of the infraspinatus/teres minor force (left) and subscapularis force (right) in comparison to the literature⁵.

⁵ In literature, large area muscles are divided into several single segments, each representing slightly different orientation in space. The overall muscle forces of the supraspinatus and deltoideus were calculated by summarising the forces of the individual muscular segments. The resulting force was then calculated as a sum of absolute values and not by summarising the force vectors, which represents a massive simplification (they were not fully published in literature).

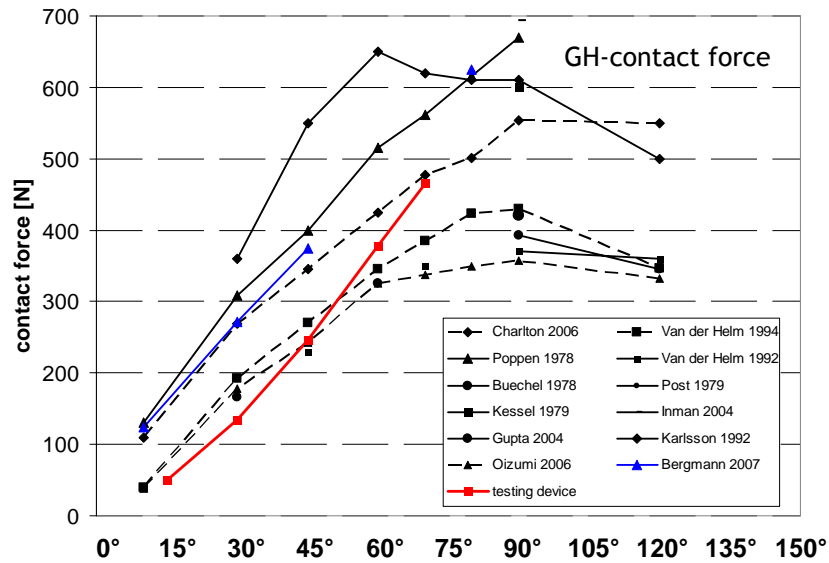


Figure 62: Force progression of the contact force in comparison to the literature.

4.1.2 Moment arms and translation of the rotation centre

4.1.2.1 Muscular moment arms

The muscular moment arm of the supraspinatus shows a constant value of around 25 mm with a slight decrease at the end of the abduction cycle. No characteristic curve progression is detectable, which is in agreement with Terrier et al. [169]. A higher variation in the moment arms has been detected in the study of Gatti et al., although only the values at an abduction angle of 30° and 40° are provided [170]. The muscular moment arm of the deltoideus is in the range of 20 - 30 mm, depending on the position in abduction. Higher values are seen in the study of Terrier et al. compared to our measurements, shown in Figure 63.

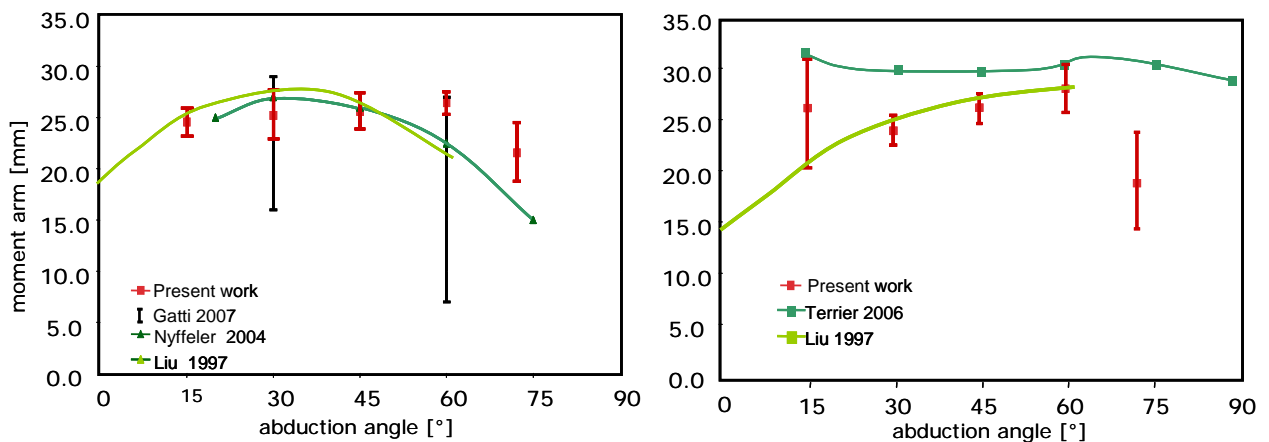


Figure 63: Muscular moment arms for the supraspinatus (left) and deltoideus (right).

4.1.2.2 Translation of the humeral head centre

Superior-to-inferior translations of the humeral head centre were detected ranging from -4 to 2.5 mm from 15° to 70° of glenohumeral abduction. The starting position of the humeral head centre of the first measurement was taken as the reference and simultaneous origin of the coordinate system. The two measured samples showed different characteristics of the curve, seen in Figure 64.

Terrier et al. calculated a superior-to-inferior translation of the humeral head centre ranging from -2 to 1.5 mm during glenohumeral abduction [169] by using a computer model. Resulting translation of the humeral rotation centre relative to the glenoid is therefore in a lower range compared to our result. This can be explained by the absence of the capsular ligaments in our model, which does provide additional stability under in vivo conditions.

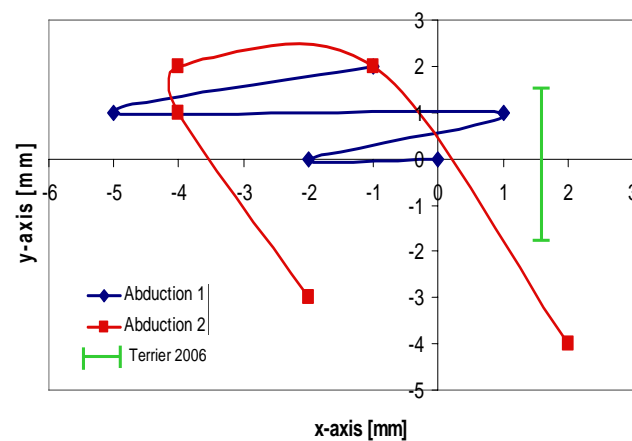


Figure 64: Translation of the glenohumeral head centre⁶.

⁶ It is to mention that no error analysis and no statistical evaluation were achieved; only two samples were measured.

4.1.3 Biomechanical failure assessment of existing fixation techniques

The general failure mechanisms were similar for all tested samples. Initially, a displacement of the fragments resulted due to increasing muscular load, leading to cutting of sutures into the bone. A steadily increasing fragment displacement resulted in a modified muscular load introduction at the proximal humerus, leading to an asymmetric load distribution at the proximal head. Subsequently, instability of the proximal humerus by a lateral tilting out of the scapular plane occurred (Figure 65). Several weak design aspects in the reconstructed humerus have been detected by analyzing the documented failure sequences. The reasons initiating instability were:

- Sutures cutting into the bone: For almost all fixation techniques, the suture cut in the humerus by plastically deforming the area in the predrilled holes.
- For fixation type A, the cutting effects of the suture were observed primarily in the fragments of greater and lesser tuberosity.
- For fixation type B, sutures cut through the bone into the proximal part of the humeral shaft. The metallic cable compressing the vertically oriented sutures against the surface of the fragments prevented a cutting through in the proximal part.
- The sutures cut in the bone parallel to the applied tensional force direction of the deltoideus and supraspinatus.
- In one sample (type B), a humeral shaft fragment was pulled out in the area of fixation. This failure resulted due to the complete cutting of sutures through the bone.
- In one sample (type A), a rupture of the supraspinatus tendon attachment was detected. Contrary to expectations, the connection did not fail in the tendon-to-bone interface. One fracture in greater tuberosity fragment occurred by pulling out the tendon and a glued part of the bone fragment. This sample was excluded from the further analysis.

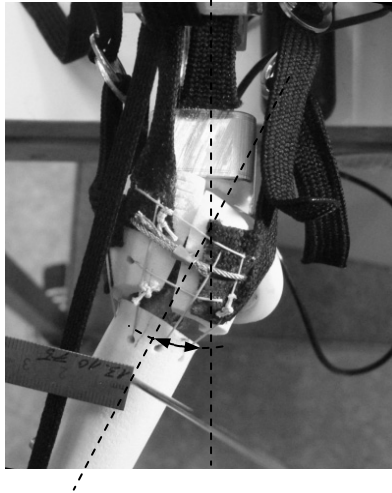


Figure 65: Instability of the reconstruction and subsequently displaced fragments resulted in a humeral tilting out of the scapular plane (top view).

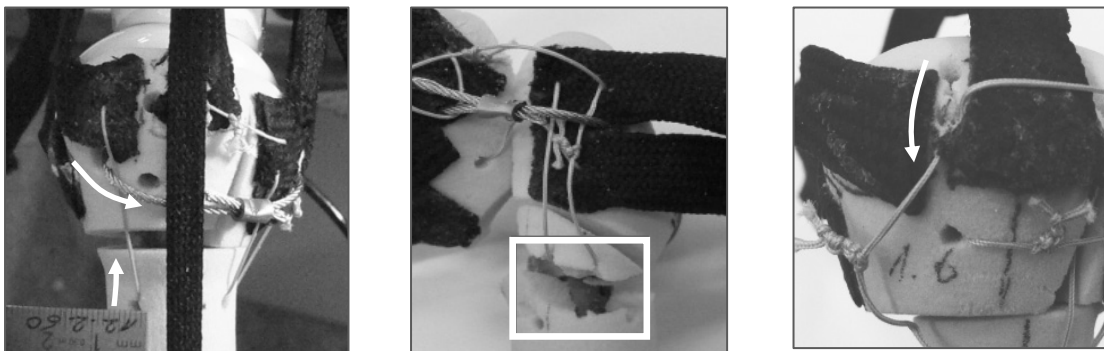


Figure 66: Failure of the fixation technique due to instability (left), fracture of the bone (middle) and cutting-in effect of the sutures (right).

As a conclusion, drilling holes in the bone should be reinforced to prevent any cutting-through of the wire (Figure 66) due to plastic deformation and subsequently leading to instability. This effect can be reduced by an evenly distributed load introduction of the sutures at the insertion holes. As a consequence, a novel design with a reinforcement of the drill holes, or a design without any drill holes should be considered.

4.1.3.1 Definition of the requirements for an optimised design

The results of testing the clinically established fixation techniques show that distinct technical requirements are necessary to provide biomechanical stability during the loading sequences. Specific (potential) advantages based on the examined failure mechanisms are hypothesized:

- Drilling holes which affect a sharp change of the cable or suture direction (at the insertion into the bone) should be avoided or reinforced.
- The presence of a bearing area at the suture or cable insertion into the bone could evenly distribute the transmitted shearing forces.
- Rigid connections, which are oriented parallel to the assumed loading direction or perpendicular to the fragment borderline, would provide stiff compression between the fragments.
- The ability of crossing or overlapping cables (due to different directions) in a variable angle on the bone surface would allow novel techniques.
- Preventing a line pressure on the bone surface or on the periosteum by distance holders is of advantage to prevent cutting effects.
- A punctually guided suture and cable on the spherical proximal humerus would prevent lateral slipping effects.

4.1.4 The novel fixation technique (Type C)

To meet the previously defined requirements, different concepts were collected and analyzed according to a systematic innovation process. The sketches and conceptual designs were evaluated in group meetings and workshops by using different searching algorithms.

The designed anchors had to be stabilized and fixed at a predetermined place on the bone surface. This was done by two circumferential wires around the bone and through the prosthesis, perpendicular to the longitudinal axis of the humerus. These horizontal wires applied a pressure to the two underlying bone anchors to fix them to the bone surface. In each case, two bone anchors are connected by two vertical wires to rigidly secure the fragments against a proximal movement. The present fixation is patented for different configurations; nevertheless, we were focussing on one solution illustrated in Figure 67.

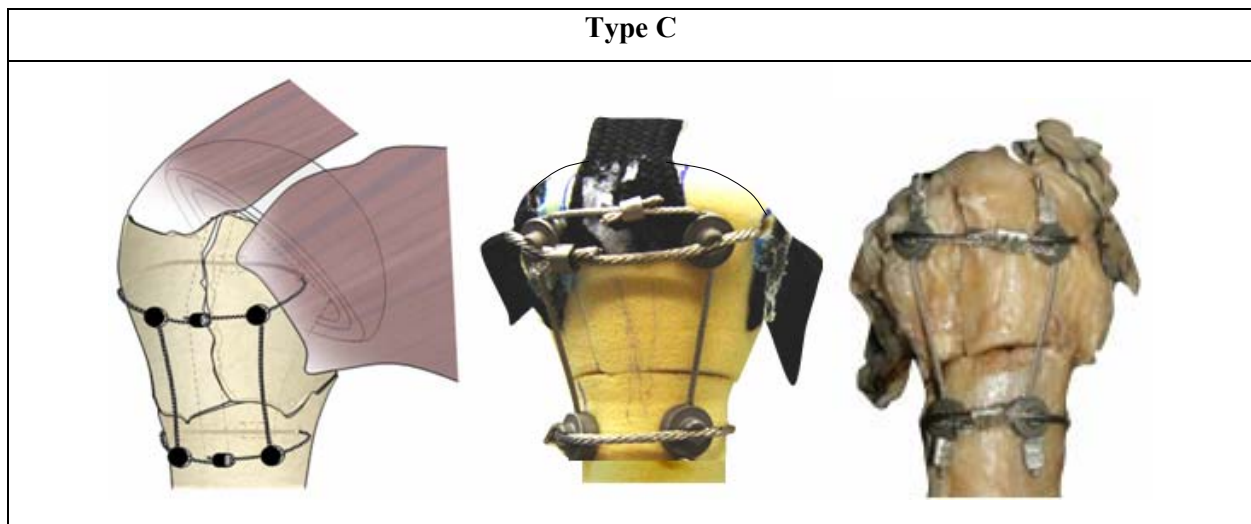


Figure 67: Cable fixation by using horizontally and vertically placed cables representing the novel design of Type C. Schematic view (left), artificial model (middle), human sample (right).

In a detailed view, the bone anchors provide longitudinal and perpendicular cable guidance. On the bottom side, three spikes with a length of 3 mm are inserted to prevent slippage on the bone surface. The diameter of the bone anchors is 8 mm (Figure 68).

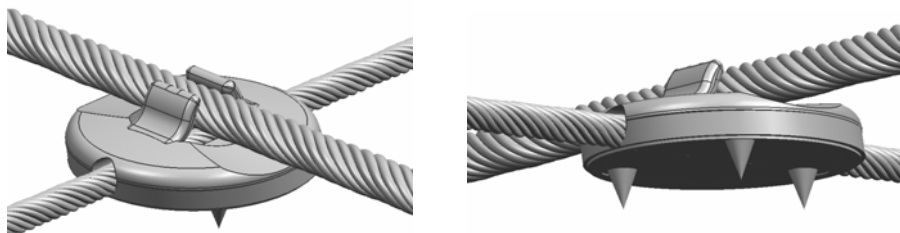


Figure 68: Design of the bone anchors to guide and cross the cables.

The placement of the bone anchors on the greater and lesser tuberosity fragment is visualised on a technical sketch in Figure 69. Each bone anchor is placed directly on the bone surface between the tendon insertions of the ISP and TM, and on the height of the SSC insertion.

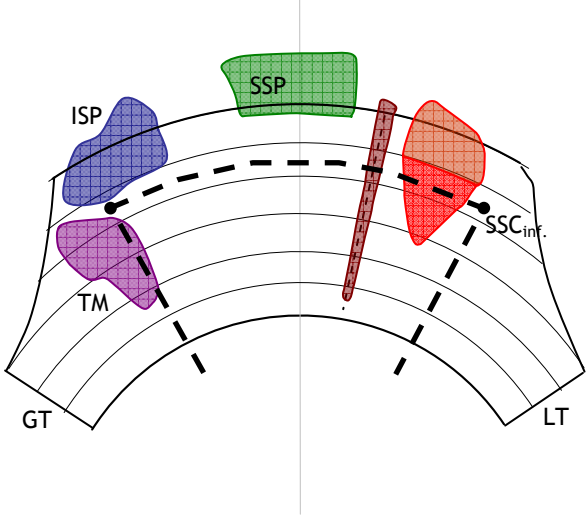


Figure 69: The placement of the bone anchors on the greater and lesser tuberosity fragment (black dotted line).

The design shown in Figure 70 enables different crossing angles of the cables due to a rotating clip on top of the bone anchor. The upper cable is secured by the clamping mechanism which prevents a gliding of the cable in direction of the cable direction.

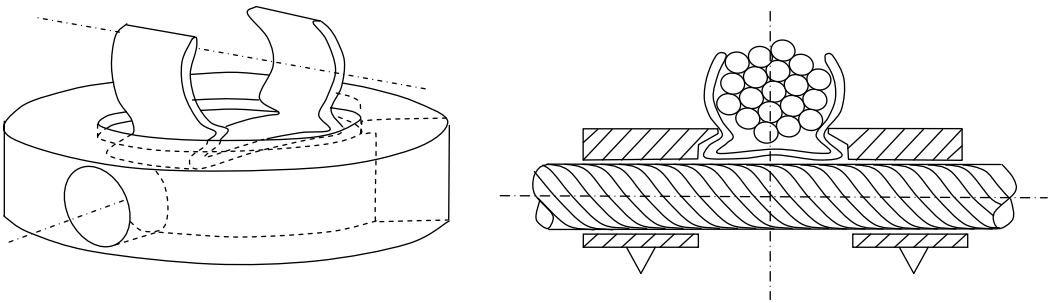


Figure 70: Concepts of bone anchors with multidirectional angulation of the cables.

4.1.5 Biomechanical performance of fixation techniques

4.1.5.1 Fragment kinematics for single plane abduction

Generally, an overall increase in the greater tuberosity (GT) displacement is observed during cyclic loading. The migration in proximal direction relative to the humerus shaft is detected for all fragments. Contradictory to expectations, no recovery or subsequent decrease of the fragment distance during unloading appeared. Measured interfragmentary distances are characterised by a linear increase until the stop criterion is reached. Two examples of a loading cycle during full abduction are shown for the different projection planes (Figure 71 and Figure 72).

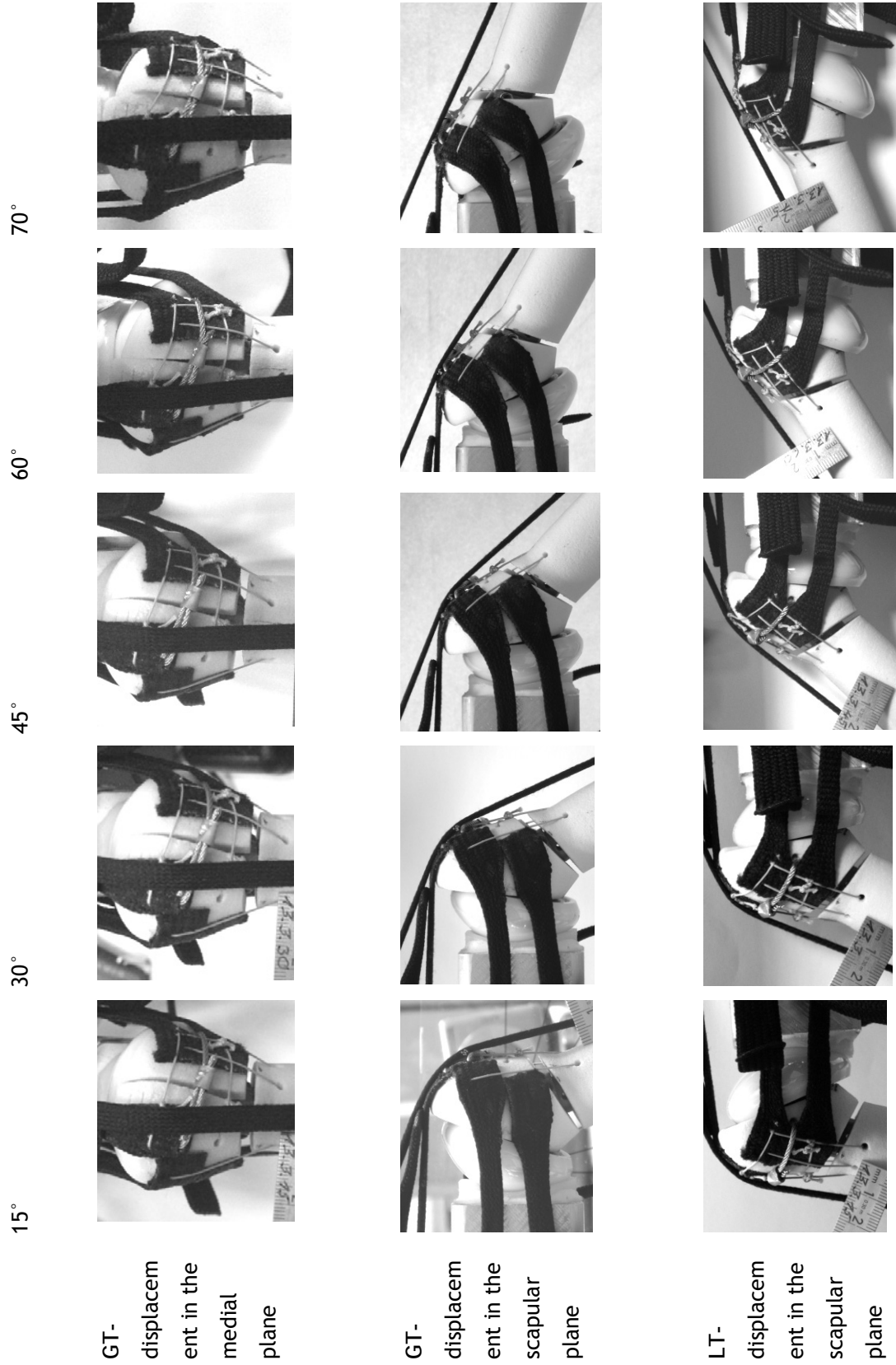


Figure 71: Abduction in the three planes of the humerus for the artificial bone samples.

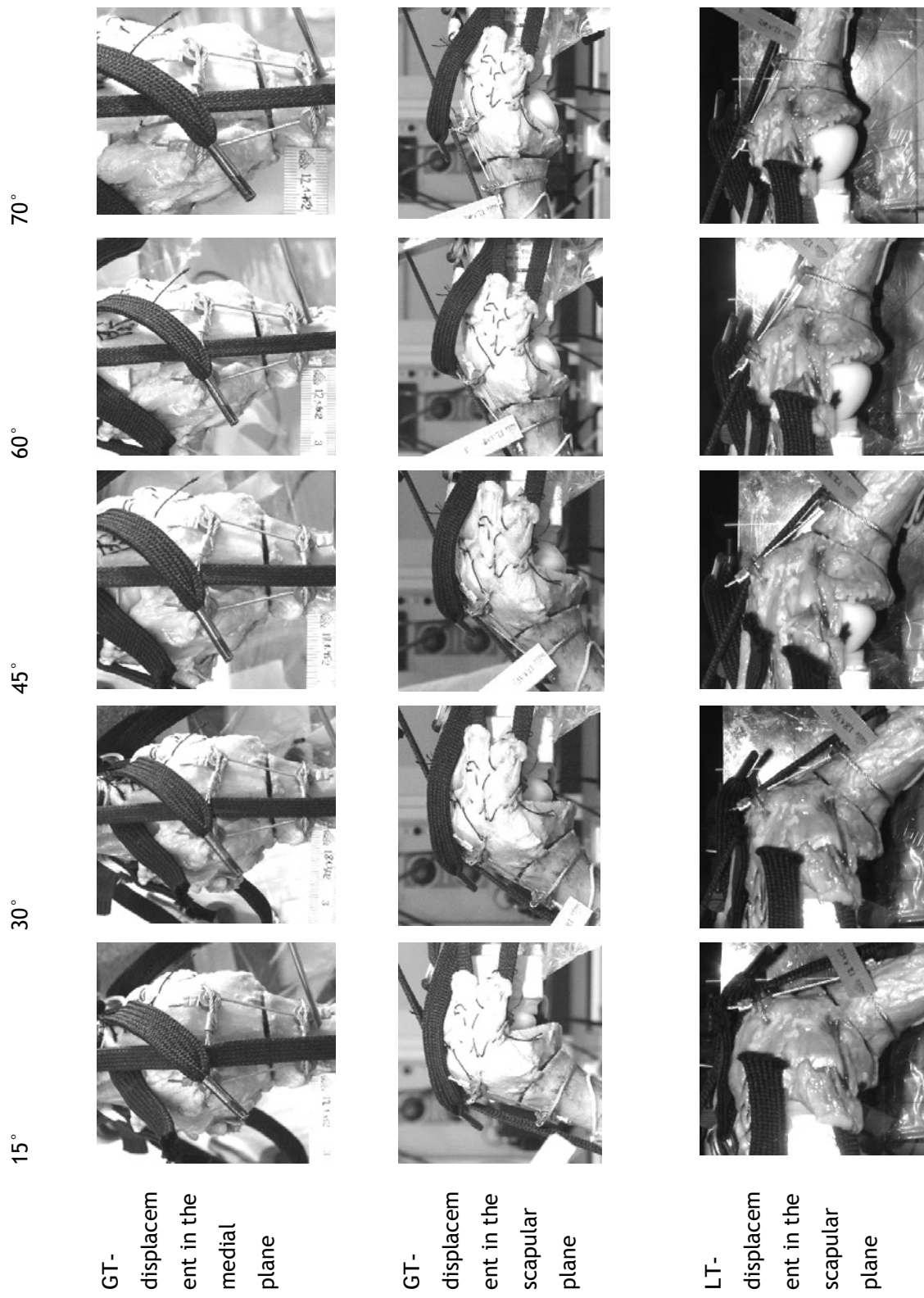


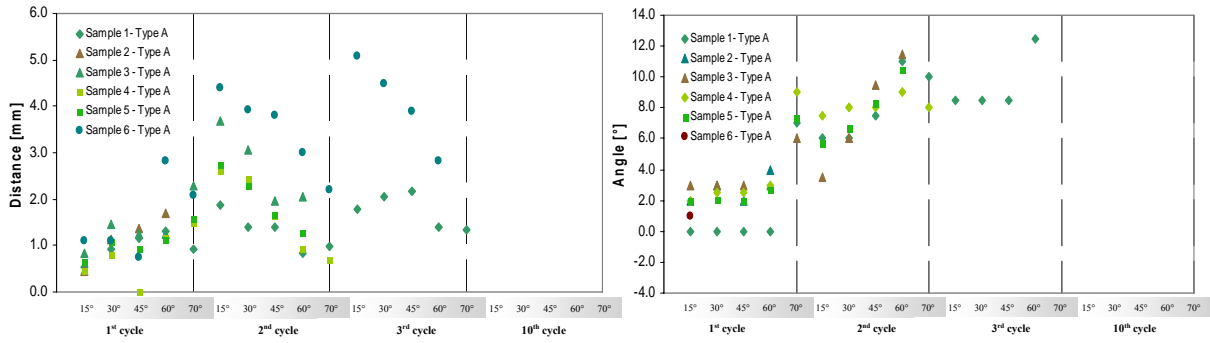
Figure 72: Abduction in the three planes of the humerus for the human bone samples.

Displacements of the greater tuberosity

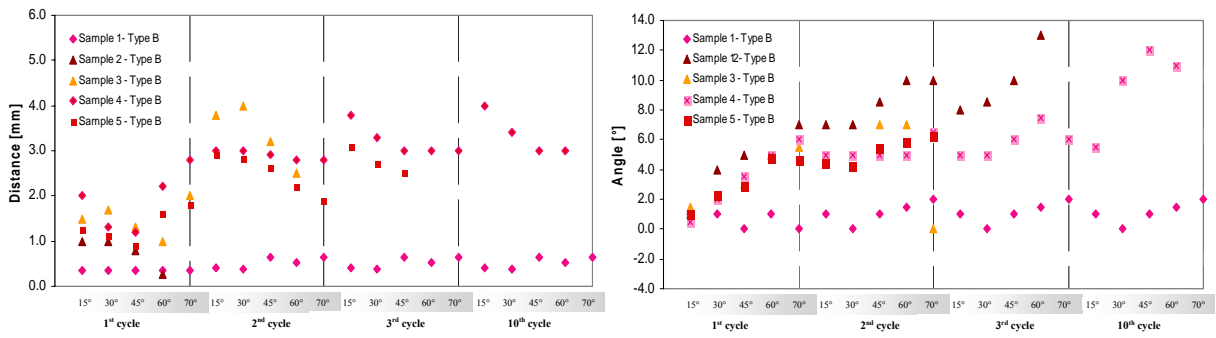
The greater tuberosity displacements in the scapular and medial planes are shown in Figure 73 and Figure 74.

For fixation type A and B, higher displacements in the scapular plane are seen for the greater tuberosity in comparison to type C. No differences were seen for the angular stability of the fragments. The increase of the greater tuberosity displacement in the medial view provides similar characteristics as in the scapular view for all three fixation techniques. This correlation is reasonable unless the projected tuberosity-to-shaft distance in the scapular plane influences as well the distance in the medial plane. The greater tuberosity-to-shaft distance for fixation types A and B is slightly reduced in the second cycle, which can be explained by the simultaneous increasing angulation of the fragment. No significant differences were seen in the angulation of the fragments, although type C tends to have smaller angular displacements.

Type A



Type B



Type C

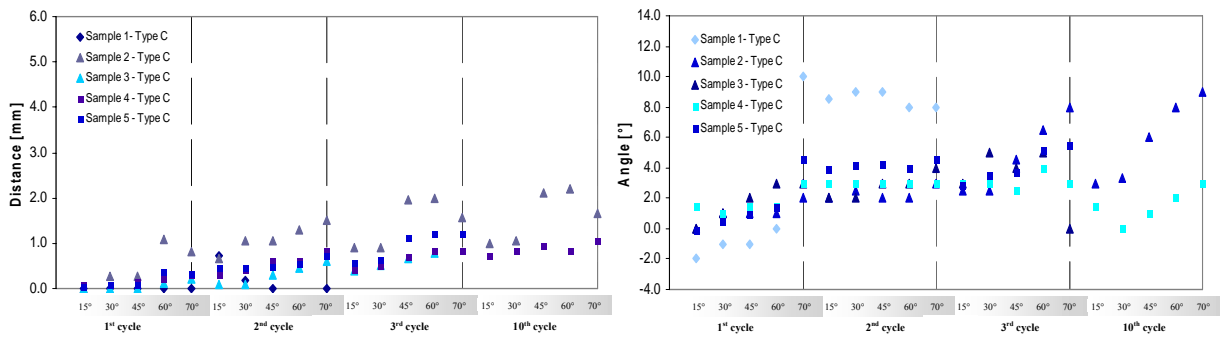
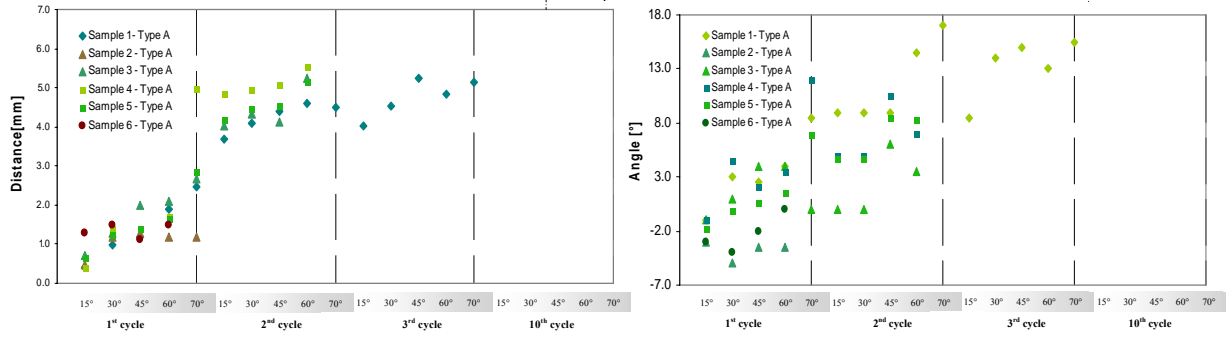
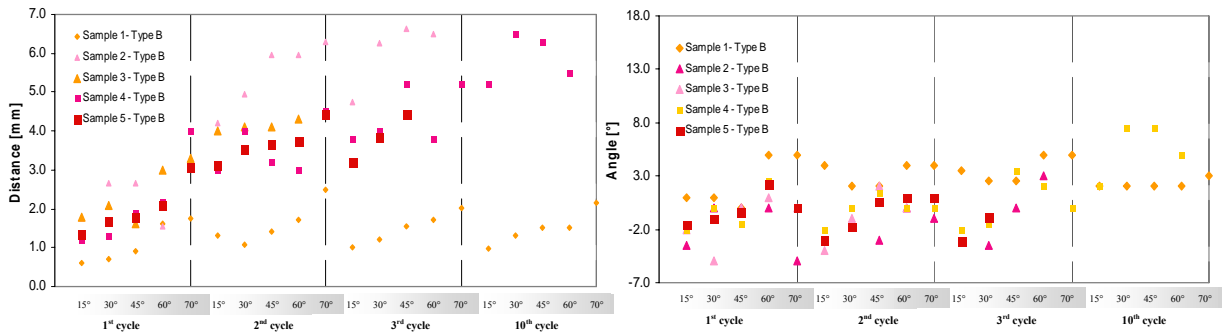


Figure 73: Greater tuberosity displacements in the scapular plane. Fragment distance is seen in the left column, the angulation in the right column.

Type A



Type B



Type C

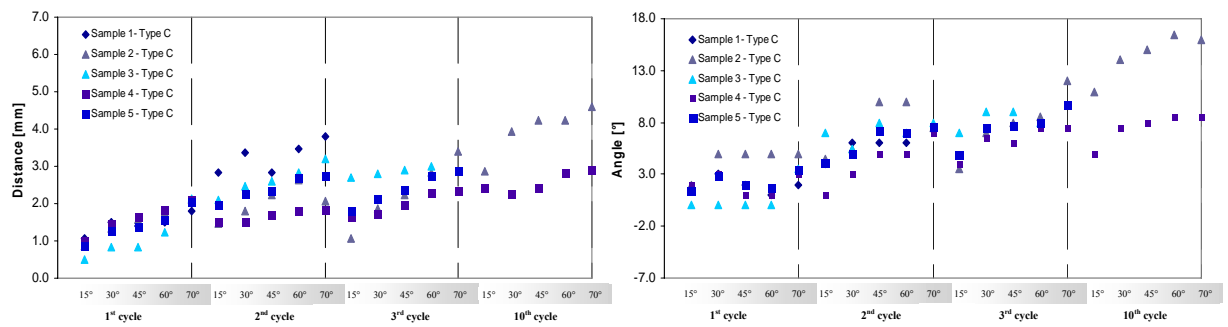


Figure 74: Greater tuberosity displacement in the medial plane. Fragment distance is seen in the left column, the angulation in the right column.

Displacements of the lesser tuberosity

The lesser tuberosity displacements in the scapular and medial planes are shown in Figure 75.

No significant changes have been observed for the lesser tuberosity-to-shaft distance with respect to the different fixation designs. The displacements remained stable in most of the tested samples and could not be used as a predictor to distinguish the stability of the reconstruction.

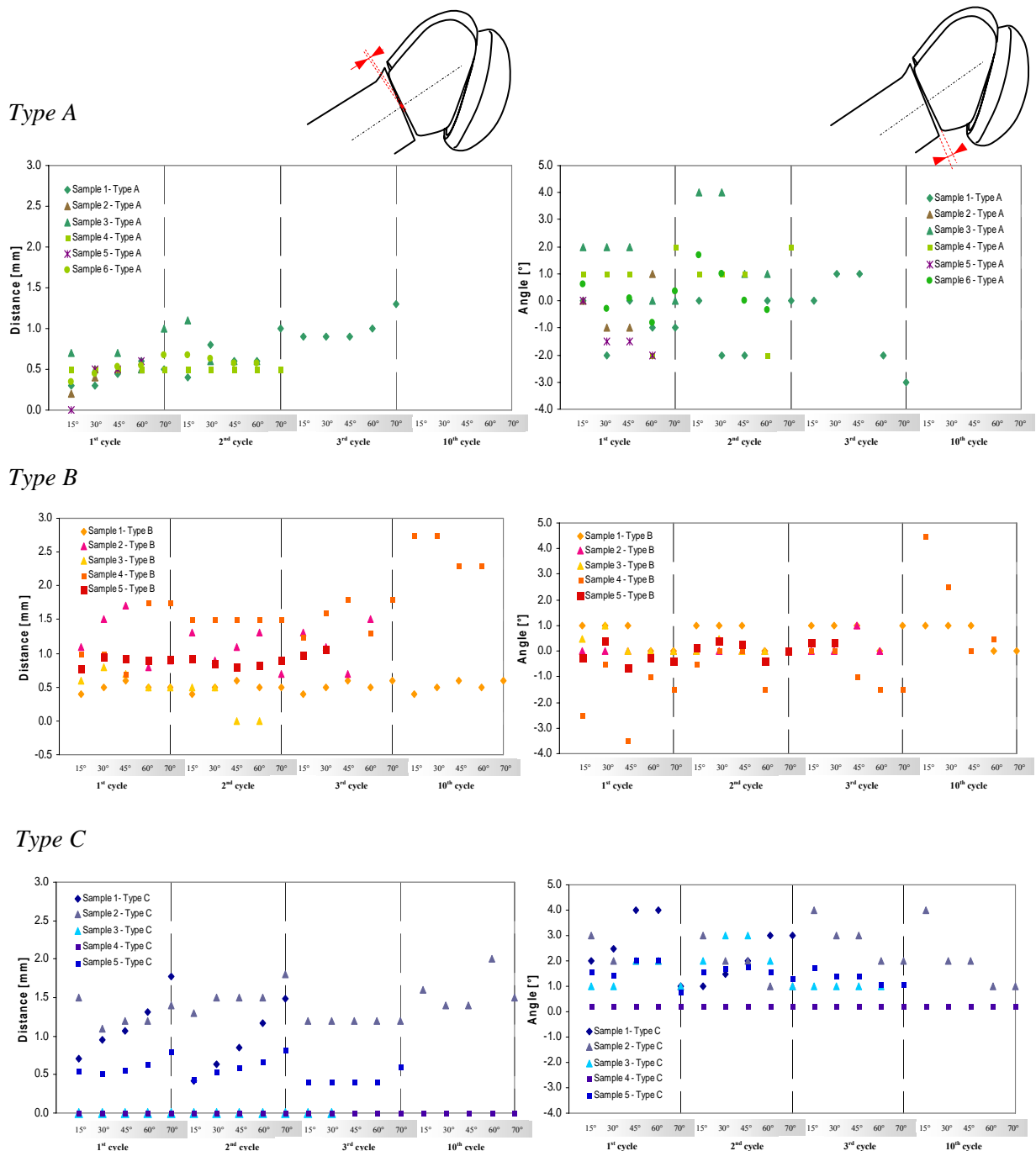


Figure 75: Lesser tuberosity displacements in the scapular plane. The fragment distance is seen in the left column, the angulation in the right column.

The fragment displacements for the first three loading cycles are displayed in Figure 76 for a better visualisation. The angulation and the increase in the distance of the greater tuberosity relative to the shaft are shown in the same picture for each loading cycle.

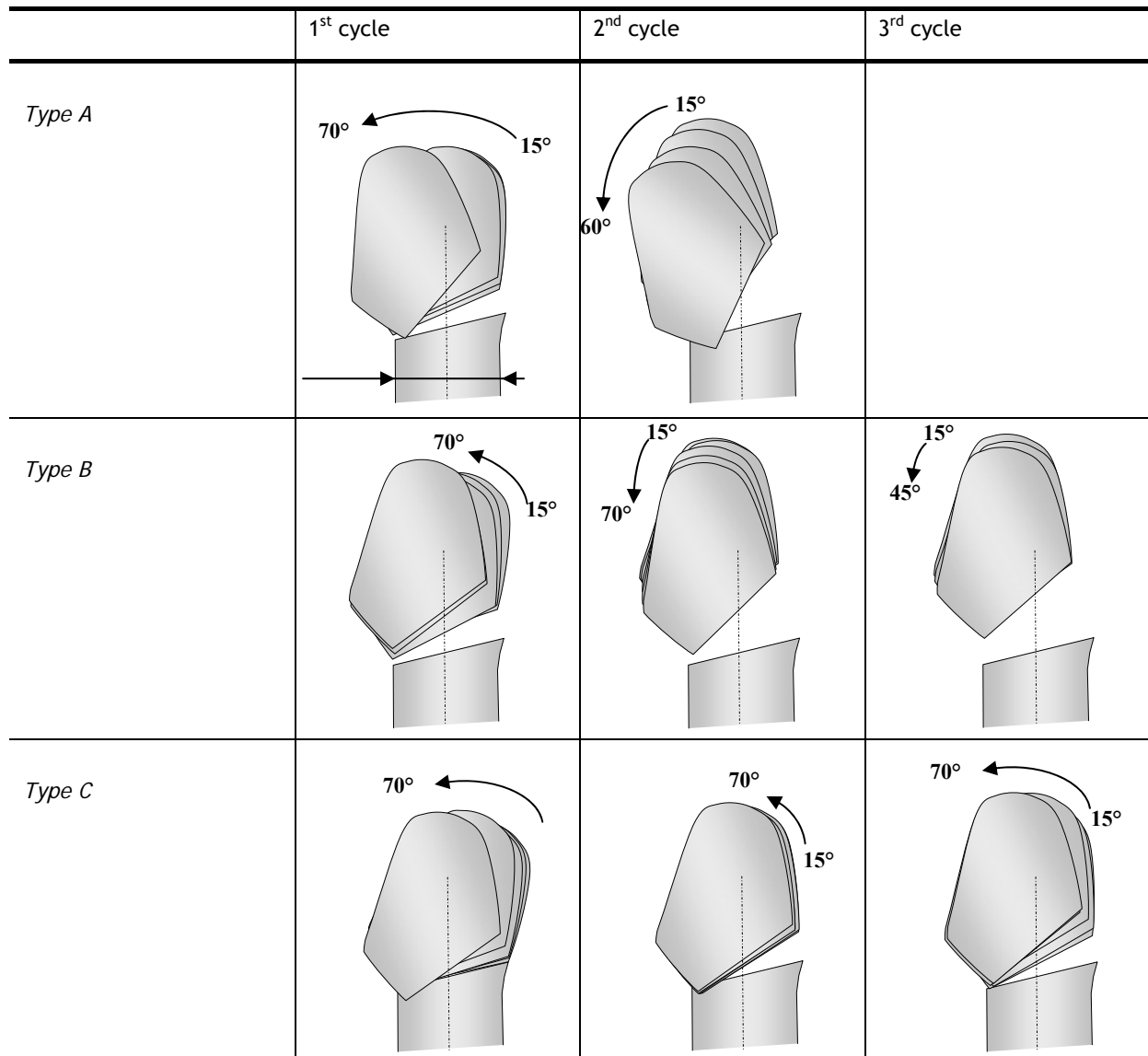


Figure 76: Fragment migration of the greater tuberosity in the scapular plane for the first three cycles.^{7, 8}
The constant shaft diameter of the humeral shaft can be taken as reference value (Ø 25 mm).

⁷ The angles and the displacements were multiplied with a factor of 5x for a better visualisation.

⁸ Rigid body translations and rotations are displayed; deformations of the fragments were not displayed. Therefore, intersections of the fragments with the shaft are illustrated, which did not occur during testing.

4.1.5.2 Fragment kinematics for internal and external rotation at a fixed abduction angle

The comparison of the two different loading sequences abduction vs. rotation at fixed abduction of 45° resulted in an increased displacement for abduction cycles (Figure 77). No failure occurred during these tests, the used weight was below the limit to damage the reconstruction. One specific fixation technique was tested (Type B, suture and cables).

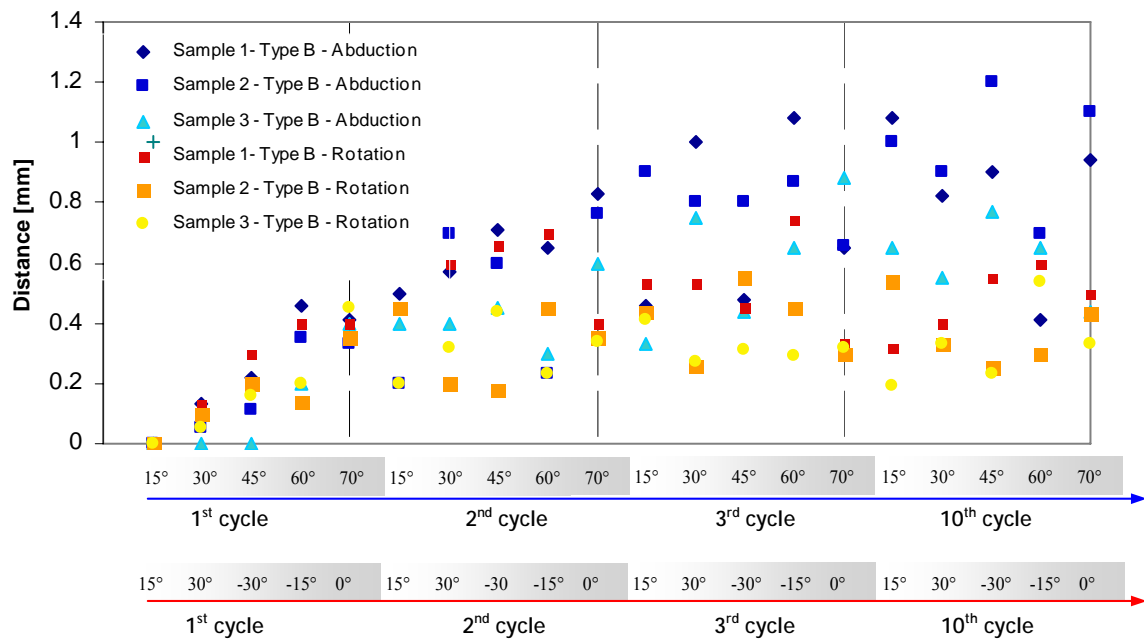


Figure 77: Displacements for the greater tuberosity in the lateral view.⁹

4.1.5.3 Comparison of the migration rate

The migration rate for the greater tuberosity is increased in fixation type A in comparison to the techniques of types B and C (Figure 78, Figure 79 and Figure 80). A significant difference is found with respect to the greater tuberosity migration rate in the scapular plane between type A and type C ($p=0.04$). This difference is as well observed by comparing the results of the human bone samples of type A and type C ($p=0.15$).

No significant difference is provided by the angular displacement for both tuberosities, although cable technique of type C tends to increase angular stability. The artificial bone model was in a similar range with respect to the migration rate of the greater tuberosity in the medial plane. Significant increase in the displacement of the lesser tuberosity is detected for type A compared to type C ($p=0.05$).

⁹ The displacements in that specific investigation were realised with a lower arm weight (1.5 kg) in comparison with the normal loading case of 2.5 kg.

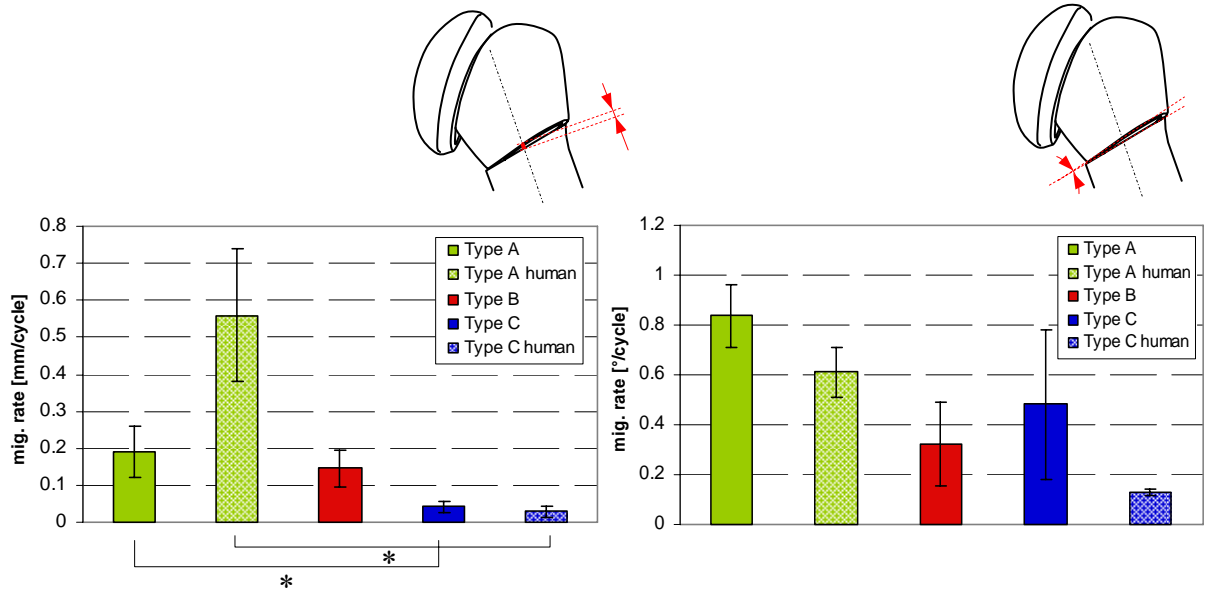


Figure 78: Greater tuberosity migration rate in the scapular plane.

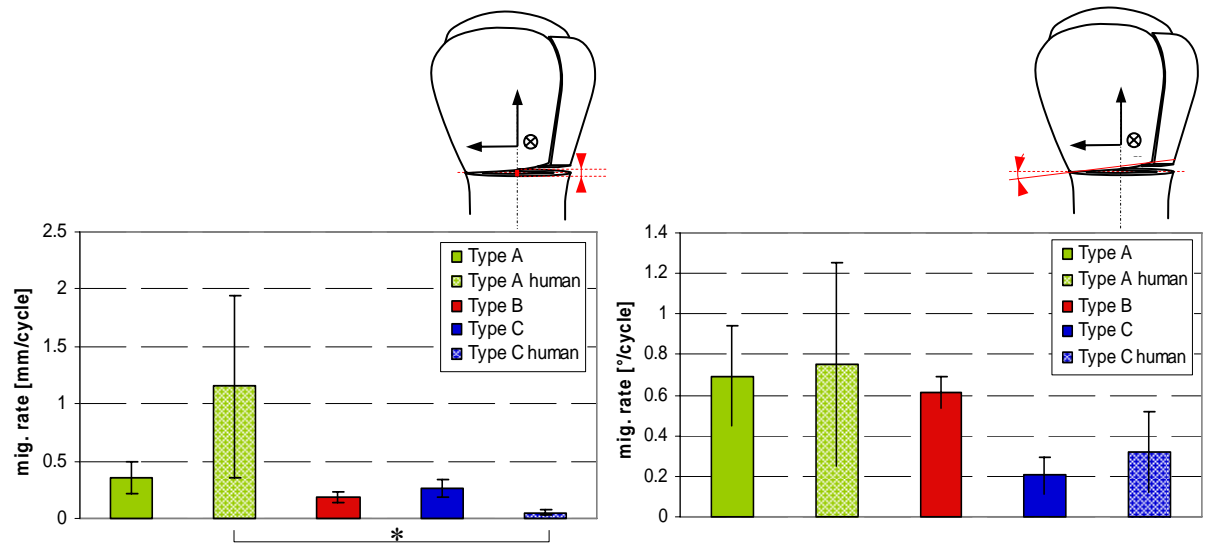


Figure 79: Greater tuberosity migration rate in the medial plane.

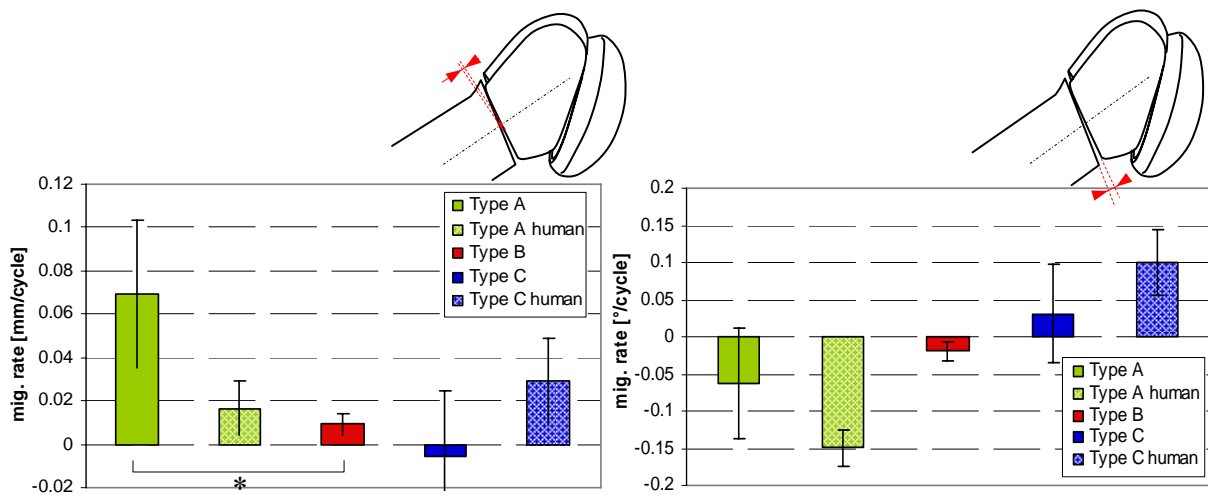


Figure 80: Lesser tuberosity migration rate in the scapular plane.

4.1.5.4 Loading cycles-to-failure

The number of sustained loading cycles-to-failure is represented by the boxplot in Figure 81. Conventional suture fixation represented by type A failed after applying 2.5 abduction cycles (mean of $n = 6$ tested samples). Type B survived 5 loading cycles-to-failure ($n = 5$). Type C showed the highest survival rate of 8 cycles (mean of $n = 5$). A statistical significance considering the type of fixation and number of applied cycles-to-failure is found between types A and C ($p = 0.02$). No statistical significance could be shown between type B and C. (Mann-Whitney-U-Test, based on a level of significance of $\alpha = 5\%$).

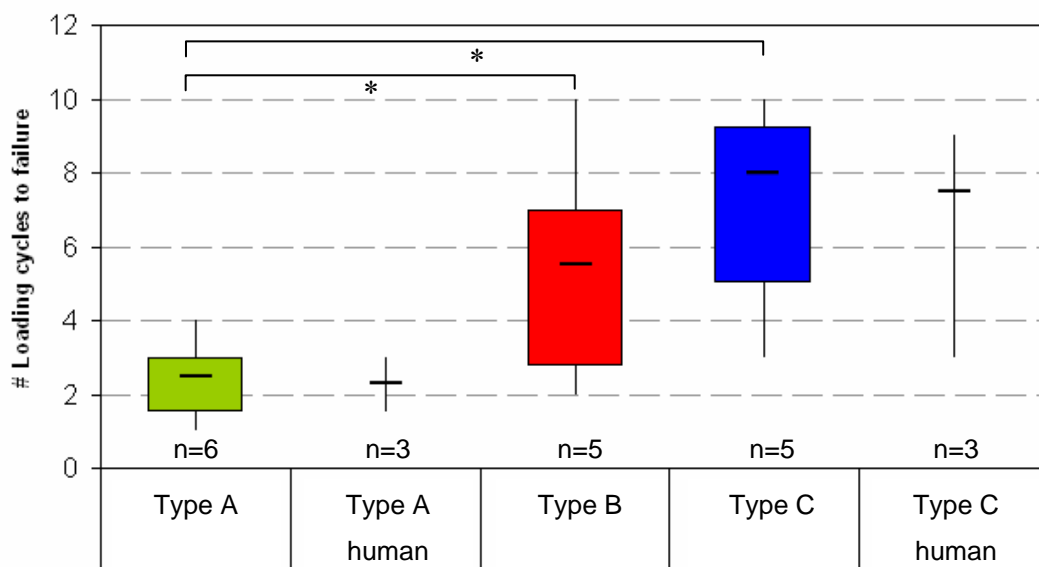


Figure 81: The number of cycles to failure is shown for the three fixation techniques, suture (type A), suture & cable (type B) and cable (type C).

4.1.5.5 Failure mechanisms of the loaded reconstructions

Similar failure mechanisms are observed in the artificial model compared to the human samples (Figure 82). For fixation type A using sutures, cutting through of the wire occurs in the greater tuberosity, as previously described in Chapter 4.1.3. This failure mechanism was also detected in the human samples, whereas the cutting distance of the wire through the bone was between 8 - 12 mm for both bone models.

Slippage of the cable supporting bone anchors of type C occurred relative to the bone surface of the greater tuberosity. Interestingly, a lateral tilting or overturning of the bone anchors was

not observed, despite the spikes below the bone anchors, opposite to the contact area of the bone.

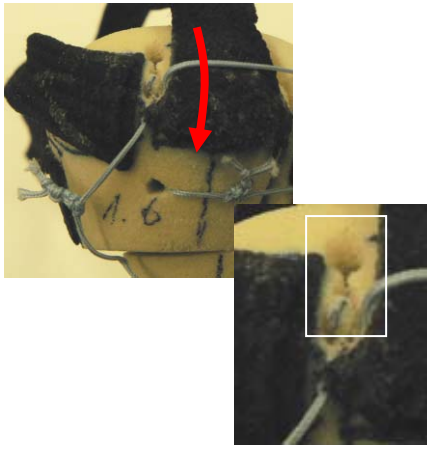
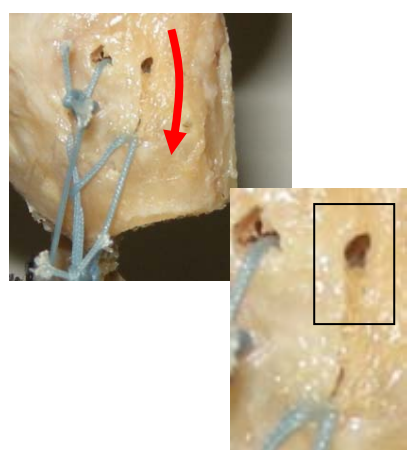
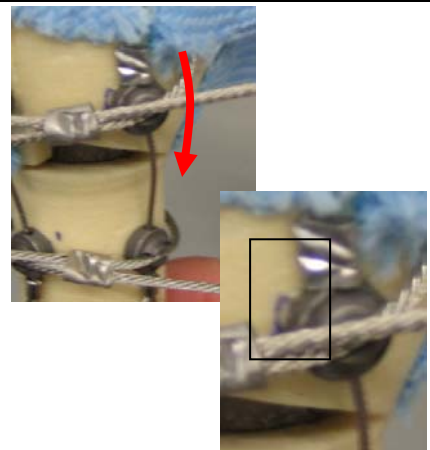
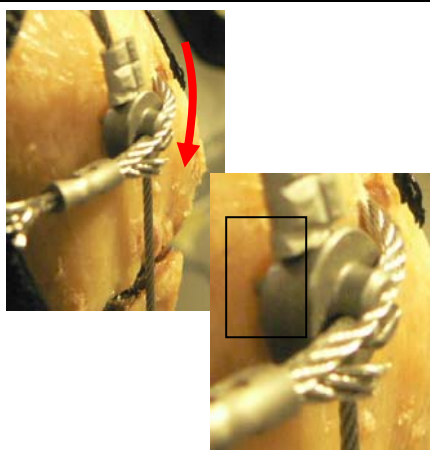
	Artificial model	Human samples
Type A, sutures	 <p>The image shows an artificial model of a bone with a suture fixation. A red arrow points to a crack in the bone that has formed, extending distally from the suture hole. An inset image shows a magnified view of the crack.</p>	 <p>The image shows a human bone sample with a suture fixation. A red arrow points to a crack in the bone that has formed, extending distally from the suture hole. An inset image shows a magnified view of the crack.</p>
Type C, cables	 <p>The image shows an artificial model of a bone with a cable fixation. A red arrow points to the cable, which has slipped and is no longer properly seated in the bone anchors. An inset image shows a magnified view of the slippage.</p>	 <p>The image shows a human bone sample with a cable fixation. A red arrow points to the cable, which has slipped and is no longer properly seated in the bone anchors. An inset image shows a magnified view of the slippage.</p>

Figure 82: Failed reconstructions of the fractured proximal humerus. For fixation type A, cutting of the bone started at the suture hole in distal direction. Type C showed a slippage of the bone anchors on the bone surface.

4.2 Results of the Finite Element Analysis

4.2.1 Regions of high von Mises stresses

4.2.1.1 Von Mises stresses in the cable-to-bone interface

Stress concentration was shown at two specific regions in the bone-to-implant interface (Figure 83). The first location of high stresses was detected in the anterior and posterior insertion hole that guides the cable of type C'. In particular, stress is higher at the hole at the lesser tuberosity than at the cable insertion at the greater tuberosity. Another area of elevated stresses was found on the lateral surface of the proximal humerus; as a result from indentations of the cables/bone anchors into the bone.

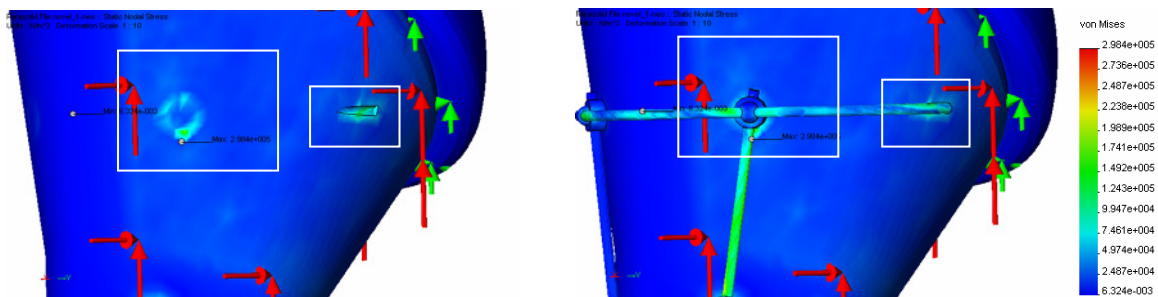


Figure 83: Local stresses in the bone-to-implant interface (left: fixation removed for a better view on the underlying bone surface, right: fixation is displayed).

The indentation of the cable or of the supporting bone anchors on the lateral part of the proximal humerus surface revealed higher stresses than the cable support on the lateral surface of the humerus. If the maximum cable-to-bone stresses of type B' are taken as a 100 % reference value, stresses in the bone anchors of type C' show an increase of about 180 %, seen in Table 9.

	Type A'	Type B'	Type C'
Lateral cable contact on the greater tuberosity	100 %	119 %	180 %
Anterior cable contact on the lesser tuberosity	- (no holes)	148 %	152 %
Posterior cable contact on the greater tuberosity	- (no holes)	110 %	122 %

Table 9: Maximum stresses at the cable insertion into the bone and in the medial interface.

4.2.1.2 Von Mises stress on the lateral humeral surface

Von Mises stresses were similar for all calculated locations P1 to P4 (Table 10). The differences in the amount of acting stresses between the three fixation techniques were similar and varied in a range of 10 – 20 %, with slightly higher values for type A'. Consequently, the refixated fragments are under very low stress in the fractured bone compared to the control.

Location:		Healed	Type A'	Type B'	Type C'
Lesser Tuberosity		bone (control)			
Stresses [Pa]	P1	18'000	211	200	251
	P2	6'100	271	250	244
Location:		Healed	Type A'	Type B'	Type C'
Greater Tuberosity		bone (control)			
Stresses [Pa]	P3	27'000	243	202	240
	P4	16'000	243	215	271

Table 10: Resulting stresses on predetermined locations P1 – P4 on the bone.

4.2.1.3 Displacement of the fragments

The greater tuberosity displacement was in a small range compared to the displacements of the lesser tuberosity. The lesser tuberosity fragment was displaced up to five times more in fixation of type A compared to type E, and approximately three times further compared to type F with respect to the locations *P1* and *P2*. Interestingly, the displacements for the interior points *P1'* – *P4'* are in a similar range to the points *P1* – *P4* (Table 11). As a consequence, the interfragmentary deformations of the fragments are in the lowest range in the model under the applied load.

Additionally to the displacement between the points, a slight fragment rotation occurred around the positive y-axis for the greater tuberosity and around the negative y-axis for the lesser tuberosity for all types of fixations. In the intact model, these displacements are up to an order of magnitude lesser than in the fractured models.

Location:		Healed			
Lesser Tuberosity		bone (control)	Type A'	Type B'	Type C'
Displacements [um]	P1	2.0	79	15	45
	P1'	1.8	46	7.9	33
	P2	1.8	52	10	24
	P2'	1.6	59	8.2	12
Location:		Healed			
Greater Tuberosity		bone (control)	Type A'	Type B'	Type C'
Displacements [um]	P3	3.2	4.3	5.2	2.2
	P3'	3.1	4.15	4.9	3.2
	P4	3.1	4.3	4.8	8.0
	P4'	2.9	4.2	3.9	7.8

Table 11: Resulting displacements d [μm] at the investigated locations P1 – P4 and P1'-P4'.

4.2.1.4 Comparison of displacements with the literature:

A comparison of our results with an experimental study by Dietz et al. was done (Table 12) [137]. A direct comparison is limited because of the different boundary conditions: In particular, forces of 40 N by the infraspinatus and subscapularis, and a constant force of 40 N for the supraspinatus, were applied in 25° abducted position. This is in contrast to our study, using a loading of 24 N for the subscapularis, 12 N for the supraspinatus and 6 N for the infraspinatus. However, a distance of 0.04 mm was detected by Dietz et al. between lesser and greater tuberosity. This corresponds to the interfragmentary distances of 0.015 – 0.09 mm. The calculated range by FEA is therefore in agreement with these experimental values.

Dietz et al. [137]	Fragment Distances	Sutures and Cable	Only sutures
Interfragmentary displacement [mm]	LT-GT	0.04 (0.02-0.1)	0.14 (0.08-0.28)

Table 12: Experimental testing of fragment displacement using the same prosthesis design compared to present investigation.

4.2.1.5 Comparison of strains with the experimental data

Fractured bone revealed only 12 % strain in comparison to a non-fractured bone by the experimental strain mapping (Figure 84). This ratio is in agreement to the results of the FE calculations, which show strains in the similar range (except that the values for the FE analysis are four times smaller for the fractured humerus).

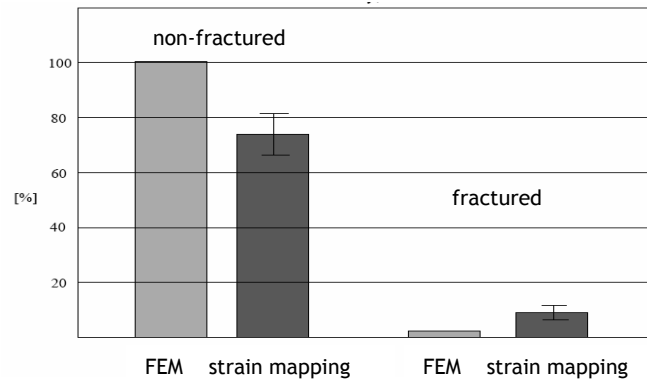


Figure 84: Experimental and computed strain values at the point P1; a decreased strain for the fractured bone is seen in the experiment and in the simulation

The strain distribution of the experiment was displayed. The regions around the fracture borderlines and on the tendon insertions had to be removed. Therefore, only a small area was available on the proximal humerus. In a direct comparison with FEA, similar strain distribution according to the loading was detected (Figure 85).

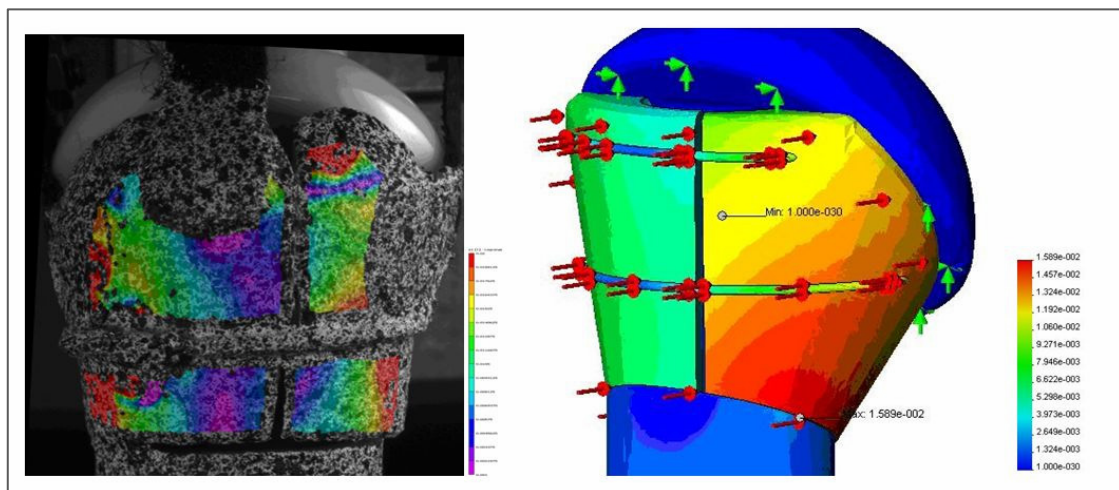
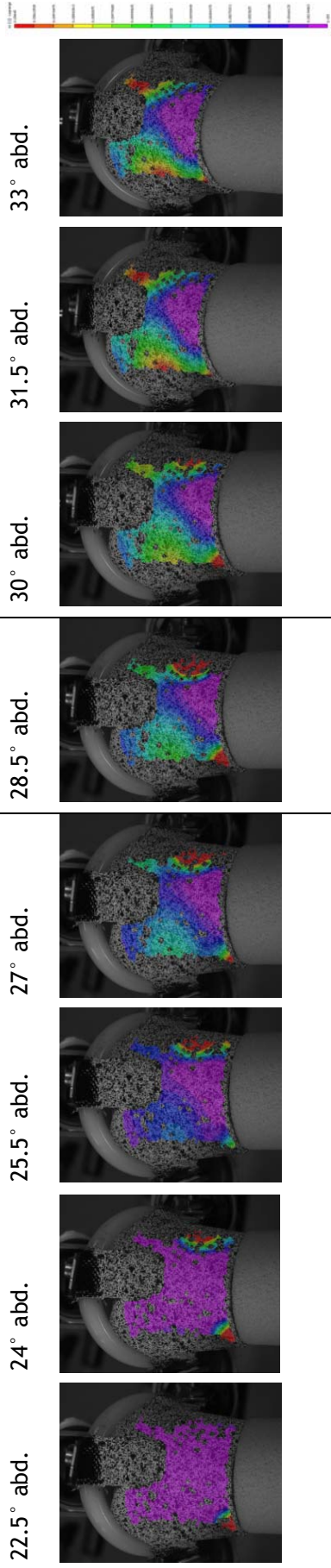


Figure 85: Strain distribution at the proximal humerus for the experiment (left) and simulation (right) for fixation technique B. (A direct comparison is not possible due to a non uniform scaling).

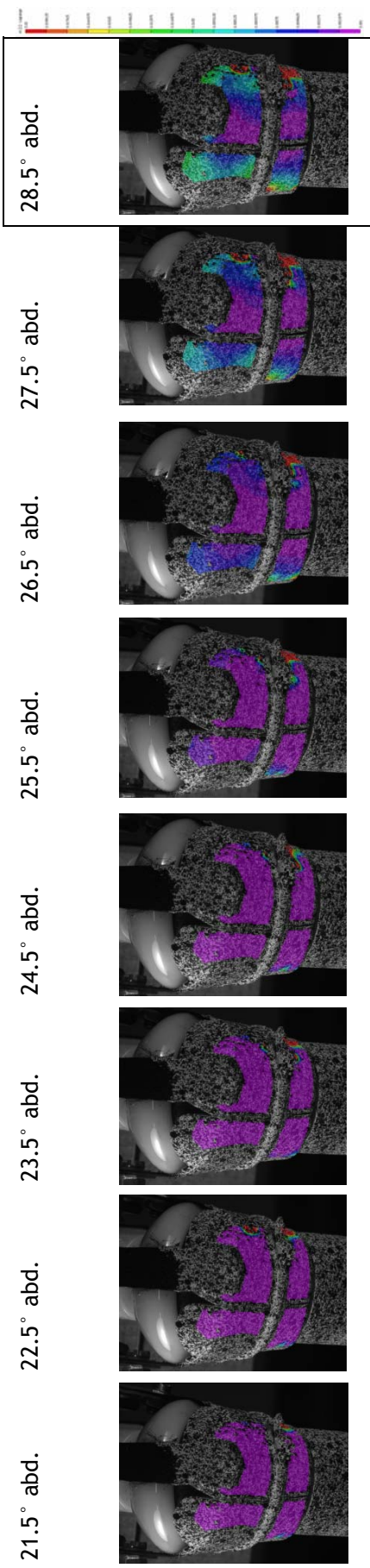
The complete strain sequence during the increased loading is displayed with the corresponding abduction angle (Figure 86).

Strain mapping at the proximal humerus during increase of the muscular load

Not fractured



fractured



- Different scale and colour gradient is used, a direct comparison is not possible.
- Comparison was done for the 28.5° abduction angle.
- Different camera positions were used, this results in a different perspective.

Figure 86: Strains at the healed and fractured bone with increasing abduction angles.

5 Discussion

5.1 Experimental testing

Testing device and loading conditions

The presented testing procedure represents a technical stability test closer to physiological conditions than existing biomechanical tests. The proximal humeral bone can be loaded by reproducible, cyclical loads. In comparison to the literature, the present testing device applies similar boundary conditions such as muscle and joint forces. The present testing procedure is sensitive enough to reveal differences between different fixation designs with respect to survival rate and kinematic behaviour of fragments during loading. A selective loading regime is used for the tests, where weak design aspects of the fixation techniques were evaluated. The uniformly distributed active load by a force ratio of 50:50 between SSP and DELT reveals forces which are in the agreement with the studies of Debsky et al. and Sharkey et al. [109, 112]. Nevertheless, Wuelker et al. describes higher forces of the DELT during abduction, which is understandable when comparing the muscular cross sections of both muscles [113]. The load ratio is still a point of discussion, as no experimental data for the supraspinatus are available. The amount of simulated muscles is still in a low range. Additional muscles such as pectoralis and latissimus would provide additional stability to the humerus.

To conclude, a novel testing procedure was designed according to the physiological movements and loads at the proximal humerus. The novel testing device simulates a high range of motion. Additionally, the middle deltoideus was integrated as a main abductor contrary to other testing devices. The necessary parameters to assess the stability of a fixation technique such as the migration rate and cycles-to-failure were defined. The observed failure mechanism during cyclic loading and the fragment kinematics allow specific optimisation of tested fixation techniques.

Analysis of fixation techniques

Analysing the number of sustained loading cycles, the higher survival rate of fixation types B and C in comparison to A confirmed the expectations in present testing. It is clear that an additional reinforcement such as the cable in type B leads to a higher survival rate in comparison to the standard suturing technique of type A. No significant differences were found for the angular displacement in all types, which shows that type C still can be optimised with regard to prevent fragment rotation.

Some investigated parameters which describe the fragment kinematics are directly related to each other: the angulation of the fragment during abduction may simultaneously reduce the measured distance between that fragment and the shaft. This circumstance was specifically detected in the scapular plane, where an increasing angulation of the fragment induced a decreased greater tuberosity –to-shaft distance. The strongest predictor for the quality of the fixation technique seems to be the greater tuberosity displacement in the medial view. Generally, higher survival rates (# loading cycles-to-failure) have been expected than the results finally revealed under these mechanical conditions.

General Limitations: This investigation was based on one specific prosthesis design using a cylindrical shape for the middle part of the prosthesis with small spikes. This prosthesis design represents a generic form without any macrostructured features such as fins on the prosthesis. Nevertheless, fragment motion pattern strongly depends on that prosthesis design. Using a squared or spherical prosthesis middle part may reveal other kinematic results. Due to the absence of moistened tissue around the rotator cuff, frictional parameters between the artificial bone material and the prosthesis do not match the physiological conditions.

The presented standard deviations for the survival rate of loaded fixation techniques are in a high range. However, a similar biomechanical study which applied unidirectional loading revealed comparable standard deviations [77]. An accurate placement of the fixation techniques on the proximal humerus by controlling the applied pretension may reduce the wide spread of the results.

Standardisation of the complex in-vivo situation of a fractured proximal humerus has to be discussed: The straight fracture lines in the proximal humeral samples presumably provide less resistance to acting muscular loads than a rough and uneven surface of real fracture borderlines. Additionally, the fragment kinematics in-vivo is influenced by the interactions of such uneven fracture planes, which was not simulated in present testing. This investigation represents therefore an idealised situation.

The testing device and applied boundary conditions directly influences the biomechanical behaviour of the reconstruction. It is therefore important, to highlight its simplifications: In total six muscles were simulated in comparison to an in-vivo situation with 27 muscles. Therefore, fewer muscles had to provide the stability of the system during movement. As a compromise between maintaining the stability with a lower number of simulated muscles, the selection of corresponding muscle segments in front of the scapula and on the rear side of the scapula was achieved.

The middle deltoideus is simulated by a thin polyester band. A distribution of the load over a larger contact zone at the rotator cuff – for example by simulating the anterior and posterior deltoideus – seems to be one further step to optimise the chosen testing setup.

Comparison of the artificial model with human samples

Human samples and the artificial bone model revealed similar behaviour in the amount of sustained loading cycles-to-failure and resulting migration rates. Comparable failure mechanisms for the fixation techniques between the two bone qualities confirmed a certain analogy of the biomechanical behaviour. The use of the artificial bone model represents therefore a reliable substitute for the cadaver specimens.

Correlation of fragment kinematics with clinical observations

No clinical study describes general patterns of postoperative fragment kinematics in case of dislocation. However, single cases are documented by Plausinis et al which describe a proximal fragment migration, resulting in an increased distance of the greater tuberosity to the humeral shaft [157]. Plausinis et al investigated that failed fixation by means of x-ray, where some limitations have to be taken into account such as an accurate analysis of the fragment dislocation. However, present literature describes similar in-vivo fragment behaviour in comparison to the experimental testing.

5.2 Finite Element Analysis FEA

Location of high von Mises stresses: Regions of increased stresses were identified in two distinct regions of the reconstructed humerus: the insertion hole of the cable into the bone, and the area of contact with the cable supporting bone anchors (on the lateral surface of the humerus, below the supraspinatus insertion). Under the assumption that evenly distributed load transmission may reduce these stress peaks, the design properties of the fixation technique have to be adapted as follows:

- An enlarged diameter of the cable supporting bone anchors would lower the local pressure on the bone, thus reducing the risk of overload and subsidence.
- Achieving a smoothed radius of the hole guiding the cable through the bone could reduce the stress peaks.

The discontinuous bone volume at fragment borderlines interrupts load transmission across the fragments. This circumstance leads to unloaded regions in fractured bone in comparison to the bone without fracture gaps (control). Such unloaded regions are characteristic for all types of cerclages. This loss of mechanical stimuli may explain the clinically observed bone resorption [168].

Displacements: The greater tuberosity shows less displacement in comparison to the lesser tuberosity; presumably this effect is due to the embracing fragment geometry, which surrounds the middle part of the prosthesis. This is in contrast to the experiments and is explained by an increased loading of the greater tuberosity for high abduction angles. The fragment dislocations for type B' and C' are smaller in comparison to type A'. This behaviour can be explained with the fewer constraints that are present in type A' fixation vs. type B', in which the surrounding cables only enclose the fragments without any direct fixation through the prosthesis. The interlocking and more constraining fixation through the prosthesis shaft provided by fixation types B' and C' seem to have a stabilising effect. Type C' fixation shows slightly higher displacements than type B', which can be explained by an increased overall cable length and a tendency to higher deformations of the free hanging cable construction.

Loading case: The applied muscular loads are in a small range and represent a static, unloaded state of the humerus. An increase of the muscular loads resulted in a non-convergent iteration process during FE post processing, apparently because of deformations beyond elastic material properties. In this work, the presence of tensile muscle forces was assumed. In some single cases, a clinically observed telescoping effect is represented by a distal migration of the fragment into the humeral shaft. This migration opposite to the muscle tensile force reveals that other loading regimes may act in vivo.

Limitations: It has to be mentioned that the results are valid specifically for the tested types of shaft design. Other designs of the middle part of the shaft may generate different results with respect to displacements of the fragments and resulting bone stresses. The absence of friction between the fragments and the prosthesis stem has to be discussed. Simulation of friction as it is obviously present in-vivo may lead to contradictory results. Interlocking shearing forces may prevent a further displacement and presumably contribute to an enhanced stability. Furthermore, the simplified humeral surfaces used for the FE calculations do not match the morphometry of real bone samples. Cavities such as the biceps groove were not modelled; the wires were placed always in contact to the proximal humerus.

The loading conditions with the small muscular loads were sensitive enough to detect differences within different fixation techniques. Nevertheless, the application of higher loads would be of interest to be able to detect failure mechanisms of the fixation technique, as it was also analysed in the experimental testing.

6 Conclusions and Outlook

Immediate mobilisation of a reconstructed shoulder joint at an early stage after trauma is important for a successful recovery. The optimisation of fixation techniques for proximal humerus fractures is therefore highly relevant in clinics, particularly since it has been generally accepted that a stable reconstruction enhances biological fracture healing. Within the framework of this thesis, two novel methodologies were developed to assess the stability of fixation techniques for a fractured proximal humerus.

A biomechanical in vitro approach was developed to experimentally analyse clinically established fracture reconstructions, taking into account physiological loads. Additionally, the testing device provides a reproducible loading to generally assess basic shoulder biomechanics, such as muscular moment arms and instantaneous axis of rotation. Finite Element Analysis (FEA) was established for a detailed investigation of implant-to-bone interactions to provide in silico optimisation of the fixation techniques. High stresses in the material and tissue interactions can be detected and reduced by modified fixation designs.

By loading a proximal humeral four-part fracture model, the illustration of fragment kinematics and failure mechanisms under physiological loading conditions was, for the first time, achieved. Greater tuberosity displacement is characterised by an almost linear increase at each abduction cycle, ranging from 0.2 to 0.4 mm/cycle for clinically established fixation techniques in the frontal view. It was found in present work that current clinically fixation techniques failed at a much earlier stage of cyclic loading as expected, despite the physiological range of applied forces. This finding has proved the necessity to improve the stability of the studied fracture reconstructions.

By analysing the failure mechanisms of the fragments during cyclic loading, the requirements for an optimised fixation technique were derived. The novel concept in this thesis was therefore based on bone anchors, which are connected by cables. One of the advantages is that the guided cables on the bone anchors are not in direct contact with the bone, in order not to damage the vascular system in the periosteum. This novel technique reduces the resulting fragment displacements during loading (0.1 mm/cycle), and thus increases the survival rate (endured cycles-to-failure) of about three times. The artificial bone model used for these tests showed similar biomechanical characteristics when used for human humeri samples, and therefore can be considered valid. Such a standardised model based on the biological bone properties enables efficient optimization of design concepts in the early stage of development, thereby eliminating the need for time consuming cadaver tests.

The Finite Element Analysis revealed regions of accumulated high stresses. These were present at two distinct regions, in particular at the cable insertion into the bone and under the bone anchors. Optimisation was done in order to achieve proportional load transmission of the cable system to the bone.

To conclude, the experimental and computational approach presented here, represent efficient methods for a detailed analysis of fracture fixation techniques. The reconstruction with the resulting prototype showed improved stability under cyclic physiological loading.

Outlook

Experiments: Future work in this context should address the following tasks: Firstly, the optimisation of the applied procedures and methods; and secondly, a further optimisation of the fixation technique itself.

Experimental testing:

- The fixation techniques were experimentally tested and optimised with respect to single plane abduction. A combined movement of abduction and rotation would represent a more complex loading case. Experiments including abduction and rotation would optimise the implant stability for multiple loading directions.
- The glenohumeral contact force in the present experimental testing was measured in the glenoid. In contrast, Bergmann et al. were able to measure in vivo contact forces in the prosthesis. A similar setup could provide measurements closer to the in vivo conditions.
- With real-time force measurements during the experiment, it would be possible to get more detailed information about the failure mechanisms, in particular regarding its temporal progress.
- The use of osteoporotic bone samples could be valuable to optimise the fixation techniques under worst case conditions.
- A tracking to estimate the exact three-dimensional humeral position would allow for a more accurate kinematic evaluation of the system as opposed to the visual determination of the abduction angle in the performed measurements.

Data evaluation: The accuracy of the fragment migration measurement by using a planar projection could be improved by using a novel technique: An optical topometry surface scanner to reconstruct the 3-D situation at the proximal humerus was pre-evaluated (Breuckmann Opto-top, Figure 87). This three dimensional optical camera system provides

photorealistic captures of shape and texture by a non contact scanning technique. The scanning system is an optical triangulation scanner that is based on pattern projection on the object to be investigated. The scanner consists of a digital camera and a projector that projects a grid pattern onto the object. The light is projected from a defined position in a defined direction. The direction of the returning light is measured by an angle sensor. With the known projection angle and the measured angle of the returning light, the coordinates of the illuminated object can be calculated [171, 172].

In a feasibility study, the topology at the proximal humerus was reconstructed based on camera snapshots. That study showed the fragments, the humeral shaft and parts of the visible shoulder implant. These reproduced 3-D data at the proximal humerus have been imported into the CAD program Geomagic (Geomagic GmbH, US) for further analysis of the fragment distances.

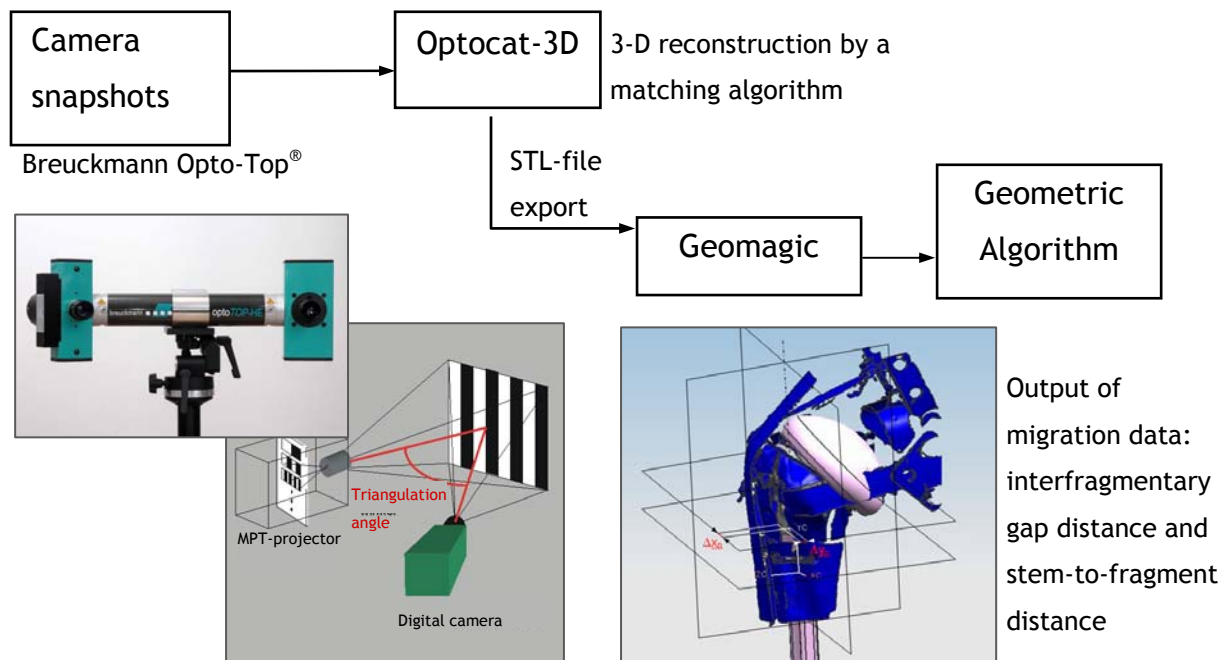


Figure 87: 3-D scan of the humerus for the measurement of the fragment migration.

Further development of the novel fixation technique: Generally, the intraoperative handling and the applicability of the novel fixation technique has to be proved in cadaver tests. Novel design features such as the application of flexible cable crossing angles on the bone anchors would allow a better fracture reconstruction. A successful long-term in vivo behaviour of the novel fixation technique still has to be proved in clinical studies.

FE-Analysis:

- A dynamic, iterative FE-model which could simulate different abduction angles and muscular lines of actions would allow a validation of the fragment displacements by simulated by the cyclic loading in the experiments (Chapter 3.1).
- The three dimensional data of a micro-CT scanned, reconstructed proximal humerus with high resolution would be of high interest. Regions with different bone qualities could be acquired and simulated as well in FEA, a more accurate and realistic fracture model could be modelled.
- The presence of an irregular bone morphometry of a proximal humerus surface shape including grooves and local elevations would allow a simulation of fixation techniques closer to in-vivo conditions.
- The simulation of a micro structured, porous prosthesis surface by defining a frictional coefficient relative to the fragments has to be discussed for a further analysis of fixation techniques.

7 Appendix A: Suture material properties

7.1 Biomechanical behaviour of sutures under dynamic loading

7.1.1 Introduction

Clinical outcome after total shoulder arthroplasty for a fractured proximal humerus is not satisfactory [31]. Resorption as a consequence of secondary displacement of the fragments was shown by Kralinger et al. in 30 - 70 % of all cases [33]. According to the suggestions of Mighell et al., optimisation of the fixation technique for the fractured tuberosities represents one of the most influencing factors on the outcome of total shoulder arthroplasties [69]. As biologically integrated tuberosities are a prerequisite for consolidation, initial postoperative dislocation should be avoided by a stable reconstruction technique.

Clinically detected fragment dislocation after humeral head fractures is often detected postoperatively. On the one hand, cutting effects of the sutures through the bone may be one reason of a failed reconstruction. On the other, material relaxation effects of suture-knot constructions or knot slippage may affect an enhanced displacement of the fragments due to plastic deformations of the suture material.

Different biomechanical material tests quantify the effects of different material properties on the elongation of sutures under loading. Load-to-failure testing is often performed to detect maximum tensile load and overall stiffness of suture-knot loop constructions, as it was done by Komatsu et al. and Viinikainen et al. [173, 174]. In contrast to that experiment of a steadily increasing load, the influence of a repetitive, cyclic loading analyses the relaxation effects of the material. Different loading criteria are found in literature: In the study of Mishra et al., the elongation of the suture loop was detected during 20 loading cycles at a maximum load of 30 N [175]. Knot slippage was analysed in a cyclic test by Mahar et al., applying a maximum load of 45 N for totally 1000 cycles [176].

Some other characteristic values were analysed such as the maximum applied compressive force of a closed loop construction immediately after knot tying: Shaw et al. investigated the influence of such an applied pretension on the maximum tensile forces by means of a load-to-failure test [177]. It is important to say that the test medium (environment around the sutures) has a significant effect on the material properties of the sutures: Kirby et al. showed that testing the sutures in saline solution of 37°C revealed different results in comparison to a dry testing with respect to the maximum tensile load [178]. Therefore, the humidity of the testing

environment has to be taken into account. Nevertheless, the test temperature (37 °C or 20 °C) does not affect the mechanical behaviour of a suture loop, as it was shown for Ethibond Excel suture in the study of Bruckner et al. [179].

In the present investigation, the aim was the analysis of a dynamic, cyclic loading on the residual elongation of suture loops.

7.1.2 Material & Methods

7.1.2.1 Tested sutures

Four commercially available sutures used for fracture fixation have been compared considering the residual elongation after cyclic loading. Orthocord (DePuy) and Fiberwire (Arthrex), (suture thickness of #5.0), Ethibond Excel (Johnson&Johnson) and Ti-Cron (Syneture) (both #7.0 metric) were used (Table 13). In total n = 3 samples were tested for each type. A closed loop-knot construction including the surgical's knot was built. In total n = 3 sutures were tested of each type. The suture loops were moistened in saline solution before testing (0.9 % NaCl, 37°C) during a defined time of 1 min. The total length of the closed loop-knot construction was 88 mm.

Name	Company	Material	Ref. No.	Thickness (Def. Eur.)
Fiberwire	Arthrex	Braided Polyester	AR-7200	5.0 metric
Ti-Cron	Syneture	Braided Polyester	XX-5054	7.0 metric
Orthocord	De Puy Mitek (J&J)	Braided Polyester	223105	5.0 metric
Ethibond Excel	Ethicon (J&J)	Braided Polyester	W-4846	7.0 metric

Table 13: Commercially available sutures.

7.1.2.2 Testing procedure

A) Static loading at a defined pretension

The tests were performed on a Zwick UPM 1475 testing machine (Zwick GmbH, Germany). The suture loops were loaded at a pretension of 50 N. This maximum load was reached after a linear increase of the force during 15 sec, describing a ramp by the force controlled actuator of the testing machine. The force relaxation was measured during 2 min by the load cell (Angewandte System Technik GmbH, Germany) which was connected to the machine actuator of the testing machine. Ti-Cron and Fiberwire were used for these tests.

B) Cyclic loading

The loops were fixed in the testing device and initially preloaded by a tensile load of 40 N. In total twenty cycles were applied to the loop at an upper and lower force level of $F_{\max} = 50$ N and $F_{\min} = 5$ N respectively (frequency = 1 Hz at room temperature = 20 °C). The maximum load was below the ultimate tensile load of the suture in order to exclude the influence of non reversible suture elongation. Tensile load on suture loops was introduced by an upper and lower titanium rod of 4.5 mm diameter (Figure 88). Residual elongation in the length of the suture-knot construction was expressed in percentage [134] of the overall initial length. Testing was performed for all presented sutures.

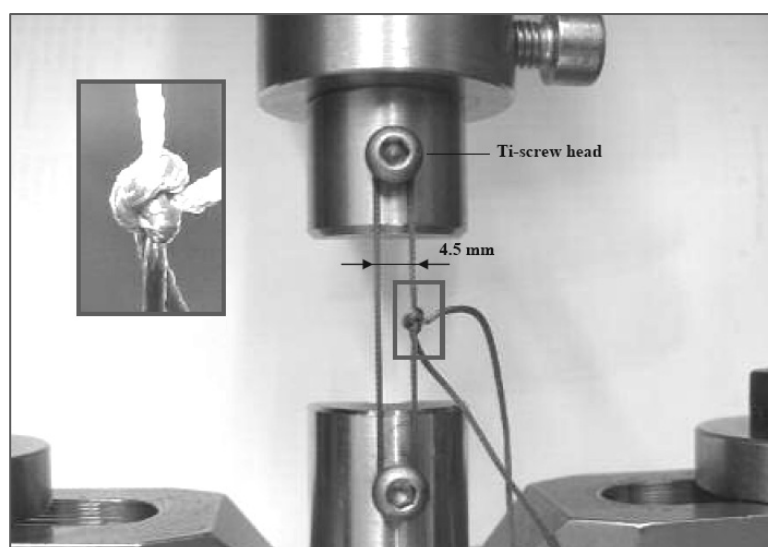


Figure 88: Test setup to apply a cyclic loading.

7.1.3 Results

A) Static loading

The pretension of the Fiberwire suture is reduced to around 30% with respect to the initial load of 50 N, whereas 50% of the pretension gets lost for Ti-Cron sutures. Although the curve displays a flattened characteristic behaviour at the end of the testing time at 2 min, a further decrease of the pretension after 2 min testing time has been assumed (Figure 89).

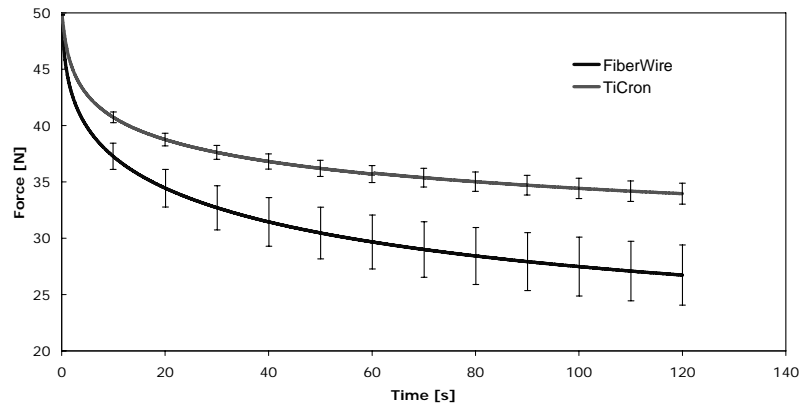


Figure 89: Relaxation of Fiberwire and Ti-Cron sutures after applying initial pretension of 50 N.

B) Cyclic loading

Fiberwire, Ethibond Excel and Ti-Cron showed comparable residual elongation values of 1.4 – 1.6 % (maximally, this refers to a total non recovering elongation length of 1.4 mm), Orthocord of 2.9 % (2.6 mm) after the cyclic loading (Figure 90). The standard deviation was around +/-15 % for the Fiberwire and Ti-Cron sutures with respect to the maximum force, whereas Ethibond and Orthocord sutures showed higher standard deviations of around +/-20 %. The force-displacement curves get flattened with increasing number of cycles and show a tendency to converge at a constant elongation. The Orthocord suture showed a hydrophilic behaviour after moistening in saline solution in contrast to the other hydrophobic suture materials.

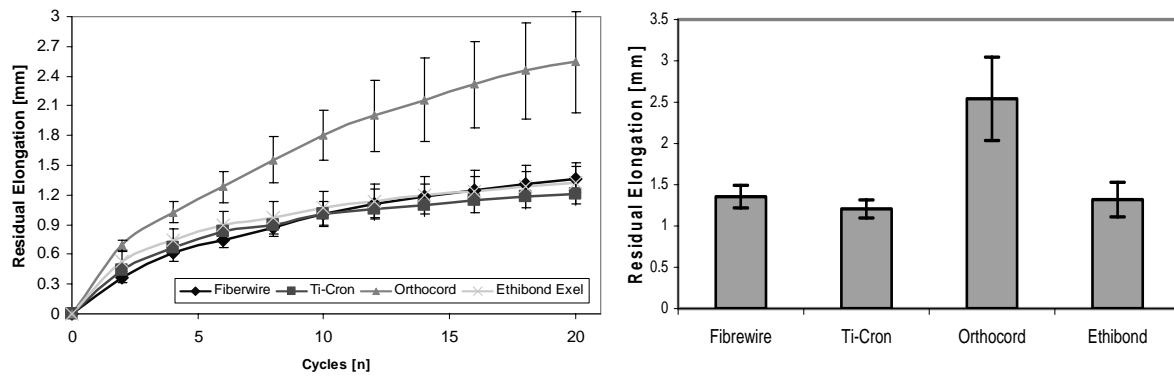


Figure 90: Progression of the suture knot-elongations (left) and maximum elongations at 20 cycles.

7.1.4 Discussion and conclusions

Good clinical results can be obtained with a non-operative treatment at patients with a greater tuberosity fragment displacement of less than 5 mm. If the displacement is more than this characteristic value, the fragment should be mobilized, repaired, and fixed into its original bed as described by Park et al. [180, 181]. Considering this criteria of maximum displacement, the suture-knot elongation revealed in present study is in a smaller range (1.2 mm – 2.4 mm) and cannot be the only reason for failure of a reconstructed humerus. Presumably, a limit value can be reached in combination with other mechanisms such as cutting of sutures through the bone or sliding effects of sutures on the bone surface.

In contrast to the other hydrophobic materials, Orthocord suture showed a hydrophilic behaviour after moistening in saline solution. This may be a reason that residual elongation of the loop after testing was significantly higher in comparison to the other types of sutures.

8 Appendix B: Artificial bone model and prosthesis design

8.1 Artificial bone model

The dimensioning of present technical drawings is not complete. Relevant distances and angles are shown. All dimensions are in millimetres.

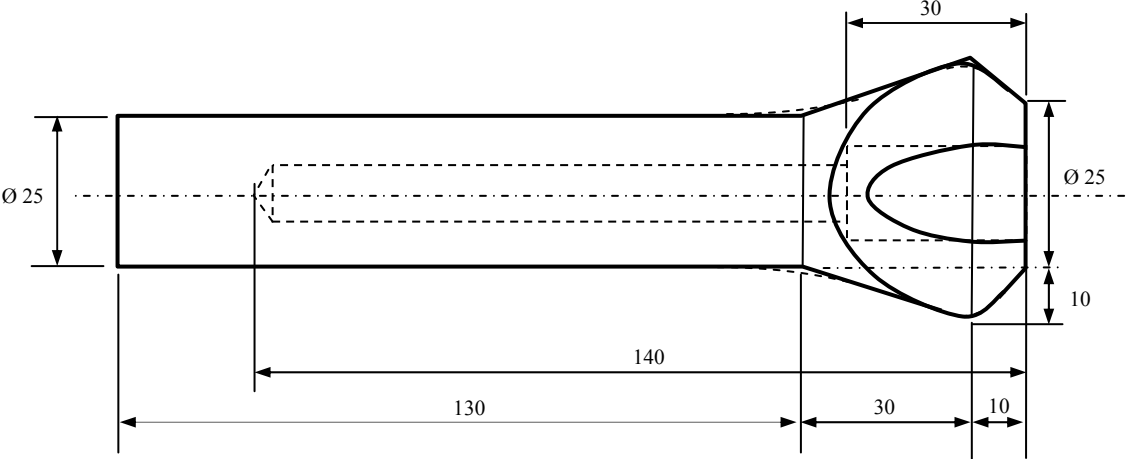


Figure 91: Artificial bone model.

8.2 Prosthesis design

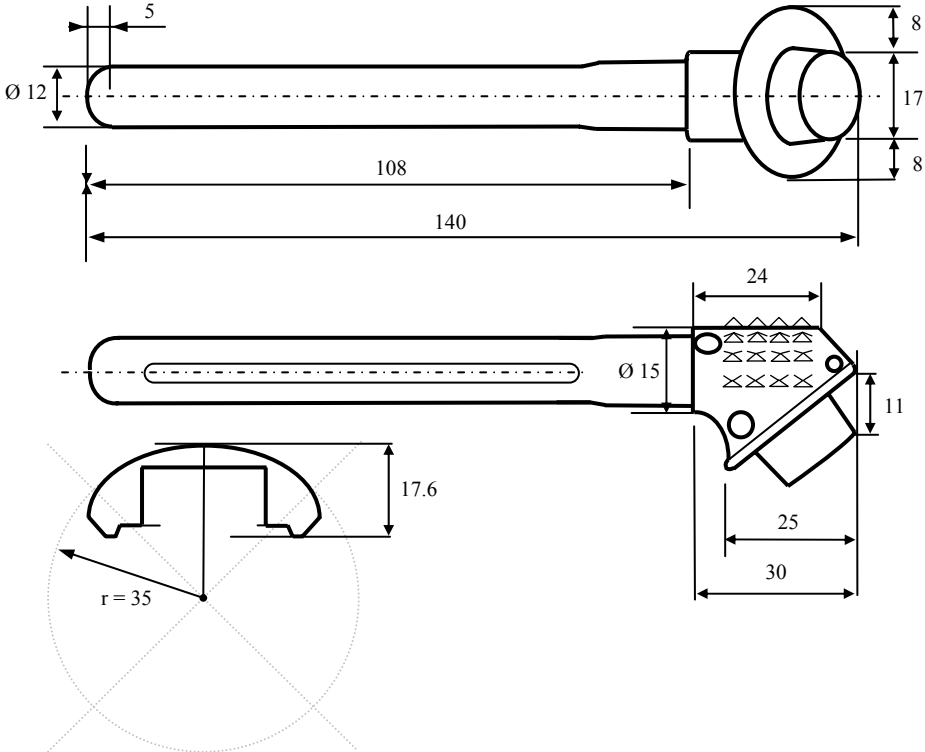


Figure 92: Humeral prosthesis stem and cross section of the prosthesis head.

9 Appendix C: Curriculum Vitae

Personal Data

Name	Daniel Baumgartner
Date of birth	October 26th, 1976 in Solothurn
Nationality	Swiss citizen

Education

Oct. 2001	Dipl. Ing ETH, Zurich, Master in Biomedical Engineering
Sept. 1993 – June 1996	Swiss Federal Maturity Solothurn
Aug. 1983 – July 1993	Primary and higher secondary school, Zuchwil and Oensingen

Working Experience

Aug. 2006 – July 2009	Institute for Biomechanics IFB	ETH Zurich, PhD Student
May 2002 – July 2006	RMS Foundation, Bettlach	Department of Biomechanics
Aug. 1999 – Feb. 2000	Volkswagen AG, Puebla, Mexico	Department of exterior car design
Feb. 1999 – Apr. 1999	Mathys Medical AG, Bettlach	Biomechanical Engineering

Internships

Mar. 2000 – Aug. 2000	Bystronic-Laser AG, Niederönz,	Laser Technologies
Feb. 1998 – Apr. 1998	Schaad AG, Subingen,	Agricultural Machines
July 1996 – Sept. 1996	Sulzer Textil AG, Zuchwil,	Weaving Machines

Knowledge

Languages	German (native), Spanish, French, English (good)
ICT	Windows, Office, Mathematica, Alias, UG NX, Patran, OpenSim

Others

Memberships	ISB, ESB, SSBE: Int., Europ. & Swiss Society for Biomechanics
Journal Reviewer	Medical & Biological Engineering and Computing, Der Orthopäde

Publications

Refixation stability in shoulder hemiarthroplasty in case of four-part proximal humeral fracture

Baumgartner D., Lorenzetti S., Gasser B., Mathys R., Stüssi E.

Journal of Medical&Biological Engineering&Computing, 2009 May;47(5):515-22

Biomechanical testing of a polymer-based biomaterial for the restoration of spinal stability

Hegewald A.A., Knecht S., Baumgartner D., Gerber H., Endres M., Kaps C., Stüssi E., Thomé C.

Journal of Orthopaedic Surgery and Research, 2009 Jul 15;4:25

Revised: Review of fixation techniques for the fractured proximal humerus in hemiarthroplasty

Baumgartner D., Lorenzetti S., Gasser B., Mathys R., Stüssi E.

The American Journal of Orthopedics

Submitted: Experimental in-vitro testing of the glenohumeral joint – a literature review

Baumgartner D., Gerber H., Butscher A., Levchuck A., Stüssi E.

Proceedings of the Institution of Mechanical Engineers, Part H

Conference Proceedings

Baumgartner D., Schlüssel, M., Gerber, H., Stüssi E.

A novel cable fixation technique reduces fragment dislocation in case of proximal humeral four-part fractures, Zurich, Switzerland, June 7th – 9th 2009, European Society for Biomechanics ESB

Baumgartner D., Mathys R., Gasser B., Stüssi E.

Primary stability testing of novel fixation strategies in case of a proximal humeral fracture

Genf, Switzerland, June 24th – 26th 2009, Schweiz. Gesellschaft für Orthopädie SGO

Baumgartner D.; Hegewald A.A.; Gerber H.; Stüssi E.;

Polymer-based annulus sealing improves nucleus implant containment

Madrid, Spain, March 24th-26th 2008; European Orthopaedic Research Society EORS

Baumgartner D.; Lorenzetti S.; Gasser B.; Stüssi E.;

Refixation stability in shoulder hemiarthroplasty in case of proximal humeral fracture

Bologna, Italy, July 10th – 13th 2008, International Shoulder Group ISG

Baumgartner D.; Lorenzetti S.; Stüssi E., **Rotator cuff load distribution during glenohumeral abduction – a literature review of various muscle force simulation models**

Brugge, Belgium, September 17th – 20th 2008, Europ. Soc. for Surgery of the Should. Elbow SECEC

Baumgartner D.; Burri A., **Ist bei Verwendung künstlicher lumbaler Bandscheibenprothesen eine korrekte Wiedergabe der Rotationsachsen möglich?**

Ulm, Deutschland, November 27th – 29th 2008, 3. Jahrestagung der dt. Wirbelsäulenges. DWG

Baumgartner, D., Lorenzetti S., et al.

An experimental shoulder model simulating postoperative physiotherapy for primary stability testing of fracture fixation, Cape Town, South Africa, July 5-9th 2009, Int. Society for Biomechanics ISB

Patents

EP1749505	2007	(publ.)	Gelenkprothese mit Elastomer- oder Federelement
EP08021326	2008	(filed)	Sitzgerät mit beweglicher Sitzfläche
	2009	(filed)	Fixationstechnik für Humerusfraktur

10 Bibliography

1. Pearce, J.M., *Henry Gray's Anatomy*. Clin Anat, 2009. 22(3): p. 291-5.
2. Boileau, P. and G. Walch, *The three-dimensional geometry of the proximal humerus. Implications for surgical technique and prosthetic design*. J Bone Joint Surg Br, 1997. 79(5): p. 857-65.
3. Ruckstuhl-Knuesel, H., *Mechanics of the shoulder complex and clinical investigation in spinal cord injured individuals*. Diss ETH No. 17638, 2008.
4. Moseley, H.F., *The Vascular Supply of the Rotator Cuff*. Surg Clin North Am, 1963. 43: p. 1521-2.
5. Moseley, H.F. and I. Goldie, *The Arterial Pattern of the Rotator Cuff of the Shoulder*. J Bone Joint Surg Br, 1963. 45: p. 780-9.
6. Laing, P.G., *The arterial supply of the adult humerus*. J Bone Joint Surg Am, 1956. 38-A(5): p. 1105-16.
7. Seggl, W., *Arterial Blood supply of the Humeral Head and its Prognostic Value in Shoulder Dislocation and Proximal Humeral Head Fractures*. Acta Chirurgica Austriaca, 1991. Supplementum 92: p. 3-19.
8. Gerber, C., A.G. Schneeberger, and T.S. Vinh, *The arterial vascularization of the humeral head. An anatomical study*. J Bone Joint Surg Am, 1990. 72(10): p. 1486-94.
9. Brooks, C.H., W.J. Revell, and F.W. Heatley, *Vascularity of the humeral head after proximal humeral fractures. An anatomical cadaver study*. J Bone Joint Surg Br, 1993. 75(1): p. 132-6.
10. Hessmann, M.H. and P.M. Rommens, *[Osteosynthesis techniques in proximal humeral fractures]*. Chirurg, 2001. 72(11): p. 1235-45.
11. Meyer, C., et al., *The arteries of the humeral head and their relevance in fracture treatment*. Surg Radiol Anat, 2005. 27(3): p. 232-7.
12. Dines, D.M. and R.F. Warren, *Modular shoulder hemiarthroplasty for acute fractures. Surgical considerations*. Clin Orthop Relat Res, 1994(307): p. 18-26.
13. Lee, C.K. and H.R. Hansen, *Post-traumatic avascular necrosis of the humeral head in displaced proximal humeral fractures*. J Trauma, 1981. 21(9): p. 788-91.
14. Tauber, M., et al., *Shoulder arthroplasty for traumatic avascular necrosis: predictors of outcome*. Clin Orthop Relat Res, 2007. 465: p. 208-14.
15. Sturzenegger, M., E. Fornaro, and R.P. Jakob, *Results of surgical treatment of multifragmented fractures of the humeral head*. Arch Orthop Trauma Surg, 1982. 100(4): p. 249-59.
16. Young, T.B. and W.A. Wallace, *Conservative treatment of fractures and fracture-dislocations of the upper end of the humerus*. J Bone Joint Surg Br, 1985. 67(3): p. 373-7.
17. Zuckerman, J.D., et al., *Interobserver reliability of acromial morphology classification: an anatomic study*. J Shoulder Elbow Surg, 1997. 6(3): p. 286-7.
18. Sanchez-Sotelo, J., *Proximal humerus fractures*. Clin Anat, 2006. 19(7): p. 588-98.
19. Chansky, H.A. and J.P. Iannotti, *The vascularity of the rotator cuff*. Clin Sports Med, 1991. 10(4): p. 807-22.
20. Lind, T., K. Kroner, and J. Jensen, *The epidemiology of fractures of the proximal humerus*. Arch Orthop Trauma Surg, 1989. 108(5): p. 285-7.
21. Palvanen, M., et al., *The injury mechanisms of osteoporotic upper extremity fractures among older adults: a controlled study of 287 consecutive patients and their 108 controls*. Osteoporos Int, 2000. 11(10): p. 822-31.
22. Widmer, M., et al., *Regional variation in orthopedic surgery in Switzerland*. Health & Place, 2009.

23. Siebenrock, K.A. and C. Gerber, *The reproducibility of classification of fractures of the proximal end of the humerus*. J Bone Joint Surg Am, 1993. 75(12): p. 1751-5.
24. Neer, C.S., 2nd, *Displaced proximal humeral fractures. II. Treatment of three-part and four-part displacement*. J Bone Joint Surg Am, 1970. 52(6): p. 1090-103.
25. Neer, C.S., 2nd, *Displaced proximal humeral fractures. I. Classification and evaluation*. J Bone Joint Surg Am, 1970. 52(6): p. 1077-89.
26. Kontakis, G., et al., *Prosthetic replacement for proximal humeral fractures*. Injury, 2008. 39(12): p. 1345-58.
27. Szyszkowitz, R., et al., *Proximal humeral fractures. Management techniques and expected results*. Clin Orthop Relat Res, 1993(292): p. 13-25.
28. Dietrich, M., et al., *[Complex fracture of the proximal humerus in the elderly. Locking plate osteosynthesis vs hemiarthroplasty]*. Chirurg, 2008. 79(3): p. 231-40.
29. Bastian, J.D. and R. Hertel, *Osteosynthesis and hemiarthroplasty of fractures of the proximal humerus: outcomes in a consecutive case series*. J Shoulder Elbow Surg, 2009. 18(2): p. 216-9.
30. Reuther, F., S. Muller, and D. Wahl, *Management of humeral head fractures with a trauma shoulder prosthesis: correlation between joint function and healing of the tuberosities*. Acta Orthop Belg, 2007. 73(2): p. 179-87.
31. Boileau, P., et al., *Tuberosity malposition and migration: reasons for poor outcomes after hemiarthroplasty for displaced fractures of the proximal humerus*. J Shoulder Elbow Surg, 2002. 11(5): p. 401-12.
32. Bosch, U., et al., *Outcome after primary and secondary hemiarthroplasty in elderly patients with fractures of the proximal humerus*. J Shoulder Elbow Surg, 1998. 7(5): p. 479-84.
33. Kralinger, F., et al., *Outcome after primary hemiarthroplasty for fracture of the head of the humerus. A retrospective multicentre study of 167 patients*. J Bone Joint Surg Br, 2004. 86(2): p. 217-9.
34. Hasan, S.S., et al., *Characteristics of unsatisfactory shoulder arthroplasties*. J Shoulder Elbow Surg, 2002. 11(5): p. 431-41.
35. Robinson, C.M. and J. Aderinto, *Posterior shoulder dislocations and fracture-dislocations*. J Bone Joint Surg Am, 2005. 87(3): p. 639-50.
36. Ruckstuhl, H., et al., *Post-traumatic glenohumeral cartilage lesions: a systematic review*. BMC Musculoskelet Disord, 2008. 9: p. 107.
37. Ambacher, T., H.J. Erli, and O. Paar, *[Treatment outcome after primary hemiarthroplasty in dislocated humeral head fractures]*. Zentralbl Chir, 2000. 125(9): p. 750-5.
38. Becker, R., et al., *Strength and motion after hemiarthroplasty in displaced four-fragment fracture of the proximal humerus: 27 patients followed for 1-6 years*. Acta Orthop Scand, 2002. 73(1): p. 44-9.
39. Boileau, P., *Operation Technique Aequalis prosthesis*. Maîtrise Orthopédique, 2005(141).
40. Boss, A.P. and B. Hintermann, *Primary endoprosthesis in comminuted humeral head fractures in patients over 60 years of age*. Int Orthop, 1999. 23(3): p. 172-4.
41. Christoforakis, J.J., et al., *Shoulder hemiarthroplasty in the management of humeral head fractures*. Acta Orthop Belg, 2004. 70(3): p. 214-8.
42. Demirhan, M., et al., *Prognostic factors in prosthetic replacement for acute proximal humerus fractures*. J Orthop Trauma, 2003. 17(3): p. 181-8; discussion 188-9.
43. Kollig, E., et al., *[Primary hemiarthroplasty after complex fracture of the humeral head--functional late results]*. Zentralbl Chir, 2003. 128(2): p. 125-30.
44. Zyto, K., M. Kronberg, and L.A. Brostrom, *Shoulder function after displaced fractures of the proximal humerus*. J Shoulder Elbow Surg, 1995. 4(5): p. 331-6.

45. Loew, M., et al., *Influence of the design of the prosthesis on the outcome after hemiarthroplasty of the shoulder in displaced fractures of the head of the humerus*. J Bone Joint Surg Br, 2006. 88(3): p. 345-50.
46. Mehlhorn, A.T., H. Schmal, and N.P. Sudkamp, *Clinical evaluation of a new custom offset shoulder prosthesis for treatment of complex fractures of the proximal humerus*. Acta Orthop Belg, 2006. 72(4): p. 387-94.
47. Fialka, C., et al., *Primary hemiarthroplasty in four-part fractures of the proximal humerus: randomized trial of two different implant systems*. J Shoulder Elbow Surg, 2008. 17(2): p. 210-5.
48. Gronhagen, C.M., et al., *Medium-term results after primary hemiarthroplasty for comminute proximal humerus fractures: a study of 46 patients followed up for an average of 4.4 years*. J Shoulder Elbow Surg, 2007. 16(6): p. 766-73.
49. Wiedemann, *Hemiarthroplasty for Humeral Head Fractures*. Operat Orthop Traumatol, 2004. 16: p. 1-27.
50. Besch, L., et al., *Hemiarthroplasty of the shoulder after four-part fracture of the humeral head: a long-term analysis of 34 cases*. J Trauma, 2009. 66(1): p. 211-4.
51. Mansat, P., et al., *Shoulder arthroplasty for late sequelae of proximal humeral fractures*. J Shoulder Elbow Surg, 2004. 13(3): p. 305-12.
52. Naranja, R.J., Jr. and J.P. Iannotti, *Displaced three- and four-part proximal humerus fractures: evaluation and management*. J Am Acad Orthop Surg, 2000. 8(6): p. 373-82.
53. Brems, J.J., *Rehabilitation following total shoulder arthroplasty*. Clin Orthop Relat Res, 1994(307): p. 70-85.
54. Ballmer, F.T. and R. Hertel, *[Indications and results of shoulder prosthetics in complex proximal humerus fractures]*. Ther Umsch, 1998. 55(3): p. 197-202.
55. Krause, F.G., L. Huebschle, and R. Hertel, *Reattachment of the tuberosities with cable wires and bone graft in hemiarthroplasties done for proximal humeral fractures with cable wire and bone graft: 58 patients with a 22-month minimum follow-up*. J Orthop Trauma, 2007. 21(10): p. 682-6.
56. Pilliar, R.M., J.M. Lee, and C. Maniopoulos, *Observations on the effect of movement on bone ingrowth into porous-surfaced implants*. Clin Orthop Relat Res, 1986(208): p. 108-13.
57. Perren, S.M., et al., *Biomechanics of fracture healing after internal fixation*. Surg Annu, 1975. 7: p. 361-90.
58. Perren, S.M., B. Rahn, and J. Cordey, *[Mechanics and biology of fracture healing]*. Fortschr Kiefer Gesichtschir, 1975. 19: p. 33-7.
59. Goldman, R.T., et al., *Functional outcome after humeral head replacement for acute three- and four-part proximal humeral fractures*. J Shoulder Elbow Surg, 1995. 4(2): p. 81-6.
60. Stableforth, P.G., *Four-part fractures of the neck of the humerus*. J Bone Joint Surg Br, 1984. 66(1): p. 104-8.
61. Hartsock, L.A., et al., *Shoulder hemiarthroplasty for proximal humeral fractures*. Orthop Clin North Am, 1998. 29(3): p. 467-75.
62. Hawkins, R.J., *Displaced proximal humeral fractures*. Orthopedics, 1993. 16(1): p. 49-53.
63. Kraulis, J. and G. Hunter, *The results of prosthetic replacement in fracture-dislocations of the upper end of the humerus*. Injury, 1976. 8(2): p. 129-31.
64. Tanner, M.W. and R.H. Cofield, *Prosthetic arthroplasty for fractures and fracture-dislocations of the proximal humerus*. Clin Orthop Relat Res, 1983(179): p. 116-28.
65. Agorastides, I., et al., *Early versus late mobilization after hemiarthroplasty for proximal humeral fractures*. J Shoulder Elbow Surg, 2007. 16(3 Suppl): p. S33-8.

66. Greiner, S.H., et al., *Tuberosity position correlates with fatty infiltration of the rotator cuff after hemiarthroplasty for proximal humeral fractures*. J Shoulder Elbow Surg, 2009. 18(3): p. 431-6.
67. Robinson, C.M., et al., *Primary hemiarthroplasty for treatment of proximal humeral fractures*. J Bone Joint Surg Am, 2003. 85-A(7): p. 1215-23.
68. Hoffmeyer, P., *The operative management of displaced fractures of the proximal humerus*. J Bone Joint Surg Br, 2002. 84(4): p. 469-80.
69. Mighell, M.A., et al., *Outcomes of hemiarthroplasty for fractures of the proximal humerus*. J Shoulder Elbow Surg, 2003. 12(6): p. 569-77.
70. Lugli, T., *Artificial shoulder joint by Pean (1893): the facts of an exceptional intervention and the prosthetic method*. Clin Orthop Relat Res, 1978(133): p. 215-8.
71. Bankes, M.J. and R.J. Emery, *Pioneers of shoulder replacement: Themistocles Gluck and Jules Emile Pean*. J Shoulder Elbow Surg, 1995. 4(4): p. 259-62.
72. Mighell, M.A., et al., *Primary semi-constrained arthroplasty for chronic fracture-dislocations of the elbow*. J Bone Joint Surg Br, 2005. 87(2): p. 191-5.
73. Voigt, C. and H. Lill, *[Primary hemiarthroplasty in proximal humerus fractures]*. Orthopade, 2007. 36(11): p. 1002-12.
74. Gerber, C., *Operation Manual of Anatomical Shoulder Fracture*. Operation manual, Zimmer Ltd., 2005.
75. De Wilde, L.F., et al., *A new prosthetic design for proximal humeral fractures: reconstructing the glenohumeral unit*. J Shoulder Elbow Surg, 2004. 13(4): p. 373-80.
76. Dimakopoulos, P., A. Panagopoulos, and G. Kasimatis, *Transosseous suture fixation of proximal humeral fractures*. J Bone Joint Surg Am, 2007. 89(8): p. 1700-9.
77. Abu-Rajab, R.B., et al., *Re-attachment of the tuberosities of the humerus following hemiarthroplasty for four-part fracture*. J Bone Joint Surg Br, 2006. 88(11): p. 1539-44.
78. Wijnman, A.J., et al., *Open reduction and internal fixation of three and four-part fractures of the proximal part of the humerus*. J Bone Joint Surg Am, 2002. 84-A(11): p. 1919-25.
79. Williams, G.R., Jr., et al., *The influence of intramedullary fixation on figure-of-eight wiring for surgical neck fractures of the proximal humerus: a biomechanical comparison*. J Shoulder Elbow Surg, 1997. 6(5): p. 423-8.
80. Lin, J.S., et al., *Effectiveness of replacement arthroplasty with calcar grafting and avoidance of greater tuberosity osteotomy for the treatment of humeral surgical neck nonunions*. J Shoulder Elbow Surg, 2006. 15(1): p. 12-8.
81. Nho, S.J., et al., *Innovations in the management of displaced proximal humerus fractures*. J Am Acad Orthop Surg, 2007. 15(1): p. 12-26.
82. Ruter, A., *[Indication and technique for shoulder endoprostheses in fractures]*. Chirurg, 2001. 72(11): p. 1246-52.
83. Schittko, A., W. Braun, and A. Ruter, *[Experiences with the OrTra-prosthesis in primary prosthetic replacement of fractures of the humeral head--indication, technique and results]*. Zentralbl Chir, 2003. 128(1): p. 12-6.
84. Sosna, A., et al., *A new technique for reconstruction of the proximal humerus after three- and four-part fractures*. J Bone Joint Surg Br, 2008. 90(2): p. 194-9.
85. Pijls, B., P. Werner, and P. Eggen, *Alternative humeral tubercle fixation in shoulder hemiarthroplasty for fractures of the proximal humerus*. Congress Abstract Book, 2008. SECEC 2008, Poster No. 105, Brugge, Belgium.
86. Saha, A.K., *Dynamic stability of the glenohumeral joint*. Acta Orthop Scand, 1971. 42(6): p. 491-505.

87. Nyffeler, R.W., et al., *Influence of humeral prosthesis height on biomechanics of glenohumeral abduction. An in vitro study.* J Bone Joint Surg Am, 2004. 86-A(3): p. 575-80.
88. Blevins, F.T., et al., *Effect of humeral head component size on hemiarthroplasty translations and rotations.* J Shoulder Elbow Surg, 1998. 7(6): p. 591-8.
89. Bono, C.M., et al., *Effect of displacement of fractures of the greater tuberosity on the mechanics of the shoulder.* J Bone Joint Surg Br, 2001. 83(7): p. 1056-62.
90. Frankle, M.A., et al., *Biomechanical effects of malposition of tuberosity fragments on the humeral prosthetic reconstruction for four-part proximal humerus fractures.* J Shoulder Elbow Surg, 2001. 10(4): p. 321-6.
91. Baumgartner, D., et al., *Refixation stability in shoulder hemiarthroplasty in case of four-part proximal humeral fracture.* Med Biol Eng Comput, 2009. 47(5): p. 515-22.
92. Halder, A.M., et al., *Dynamic contributions to superior shoulder stability.* J Orthop Res, 2001. 19(2): p. 206-12.
93. Liu, J., et al., *Roles of deltoid and rotator cuff muscles in shoulder elevation.* Clin Biomech (Bristol, Avon), 1997. 12(1): p. 32-38.
94. Nakajima, T., et al., *Abduction moment arm of transposed subscapularis tendon.* Clin Biomech (Bristol, Avon), 1999. 14(4): p. 265-70.
95. Otis, J.C., et al., *Changes in the moment arms of the rotator cuff and deltoid muscles with abduction and rotation.* J Bone Joint Surg Am, 1994. 76(5): p. 667-76.
96. Ovesen, J. and S. Nielsen, *Anterior and posterior shoulder instability. A cadaver study.* Acta Orthop Scand, 1986. 57(4): p. 324-7.
97. Roetman, B., N. Wuelker, and W. Plitz, *[A dynamic shoulder model for biomechanical measurements of shoulder specimen].* Biomed Tech (Berl), 1996. 41(12): p. 359-63.
98. Tang, C.Y., et al., *Reconstruction of shoulder function using a reflected long head biceps: a moment arm study.* J Biomech, 2002. 35(8): p. 1143-7.
99. Kedgley, A.E., et al., *The effect of muscle loading on the kinematics of in vitro glenohumeral abduction.* J Biomech, 2007. 40(13): p. 2953-60.
100. Wuelker, N., M. Korell, and K. Thren, *Dynamic glenohumeral joint stability.* J Shoulder Elbow Surg, 1998. 7(1): p. 43-52.
101. Poppen, N.K. and P.S. Walker, *Normal and abnormal motion of the shoulder.* J Bone Joint Surg Am, 1976. 58(2): p. 195-201.
102. Klages, A., et al., *[Muscle efficiency in total shoulder prosthesis implantation: dependence on position of the humeral head and rotator cuff function].* Biomed Tech (Berl), 2001. 46(9): p. 241-6.
103. Veeger, H.E., et al., *Inertia and muscle contraction parameters for musculoskeletal modelling of the shoulder mechanism.* J Biomech, 1991. 24(7): p. 615-29.
104. Soslowky, L.J., et al., *Quantitation of in situ contact areas at the glenohumeral joint: a biomechanical study.* J Orthop Res, 1992. 10(4): p. 524-34.
105. Perry, J., *Anatomy and biomechanics of the shoulder in throwing, swimming, gymnastics, and tennis.* Clin Sports Med, 1983. 2(2): p. 247-70.
106. Kelkar, R., et al., *Glenohumeral mechanics: a study of articular geometry, contact, and kinematics.* J Shoulder Elbow Surg, 2001. 10(1): p. 73-84.
107. Karduna, A.R., et al., *Kinematics of the glenohumeral joint: influences of muscle forces, ligamentous constraints, and articular geometry.* J Orthop Res, 1996. 14(6): p. 986-93.
108. Apreleva, M., et al., *Experimental investigation of reaction forces at the glenohumeral joint during active abduction.* J Shoulder Elbow Surg, 2000. 9(5): p. 409-17.
109. Debski, R.E., et al., *A new dynamic testing apparatus to study glenohumeral joint motion.* J Biomech, 1995. 28(7): p. 869-74.

110. Halder, A.M., et al., *Dynamic inferior stabilizers of the shoulder joint*. Clin Biomech (Bristol, Avon), 2001. 16(2): p. 138-43.
111. Itoi, E., et al., *Dynamic anterior stabilisers of the shoulder with the arm in abduction*. J Bone Joint Surg Br, 1994. 76(5): p. 834-6.
112. Sharkey, N.A., R.A. Marder, and P.B. Hanson, *The entire rotator cuff contributes to elevation of the arm*. J Orthop Res, 1994. 12(5): p. 699-708.
113. Wuelker, N., et al., *A dynamic shoulder model: reliability testing and muscle force study*. J Biomech, 1995. 28(5): p. 489-99.
114. McMahan, P.J., et al., *Shoulder muscle forces and tendon excursions during glenohumeral abduction in the scapular plane*. J Shoulder Elbow Surg, 1995. 4(3): p. 199-208.
115. Konrad, G.G., et al., *Thoracohumeral muscle activity alters glenohumeral joint biomechanics during active abduction*. J Orthop Res, 2006. 24(4): p. 748-56.
116. Hughes, R.E. and K.N. An, *Force analysis of rotator cuff muscles*. Clin Orthop Relat Res, 1996(330): p. 75-83.
117. Sharkey, N.A. and R.A. Marder, *The rotator cuff opposes superior translation of the humeral head*. Am J Sports Med, 1995. 23(3): p. 270-5.
118. Halder, A., et al., *Structural properties of the subscapularis tendon*. J Orthop Res, 2000. 18(5): p. 829-34.
119. Smith, C.D., et al., *A biomechanical comparison of single and double-row fixation in arthroscopic rotator cuff repair*. J Bone Joint Surg Am, 2006. 88(11): p. 2425-31.
120. Nyffeler, R.W., et al., *Effects of glenoid component version on humeral head displacement and joint reaction forces: an experimental study*. J Shoulder Elbow Surg, 2006. 15(5): p. 625-9.
121. Harryman, D.T., 2nd, et al., *Translation of the humeral head on the glenoid with passive glenohumeral motion*. J Bone Joint Surg Am, 1990. 72(9): p. 1334-43.
122. Novotny, J.E., C.E. Nichols, and B.D. Beynon, *Normal kinematics of the unconstrained glenohumeral joint under coupled moment loads*. J Shoulder Elbow Surg, 1998. 7(6): p. 629-39.
123. Werner, C.M., et al., *The effect of capsular tightening on humeral head translations*. J Orthop Res, 2004. 22(1): p. 194-201.
124. Cain, P.R., et al., *Anterior stability of the glenohumeral joint. A dynamic model*. Am J Sports Med, 1987. 15(2): p. 144-8.
125. Williams, G.R., Jr., et al., *The effect of articular malposition after total shoulder arthroplasty on glenohumeral translations, range of motion, and subacromial impingement*. J Shoulder Elbow Surg, 2001. 10(5): p. 399-409.
126. Werner, C.M., P. Favre, and C. Gerber, *The role of the subscapularis in preventing anterior glenohumeral subluxation in the abducted, externally rotated position of the arm*. Clin Biomech (Bristol, Avon), 2007. 22(5): p. 495-501.
127. Yu, J., et al., *Biomechanical effects of supraspinatus repair on the glenohumeral joint*. J Shoulder Elbow Surg, 2005. 14(1 Suppl S): p. 65S-71S.
128. Huffman, G.R., et al., *Neer Award 2006: Biomechanical assessment of inferior tuberosity placement during hemiarthroplasty for four-part proximal humeral fractures*. J Shoulder Elbow Surg, 2008. 17(2): p. 189-96.
129. Blasler, R.B., et al., *Posterior glenohumeral subluxation: active and passive stabilization in a biomechanical model*. J Bone Joint Surg Am, 1997. 79(3): p. 433-40.
130. Kido, T., et al., *Dynamic stabilizing function of the deltoid muscle in shoulders with anterior instability*. Am J Sports Med, 2003. 31(3): p. 399-403.
131. Shapiro, T.A., et al., *Biomechanical effects of glenoid retroversion in total shoulder arthroplasty*. J Shoulder Elbow Surg, 2007. 16(3 Suppl): p. S90-5.

132. Bergmann, G., et al., *In vivo glenohumeral contact forces--measurements in the first patient 7 months postoperatively*. J Biomech, 2007. 40(10): p. 2139-49.
133. Gagey, O. and E. Hue, *Mechanics of the deltoid muscle. A new approach*. Clin Orthop Relat Res, 2000(375): p. 250-7.
134. Frankle, M.A., et al., *Stability of tuberosity reattachment in proximal humeral hemiarthroplasty*. J Shoulder Elbow Surg, 2002. 11(5): p. 413-20.
135. Coley, B., et al., *Detection of the movement of the humerus during daily activity*. Med Biol Eng Comput, 2009.
136. Coley, B., et al., *Arm position during daily activity*. Gait Posture, 2008. 28(4): p. 581-7.
137. Dietz, S.O., et al., *Tuberosity fixation in Shoulder Arthroplasty - Biomechanical and CT-findings*. 21 st Congress of the European Society of the Shoulder and the Elbow, 2008. Congress Abstract, Brugge Belgium.
138. Ruckstuhl, H., et al., *A quantitative study of humeral cartilage in individuals with spinal cord injury*. Spinal Cord, 2008. 46(2): p. 129-34.
139. Wu, G., et al., *ISB recommendation on definitions of joint coordinate systems of various joints for the reporting of human joint motion--Part II: shoulder, elbow, wrist and hand*. J Biomech, 2005. 38(5): p. 981-992.
140. Anglin, C., et al., *Glenoid cancellous bone strength and modulus*. J Biomech, 1999. 32(10): p. 1091-7.
141. Anglin, C., et al., *Loosening performance of cemented glenoid prosthesis design pairs*. Clin Biomech (Bristol, Avon), 2001. 16(2): p. 144-50.
142. Brown, G.A., et al., *Mechanical performance of standard and cannulated 4.0-mm cancellous bone screws*. J Orthop Res, 2000. 18(2): p. 307-12.
143. Gonzalez, J.V., et al., *Time analysis for screw application: traditional lag technique versus self-tapping lag technique*. J Foot Ankle Surg, 1997. 36(6): p. 422-4; discussion 466, 467-8.
144. Nien, Y.H., S.R. Kalidindi, and S. Siegler, *Fixation strength of swellable bone anchors in low-density polyurethane foam*. J Biomed Mater Res, 2001. 58(2): p. 137-46.
145. Zhu, M., K. TS., and S. DM., *Effects of specimen height on compressive mechanical properties of cellular materials*. Kongress of the American Society of Biomechanics, 1991. Tempe, Arizona.
146. Fuchs, S., et al., *[What influence do size and placement of patella resurfacing have on knee endoprosthesis?]*. Unfallchirurg, 2002. 105(1): p. 44-8.
147. Curtis, A.S. and S.J. Snyder, *Evaluation and treatment of biceps tendon pathology*. Orthop Clin North Am, 1993. 24(1): p. 33-43.
148. Favre, P., et al., *An algorithm for estimation of shoulder muscle forces for clinical use*. Clin Biomech (Bristol, Avon), 2005. 20(8): p. 822-33.
149. Graichen, H., et al., *Effect of abducting and adducting muscle activity on glenohumeral translation, scapular kinematics and subacromial space width in vivo*. J Biomech, 2005. 38(4): p. 755-60.
150. Lilly, J.H. and P.M. Quesada, *A two-input sliding-mode controller for a planar arm actuated by four pneumatic muscle groups*. IEEE Trans Neural Syst Rehabil Eng, 2004. 12(3): p. 349-59.
151. Curtis, A.S., et al., *The insertional footprint of the rotator cuff: an anatomic study*. Arthroscopy, 2006. 22(6): p. 609 e1.
152. D'Addesi, L.L., et al., *The subscapularis footprint: an anatomic study of the subscapularis tendon insertion*. Arthroscopy, 2006. 22(9): p. 937-40.
153. Ide, J., et al., *An anatomic study of the subscapularis insertion to the humerus: the subscapularis footprint*. Arthroscopy, 2008. 24(7): p. 749-53.

154. Johnson, G.R., et al., *Modelling the muscles of the scapula morphometric and coordinate data and functional implications*. J Biomech, 1996. 29(8): p. 1039-51.
155. Kaptein, B.L. and F.C. van der Helm, *Estimating muscle attachment contours by transforming geometrical bone models*. J Biomech, 2004. 37(3): p. 263-73.
156. Mochizuki, T., et al., *Humeral insertion of the supraspinatus and infraspinatus. New anatomical findings regarding the footprint of the rotator cuff*. J Bone Joint Surg Am, 2008. 90(5): p. 962-9.
157. Plausinis, D., Y.W. Kwon, and J.D. Zuckerman, *Complications of humeral head replacement for proximal humeral fractures*. Instr Course Lect, 2005. 54: p. 371-80.
158. Maldonado, Z.M., et al., *Straining of the intact and fractured proximal humerus under physiological-like loading*. J Biomech, 2003. 36(12): p. 1865-73.
159. Schmachtenberg, E., *Comparative Biomechanical Examination on the Conventional AO-T plate and the humerus fixator plate with the Finite Element Method*. Materialwissenschaft und Werkstofftechnik, 2001. 32: p. 121-125.
160. Buchler, P., et al., *A finite element model of the shoulder: application to the comparison of normal and osteoarthritic joints*. Clin Biomech (Bristol, Avon), 2002. 17(9-10): p. 630-9.
161. Gupta, S. and F.C. van der Helm, *Load transfer across the scapula during humeral abduction*. J Biomech, 2004. 37(7): p. 1001-9.
162. Frankle, M.A. and M.A. Mighell, *Techniques and principles of tuberosity fixation for proximal humeral fractures treated with hemiarthroplasty*. J Shoulder Elbow Surg, 2004. 13(2): p. 239-47.
163. Orr, T.E. and D.R. Carter, *Stress analyses of joint arthroplasty in the proximal humerus*. J Orthop Res, 1985. 3(3): p. 360-71.
164. van der Helm, F.C., *Analysis of the kinematic and dynamic behavior of the shoulder mechanism*. J Biomech, 1994. 27(5): p. 527-50.
165. Karlsson, D. and B. Peterson, *Towards a model for force predictions in the human shoulder*. J Biomech, 1992. 25(2): p. 189-99.
166. Hogfors, C., D. Karlsson, and B. Peterson, *Structure and internal consistency of a shoulder model*. J Biomech, 1995. 28(7): p. 767-77.
167. Oizumi, N., et al., *Numerical analysis of cooperative abduction muscle forces in a human shoulder joint*. J Shoulder Elbow Surg, 2006. 15(3): p. 331-8.
168. Scepi, M., et al., *A three-dimensional model of the shoulder girdle. Forces developed in deltoid and supraspinatus muscles during abduction*. Surg Radiol Anat, 2004. 26(4): p. 290-6.
169. Terrier, A., P. Buchler, and A. Farron, *Influence of glenohumeral conformity on glenoid stresses after total shoulder arthroplasty*. J Shoulder Elbow Surg, 2006. 15(4): p. 515-20.
170. Gatti, C.J., et al., *Comparison of model-predicted and measured moment arms for the rotator cuff muscles*. Clin Biomech (Bristol, Avon), 2007. 22(6): p. 639-44.
171. Henke, W. and I. Tattersall, *Handbook of Paleoanthropology: Vol I: Principles, Methods and Approaches*. LXXVI ed. 2007: Springer-Verlag, Heidelberg. 800-811.
172. Ulhaast, L., O. Kullmer, and F. S., *Tooth wear and diversity in early hominid molars: A case study*. Dental Perspectives on Human Evolution. 2007: Springer-Verlag, Heidelberg. 369 - 390.
173. Komatsu, F., R. Mori, and Y. Uchio, *Optimum surgical suture material and methods to obtain high tensile strength at knots: problems of conventional knots and the reinforcement effect of adhesive agent*. J Orthop Sci, 2006. 11(1): p. 70-4.
174. Viinikainen, A., et al., *Material and knot properties of braided polyester (Ticron) and bioabsorbable poly-L/D-lactide (PLDLA) 96/4 sutures*. J Mater Sci Mater Med, 2006. 17(2): p. 169-77.

175. Mishra, D.K., et al., *Elongation of arthroscopically tied knots*. Am J Sports Med, 1997. 25(1): p. 113-7.
176. Mahar, A.T., et al., *Comparison and performance characteristics of 3 different knots when tied with 2 suture materials used for shoulder arthroscopy*. Arthroscopy, 2006. 22(6): p. 614 e1-2.
177. Shaw, J.A. and H.B. Daubert, *Compression capability of cerclage fixation systems. A biomechanical study*. Orthopedics, 1988. 11(8): p. 1169-74.
178. Kirby, B.M. and J.W. Wilson, *Knot strength of nylon-band cerclage*. Acta Orthop Scand, 1989. 60(6): p. 696-8.
179. Bruckner, P., *Influence of Temperature on Biomechanical Properties of All-Inside Meniscal Fixation Devices and Native Meniscus*. Swiss Medical forum, Supplementum 32, Schweizerische Gesellschaft für Orthopädie SGO, Luzern, 2006.
180. Park, M.C., et al., *Two-part and three-part fractures of the proximal humerus treated with suture fixation*. J Orthop Trauma, 2003. 17(5): p. 319-25.
181. Park, T.S., et al., *A new suggestion for the treatment of minimally displaced fractures of the greater tuberosity of the proximal humerus*. Bull Hosp Jt Dis, 1997. 56(3): p. 171-6.